

**University of Alberta**

Understanding Stability of Water-in-Diluted Bitumen Emulsions by  
Colloidal Force Measurements

by

Shengqun Wang

A thesis submitted to the Faculty of Graduate Studies and Research  
in partial fulfillment of the requirements for the degree of

Doctor of Philosophy

in

Chemical Engineering

Department of Chemical & Materials Engineering

©Shengqun Wang

Spring 2011

Edmonton, Alberta

Permission is hereby granted to the University of Alberta Libraries to reproduce single copies of this thesis and to lend or sell such copies for private, scholarly or scientific research purposes only. Where the thesis is converted to, or otherwise made available in digital form, the University of Alberta will advise potential users of the thesis of these terms.

The author reserves all other publication and other rights in association with the copyright in the thesis and, except as herein before provided, neither the thesis nor any substantial portion thereof may be printed or otherwise reproduced in any material form whatsoever without the author's prior written permission.

**Examining Committee**

Zhenghe Xu, Department of Chemical and Materials Engineering

Jacob Masliyah, Department of Chemical and Materials Engineering

Tony Yeung, Department of Chemical and Materials Engineering

Tayfun Babadagli, Department of Civil and Environmental Engineering

Harvey Yarranton, University of Calgary

## **Abstract**

Removal of emulsified water is a challenge in oil sands and heavy oil processing. The flocculation and coagulation of emulsified water droplets depend on the interactions between the water droplets covered mainly by asphaltenes and oil-contaminated fine solids. To quantitatively evaluate the stability of water-in-diluted bitumen emulsions, this research determined the interactions between asphaltene surfaces in model oils, heptane, toluene or a mixture of the two known as heptol, by colloidal force measurements using atomic force microscopy (AFM) in combination with the Langmuir-Blodgett technique. The effect of aromaticity of the solvents, temperature and water content of the solvents on asphaltene-asphaltene interactions was systematically investigated.

The results showed that the interaction forces between asphaltenes are highly sensitive to the aromaticity of the organic solvents. In solvents of higher aromaticity, a repulsive force existed between asphaltene surfaces; whereas in solvents of lower aromaticity, a weak attraction was detected. The transition from repulsion to attraction indicates that it is possible to control asphaltene-asphaltene interactions, and ultimately to control the stability of asphaltene-stabilized water droplets in oil, through tuning the aromaticity of the organic solvents. By fitting the measured force profiles with theoretical models, the nature of the forces was determined, which provides insights into the mechanisms of asphaltene-stabilized water-in-oil emulsions. The concomitant benefit of the results from the direct force measurement is to predict asphaltene precipitation with change of solvent composition.

Oil-contaminated fine solids not only help stabilize water-in-diluted bitumen emulsions but are detrimental to bitumen upgrading. To control the wettability of these fine solids, a preliminary study was carried out in this work to explore the potential of ethyl cellulose (EC), an effective demulsifier for water-in-diluted bitumen emulsion, as a surface wettability modifier of the oil-contaminated solids. It was found that EC is able to reduce the surface hydrophobicity of the asphaltene- and bitumen-contaminated solids and thus enhances their removal from bitumen froth. The mechanism of increased wettability by EC addition was determined by quartz crystal microbalance with dissipation (QCM-D) and AFM topographical imaging. The results from this study can help establish the criteria for selecting and developing chemical modifiers for applications in wettability control of oil-contaminated solids.

## **Acknowledgement**

There are many people to whom I owe an enormous thank you for their help and advice over the course of this work.

First, I would like to thank my supervisors Dr. Zhenghe Xu and Dr. Jacob Masliyah for their guidance and support through out this work. Their constant encouragement and assistance enabled me to overcome challenges from the beginning of my doctoral program till the end of completing this thesis. Their advice in many respects, especially that regarding how the academic/industrial research work is performed, will be extremely helpful as I move forward in my career.

Second, I would like to thank my colleagues who helped me in finishing this thesis in many ways. Thank Dr. Jun Long for his help with AFM and discussions about the experiment at the beginning of my program, Drs Hongying Zhao and Sili Ren for sharing their experiences with AFM, Dr. Phillip Choi for his helpful discussions with polymer scaling theory, Dr. Xianhua Feng for his discussions on research work as well as writing, Dr. Paolo Mussone for the demonstration of Langmuir trough, Ms. Nataliya Segin for her working with me as a summer student in 2009 (summer), Ms. Tuyet Le for her help with elemental analysis and Ms Ni Yang for ellipsometry. Thank Mr. Jim Skwarok, Ms. Shiau-Yin Wu, Ms Leanne Swekla and Ms. Lisa Carreiro for their assistance on every occasion. Every bit of help from other group members is also much appreciated.

Third, I would also like to acknowledge the administrative staff of the Chemical & Materials Engineering Department at University of Alberta for creating a supportive environment for the graduate students.

Fourth, I appreciate the financial support from NSERC Industrial Research Chair in Oil Sands Engineering.

Finally, I would like to thank my family for their faith in me. They supported me through the graduate study and on all the decisions I have made in life.

## Table of Contents

<b>Chapter 1 Introduction</b> .....	1
<b>1.1 Bitumen extraction from oil sands ore</b> .....	1
1.1.1 Oil sands deposit and mining.....	1
1.1.2 Bitumen extraction.....	2
1.1.3 Bitumen froth treatment and challenges .....	2
<b>1.2 Suggestions for improvement of bitumen froth treatment</b> .....	5
<b>1.3 Objectives and techniques</b> .....	8
1.3.1 Objectives .....	8
1.3.2 AFM force measurements .....	11
<b>1.4 Literature review</b> .....	12
1.4.1 Bitumen and asphaltenes.....	12
1.4.2 Characterization of asphaltenes .....	13
1.4.2.1 Chemical composition of asphaltenes.....	14
1.4.2.2 Structure of asphaltene molecules .....	15
1.4.3 Properties of asphaltenes and effect on oil sands processing.....	17
1.4.3.1 Self-association and aggregation .....	17
1.4.3.2 Flocculation and precipitation.....	21
1.4.3.3 Interfacial activity .....	23
<b>1.5 Outline of thesis</b> .....	25
<b>Chapter 2 Materials and experimental techniques</b> .....	28
<b>2.1 Materials and chemicals</b> .....	28
<b>2.2 Atomic force microscopy (AFM)</b> .....	30
2.2.1 Fundamentals of AFM.....	30
2.2.2 Surface force measurement by AFM .....	32
2.2.3 Issues with AFM force measurement in organic solvents .....	34
2.2.4 AFM used in this work .....	36
2.2.5 Typical setup of AFM force measurement .....	37
2.2.6 Typical setup of AFM imaging.....	38
<b>2.3 Langmuir-Blodgett (LB) trough</b> .....	38
2.3.1 Asphaltene deposition onto silica wafer and AFM silica probe .....	40

2.3.2	Compression isotherms of asphaltene interfacial films .....	42
<b>2.4</b>	<b>Quartz crystal microbalance with dissipation (QCM-D)</b> .....	42
2.4.1	Adsorption of asphaltenes and EC on silica surface .....	44
<b>2.5</b>	<b>Other techniques</b> .....	46
2.5.1	Elemental analysis .....	46
2.5.2	Water contact angle measurement .....	47
2.5.3	Karl fisher titration.....	47
<b>Chapter 3</b>	<b>Colloidal interactions between asphaltene surfaces in toluene</b> .....	48
<b>3.1</b>	<b>Introduction</b> .....	48
<b>3.2</b>	<b>Scaling theory for polymer brushes and force measurements between polymer brushes by AFM</b> .....	50
3.2.1	Polymer brushes.....	50
3.2.2	Theoretical modeling of polymer brushes - scaling theory.....	52
3.2.3	Steric repulsions between polymer brushes described by scaling theory .....	52
3.2.4	Forces between two polymer brushes measured by AFM .....	54
<b>3.3</b>	<b>Experimental</b> .....	57
3.3.1	Materials .....	57
3.3.2	Preparation of asphaltene films.....	57
3.3.3	Surface force measurement (AFM technique).....	58
<b>3.4</b>	<b>Results</b> .....	59
3.4.1	Characteristics of asphaltene films .....	59
3.4.2	Interaction forces in toluene.....	64
3.4.3	Effect of water content in solvents on interaction forces.....	71
3.4.4	Effect of temperature on interaction forces.....	72
3.4.5	Nature of interaction forces.....	74
3.4.6	Colloidal forces and stability of water-in-oil emulsions.....	75
<b>3.5</b>	<b>Conclusions</b> .....	76
<b>Chapter 4</b>	<b>Interaction forces between asphaltene films in organic solvents</b> ..	78
<b>4.1</b>	<b>Introduction</b> .....	78
<b>4.2</b>	<b>Experimental</b> .....	82

4.2.1 Materials .....	82
4.2.2 LB asphaltene films and compression isotherms.....	83
4.2.3 Surface force measurements (AFM technique) .....	83
<b>4.3 Results</b> .....	84
4.3.1 Characteristics of asphaltene films .....	84
4.3.2 Interaction forces in toluene (good solvent) .....	85
4.3.3 Interaction forces in heptane (poor solvent) .....	87
4.3.4 Interaction forces in heptol .....	89
4.3.5 Langmuir compression isotherms of asphaltene interfacial films .....	91
<b>4.4 Discussion</b> .....	93
4.4.1 Nature of forces between asphaltene surfaces in heptol .....	93
4.4.2 Relation between solution quality and interaction forces .....	97
<b>4.5 Conclusions</b> .....	101
<b>Chapter 5 Wettability control mechanism of highly contaminated hydrophilic silica/alumina surfaces by an ethyl cellulose</b> .....	103
<b>5.1 Introduction</b> .....	103
<b>5.2 Experimental</b> .....	108
5.2.1 Materials and chemicals.....	109
5.2.2 Preparation of hydrophobic silica surfaces .....	109
5.2.3 QCM-D adsorption experiment .....	110
5.2.4 Soaking experiment .....	110
5.2.5 Contact angle measurement .....	112
5.2.6 AFM imaging.....	112
5.2.7 Langmuir compression isotherms of asphaltenes+EC films.....	112
<b>5.3 Results and discussion</b> .....	113
5.3.1 Adsorption of EC on asphaltene pre-adsorbed surface .....	113
5.3.2 Adsorption of asphaltenes on EC pre-adsorbed surface .....	117
5.3.3 Water wettability of sample surface.....	121
5.3.4 Topography of sample surface .....	124
5.3.5 Langmuir isotherms of asphaltenes+EC films at toluene/water interface .....	132



5.3.6 Effect of EC on water wettability of silane-treated hydrophobic silica surfaces .....	134
5.3.7 Solids removal with EC addition in froth treatment in oil sands processing .....	136
<b>5.4 Conclusions</b> .....	137
<b>Chapter 6 Summaries and Conclusions</b> .....	139
<b>6.1 Major conclusions</b> .....	140
<b>6.2 Major contributions</b> .....	141
<b>6.3 Suggestions for future work</b> .....	142
<b>References</b> .....	145


## List of Tables

Table 1.1. Comparison of operation conditions of paraffin- and naphtha-based froth treatment processes .....	5
Table 1.2. Elemental composition of bitumen and asphaltenes precipitated with n-heptane .....	14
Table 3.1. Water content in toluene .....	57
Table 3.2. Interaction force curve fitting parameters by scaling theory .....	68
Table 4.1. Fitting parameters by scaling theory of repulsive force profiles in Figure 4.2 .....	87
Table 5.1. Fitting parameters of Figure 5.7d .....	124
Table 5.2. Water contact angle of silanized silica surface treated with EC .....	134

## List of Figures

Figure 1.1. Industrial froth treatment processes.....	3
Figure 1.2. Structure of emulsified water droplets and solids in bitumen froth .....	6
Figure 1.3. Structure of water/oil and hydrophilic solid/oil interfaces .....	11
Figure 1.4. Separation of bitumen based on solubility into four classes (SARA fractionation).....	13
Figure 2.1. Schematic of AFM working mechanisms .....	31
Figure 2.2. AFM force profile and a colloidal probe attached cantilever.....	32
Figure 2.3. AFM force measurement setup .....	36
Figure 2.5. AFMs used in this work. (a) Nanoscope Multimode; (b) Agilent 5500 .....	37
Figure 2.6. (a) Schematic of Langmuir trough; (b) Langmuir-Blodgett upstroke technique to prepare asphaltene surfaces .....	39
Figure 2.7. (a) QCM-D equipment and experimental setup; (b) Quartz crystal sensor .....	45
Figure 3.1. Schematic of a polymer brush .....	51
Figure 3.2. Polymer brushes under compression during AFM force measurements .....	56
Figure 3.3. Interfacial pressure-area isotherm for asphaltene interfacial film at toluene/water interfaces at 20 °C.....	60
Figure 3.4. AFM images of asphaltene films. (a) LB asphaltene film from toluene/water interface; (b) Dip-coated asphaltene film from toluene/silicon interface.....	61
Figure 3.5. Normalized interaction forces between LB asphaltene films and silica surface in toluene at 20 °C .....	63
Figure 3.6. Normalized interaction forces between dip-coated asphaltene films and silica surface in toluene at 20 °C.....	63
Figure 3.7. Normalized interaction forces between silica-silica in toluene at 20 °C. Solid line: theoretical van der Waals interactions calculated with an effective Hamaker constant of $6.0 \times 10^{-22}$ J .....	64
Figure 3.8. Normalized interaction forces between LB asphaltene films in dry toluene as a function of separation distance at 20 °C. Solid line: fitting with scaling theory, $L_o=43$ nm, $s=17$ nm and $\delta =6$ nm .....	66

Figure 3.9. Normalized interaction forces between dip-coated asphaltene films in dry toluene as a function of separation distance at 20 °C. Solid line: fitting with scaling theory, $L_o=36$ nm, $s=19$ nm and $\delta =3.5$ nm .....	67
Figure 3.10. Normalized interaction forces in toluene at separation distance of 10 nm to demonstrate the variation of long-range forces. The results are derived from 30 force profiles at a separation distance of 10nm. For LB films, $F/R= 1.26\pm 0.15$ mN/m; for dip-coated films, $F/R = 0.93\pm 0.14$ mN/m.....	70
Figure 3.11. Effect of water content on the interactions between LB asphaltene films in toluene at 20 °C. Solid line: fitting with scaling theory, $L_o= 43$ nm (16 ppm water), 40.5 nm (68 ppm water) and 38.6 nm (365 ppm water).....	71
Figure 3.12. Effect of temperature on the interactions between LB asphaltene films in toluene .....	73
Figure 3.13. Effect of temperature on the interactions between dip-coated asphaltene films in toluene.....	73
Figure 4.1. AFM image of (a) bare silica surface and (b) asphaltene film .....	85
Figure 4.2. Interaction forces upon approach between two asphaltene surfaces as well as an asphaltene surface and a bare silica surface in toluene. ■: Interactions between two asphaltene surfaces; ●: Interactions between two bare silica surfaces; ▲: Interactions between a silica substrate – an asphaltene probe; ○: Interactions between an asphaltene substrate – a silica probe; Green solid lines: scaling theory fitted curves.....	86
Figure 4.3. Interactions between asphaltene surfaces in <i>n</i> -heptane. ●: Approach force; ▲: Retraction force/adhesion force; Solid lines: calculated van der Waals forces between asphaltene surfaces in heptane with a Hamaker constant $A_{eff}=1.1\times 10^{-21}$ J .....	88
Figure 4.4. Interactions between asphaltene surfaces upon approach in heptol. Symbols: AFM experimental data for different $\Phi_T$ ; Solid lines: scaling theory fitting of force curve ( $\Phi_T$ in the range of 0.3 to 1.0).....	90
Figure 4.5. Adhesion force as a function of $\Phi_T$ . Symbols: experimental data; Solid line: fitted trend line.....	91
Figure 4.6. Interfacial pressure-area isotherms for asphaltene monolayers at various heptol/water interfaces with a toluene volume fraction ( $\Phi_T$ ) of 0, 0.1, 0.25, 0.8, and 1 .....	92
Figure 4.7. Effective Hamaker constant of asphaltenes-heptol-asphaltenes system as a function of toluene fraction in heptol ( $\Phi_T$ ) .....	94
Figure 4.8. Fitting parameters in equation (4-1) as a function of toluene fraction in heptol ( $\Phi_T$ ). Symbols: experimental data; Solid lines: trend lines.....	96

Figure 4.9. Schematic plot of conformational transition of asphaltene layers with $\Phi_T$ of heptol (  represent the fused aromatic ring sheet or consolidated part of asphaltenes) .....	97
Figure 4.10. Interaction parameter of asphaltene/heptol as a function of $\Phi_T$ of heptol.....	100
Figure 4.11. Relationship of adhesion force to interaction parameter of asphaltenes-heptol.....	101
Figure 5.1. Effect of amphiphilic chemical modifier on organic contaminated solid surface (red circles and blue squares are polar groups on chemical modifier and solid surface, respectively). (a) Chemical modifiers adsorb on the top of organic contaminants through non-specific interaction and leave the polar segments exposed; (b) Chemical modifiers displace the organic contaminant and adsorb on the solid surface.....	106
Figure 5.2. Molecular structure of ethyl cellulose (EC) .....	107
Figure 5.3. Soaking experiment procedures and corresponding sample codes ..	111
Figure 5.4. Frequency and dissipation shift as a function of adsorption time in QCM-D experiments. (a) EC adsorption on asphaltene-coated silica surface; (b) EC adsorption on asphaltene-coated alumina surface; (c) Asphaltene adsorption on EC-coated silica surface.....	115
Figure 5.5. Mass uptake on QCM-D sensor surface in each adsorption event in Figure 5.4 .....	118
Figure 5.6. $D_{qcm}$ - $f$ plot of the QCM-D adsorption results in Figure 5.4.....	120
Figure 5.7. Water contact angles of the sample surfaces after soaking in EC-in-toluene solutions (Scatters: experiment data; Lines: fitted lines by exponential decay model). (a) Asphaltene-coated silica surfaces; (b) Bitumen-coated silica surfaces; (c) Asphaltene-coated alumina surfaces; (d) $f_{AB}(t)$ profiles of plot (a) and (b) with the exponentially fitted curves by equation (5-1) .....	122
Figure 5.8. AFM topographical images of the samples in soaking experiment. (a) Asphaltenes and AE-i (asphaltene-coated sample surface soaked in EC-in-toluene solution for i hours, i = 0, 6, and 7); (b) Bitumen and BE-i (bitumen-coated sample surface soaked in EC-in-toluene solution for i hours, i = 0, 6, and 7); (c) EC (EC-coated sample surface), EC-A-12 (EC-coated sample surface soaked in asphaltene-in-toluene solution for 12 hours) and EC-B-12 (EC-coated sample surface soaked in bitumen-in-toluene solution for 12 hours). The dimension of images is $2 \mu\text{m} \times 2 \mu\text{m}$ .....	126
Figure 5.9. Statistical analysis of the AFM images in Figure 5.8. (a) Step height of the aggregates (columns) and surface coverage of the domains with height > 0.5 nm (Dots: calculated data from images; Lines: polynomial fitting curve) as a	

function of soaking time in EC-in-toluene solution; (b) Step height profile across asphaltene (bitumen) domains (A, B, C and D correspond to four locations on the image along the line A→B→C→D)..... 128

Figure 5.10. Schematics of asphaltenes displacement by EC on a hydrophilic solid surface..... 130

Figure 5.11. Langmuir isotherms of asphaltenes+EC films at toluene/water interface..... 133

Figure 5.12. AFM image of: (a) Butyltrichlorosilane-treated silica surface and (b) EC on butyltrichlorosilane-treated silica surface; and (c) Height profile of EC image in (b). The dimension of the images is  $2\ \mu\text{m} \times 2\ \mu\text{m}$ ..... 136

## List of Symbols

$R$	Radius of the AFM probe (micro-sphere attached to the AFM cantilever tip), m
$D'$	Separation distance between the two solid surfaces, m
$D$	Distance between the outer-layers of the two compressed polymer layers, m
$E(D')$	Interaction energy between two parallel flat plates per unit area, $\text{J/m}^2$
$F(D')/R$	Normalized interaction force between a solid flat surface and a solid sphere with radii of $R$ at a closest separation of $D'$ between the solid surfaces, $\text{mN/m}$
$F(D)/R$	Normalized interaction force between a flat asphaltene surface and a spherical asphaltene surface with radius of $R$ at a closest separation of $D$ between the compressed outer-layers of polymer layers, $\text{mN/m}$
$F_C$	Free energy of a polymer chain in a polymer brush, J
$k_B$	Boltzmann constant, $\text{J}\cdot\text{K}^{-1}$
$T$	Temperature, K
$N$	Number of monomers per polymer chain
$\phi$	Volume fraction of polymer in a polymer brush
$a$	Effective size of the monomer of a polymer, m
$s$	Average distance between two polymer grafting sites on a solid surface, m
$\pi_{os}$	Osmotic pressure, Pa
$L_o$	Length of a polymer brush at the equilibrium state (without compression), m
$L$	Length of a polymer brush, m
$\xi$	Thickness of polymer brushes compressed during AFM force measurements, m
$F_{vdW}/R$	Normalized van der Waals forces between a sphere with radius $R$ and a flat surface calculated using Derjaguin's approximation, $\text{N/m}$
$A_{eff}$	Effective Hamaker constant, J
$\Phi_T$	Volume fractions of toluene in heptol

$A_c, \pi_c$	Critical trough area and critical surface pressure at which an asphaltene monolayer begins to buckle, $m^2, N/m$
$\chi$	Interaction parameter describing the stability behavior of polymer solutions
$\delta_{asp}, \delta_{heptol}$	Hildebrand solubility parameters of asphaltenes and heptol, $MPa^{1/2}$
$R_{gas}$	Universal gas constant, $8.314 J \cdot mol^{-1} \cdot K^{-1}$
$V_{heptol}$	Molar volume of heptol, $m^3 \cdot mol^{-1}$
$y_{heptane},$ $y_{toluene}$	Mole fraction of heptane or toluene in heptol
$\theta$	Water contact angle, degree
$\Delta m$	Adsorbed mass on a QCM-D sensor, $mg/m^2$
$n$	Number of harmonic overtones of the crystal sensor, $n = 1, 3, 5, 7, 9, 11$ and $13$
$C$	Constant of the QCM-D sensor, $C = 17.7 ng/(Hz \cdot cm^2)$ in this study
$f, \Delta f$	Frequency and frequency shift, Hz
$D_{qcm},$ $\Delta D_{qcm}$	Dissipation and dissipation shift
$E_{lost}, E_{stored}$	Energy lost (dissipated) and energy stored in the oscillator during one oscillation cycle of QCM-D sensor, J
$f_{AB}(t)$	Fraction coverage of asphaltene or bitumen on a surface at exposure time $t$



## List of Acronyms

AFM	Atomic force microscope
CAC	Critical aggregation concentration
CMC	Critical micelle concentration
EC	Ethyl cellulose
F-H	Flory-Huggins
FTIR	Fourier transform infrared spectroscopy
LB	Langmuir-Blodgett
QCM-D	Quartz crystal microbalance with dissipation
SAGD	Steam-assisted gravity drainage

# **Chapter 1 Introduction**

## **1.1 Bitumen extraction from oil sands ore**

### **1.1.1 Oil sands deposit and mining**

Oil sands are mineral sands with bitumen impregnated in the unconsolidated sand deposits.<sup>1</sup> Bitumen is an extremely heavy oil that must be upgraded and refined before it can be used as gasoline and other fuels.<sup>1</sup> A typical composition of oil sands is 80-85 wt% solids, 7-12 wt% bitumen and 5 wt% connate (formation) water. Depending on the depth of the oil sands deposit, two bitumen production technologies are currently employed: open-pit mining-extraction and in-situ recovery (e.g., steam-assisted gravity drainage, SAGD). Open-pit mining is an economical and a viable way for developing the relatively shallow deposits of oil sands (less than 75 m in depth), where the overburden on the top of the deposit is removed and the ore is mined with shovels. Hot water and chemical additives are added to the ore at the slurring stage. Bitumen is liberated and aerated within the hydrotransport pipeline, and separated from the solids in gravity separation vessels. To recover the bitumen from deeper oil sands deposits, in-situ bitumen recovery has to be employed. During steam-assisted in-situ recovery, bitumen is separated in situ from the solids and recovered by injecting steam into a horizontal well drilled through the oil sands formation. The viscosity of bitumen is reduced due to increased temperature or dilution with solvents. Under the gravity, the less viscous bitumen flows to the production well where it is transported to the surface. It is estimated that among the oil sands deposits in Alberta, about 20% can be economically recovered by open-pit mining

technology.<sup>1</sup> Currently, about 60% of the bitumen produced from oil sands is by open-pit mining and water-based bitumen extraction technologies.<sup>1</sup>

### **1.1.2 Bitumen extraction**

In open-pit mining, water-based bitumen extraction technologies are used for bitumen recovery.<sup>1</sup> The oil sands ore is shoveled and then sent to bitumen extraction site by truck. Prior to bitumen extraction, the oil sands ore lumps are crushed to smaller sizes and mixed with warm process water and chemical additives, e.g., caustic soda, to form an oil sands slurry. Usually the slurry has a temperature of 35-55 °C and pH of 8-8.5. Under this condition, bitumen is liberated from the mineral solid surface. Usually the bitumen conditioning process takes place in a tumbler (earlier technology) or hydrotransport pipeline (current technology). During the conditioning, air is introduced or entrained into the slurry to aerate the liberated bitumen droplets. The aerated bitumen droplets float to the top of the slurry and form a froth layer in a gravity separation vessel. The bitumen froth contains a considerable amount of water and solids that have to be removed in the bitumen froth treatment process prior to bitumen upgrading.

### **1.1.3 Bitumen froth treatment and challenges**

Typically bitumen froth contains about 60 wt% bitumen, 30 wt% water and 10 wt% solids. The majority of the water is free water, but about 5 wt% of the water is in an emulsified form.<sup>2</sup> The solids are entrained in the bitumen phase or accumulated at the water/oil interface.<sup>3,4</sup> Over the temperature range of the froth treatment (cleaning) operation, bitumen has an almost identical density to that of water.<sup>1,2</sup> To create a density difference between bitumen and water and to reduce

the viscosity of bitumen, a diluent (e.g., naphthenic or paraffinic solvent) is added to the froth to facilitate the separation of water and solids by gravity settling, or by cycloning or centrifugation. Based on the types of diluents used, two froth treatment methods are commercially employed in the industry, know as naphtha-based froth treatment and paraffin-based froth treatment.<sup>3</sup>

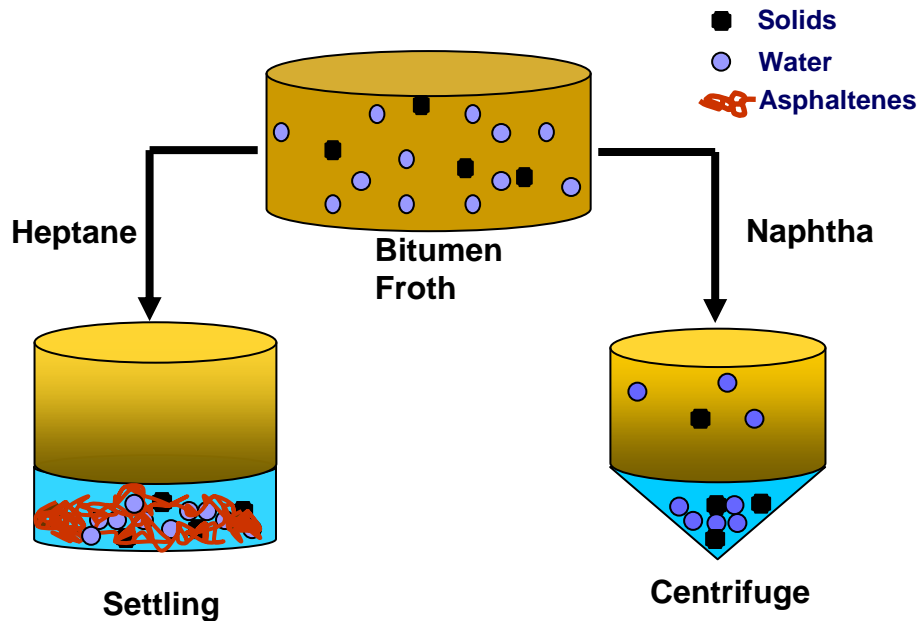


Figure 1.1. Industrial froth treatment processes

In the naphtha-based froth treatment, mechanical separation equipment such as cyclones and centrifuges is necessary for the separation of the water droplets and solids. Usually the water/oil droplets and solids form a rag layer that builds up at the water/oil interface, hindering effective phase separation.<sup>2</sup> The emulsified water droplets do not coalesce easily due to a rigid “skin” composed of asphaltenes/bitumen and asphaltenes/bitumen-contaminated fine solid particles.<sup>5</sup> As shown in Figure 1.1, after centrifugation, most of the water and solids can be removed. However, there are still about 2 wt% emulsified water and 0.5 wt% fine

solids dispersed in the diluted-bitumen phase.<sup>3</sup> These solids and emulsified water droplets are only a few microns in diameter and are partly to wholly covered with a layer of hydrocarbons, e.g., asphaltenes and natural surfactants in bitumen.<sup>6-12</sup> Therefore, they can disperse stably in the diluted bitumen (bitumen-solvent) due to a solvent-like outer-layer. Although small in quantity, these solids and water droplets can cause corrosion and fouling problems in downstream upgrading operations.<sup>1</sup> It is thus necessary to develop new technologies to remove these solids and emulsified water droplets.

As a relatively new technique, the paraffin-based froth treatment process amends the drawbacks of the naphtha-based process by producing a very clean bitumen product. When paraffinic solvents, hexane for example, are added to bitumen at a sufficiently high diluent to bitumen ratio, asphaltenes would precipitate from bitumen due to low solubility of asphaltenes in alkane (paraffinic) solvents. The precipitating asphaltenes can flocculate the dispersed water droplets and fine solids together to form complex floccules or clusters of water-solids-asphaltene precipitates that settle quickly under gravity to produce bitumen with a negligible amount of water and solids.<sup>13</sup> Despite of the high quality of bitumen produced by paraffin-based froth cleaning process, entrainment of bitumen in the clusters of flocculated water-solids-asphaltene precipitates significantly reduces the recovery of bitumen in the froth cleaning process. In addition, low recovery of solvents reduces the economic benefit of the paraffin-based process. A comparison of the operation conditions of the two froth treatment processes is listed in Table 1.1.

Table 1.1. Comparison of operation conditions of paraffin- and naphtha-based froth treatment processes

	Paraffinic diluents	Naphthenic diluents
Solvents	Alkanes of C <sub>5</sub> -C <sub>6</sub> mixture (e.g., hexane)	Naphtha
Aromatics content of diluent	0 wt%	*~14 wt%
Critical S/B ratio	1.8-2	~4
solvent/bitumen ratio in industrial operation (S/B)	2.1-2.5	0.6-0.75
Temperature	30-32 °C	75-78 °C
Asphaltene precipitation	~50% of the asphaltenes in bitumen rejected (8-10% of total bitumen)	No asphaltene precipitation
Product quality	Solids & water < 0.1 wt%	Water: 1.0-2.5 wt%; Solids: 0.3-0.8 wt%
Bitumen recovery	88-94%	~98%

Table is mainly taken according to *Fundamentals of Oilsands Extraction (ChE534 text book)*.<sup>1</sup>

\*Data from Syncrude Ltd.

## 1.2 Suggestions for improvement of bitumen froth treatment

Table 1.1 shows that the two froth treatment processes have their pros and cons. Both processes are aimed at achieving a maximum water and solids removal as well as maximum bitumen recovery. The naphtha-based process can achieve high bitumen recovery but at the cost of relatively low product quality in terms of solid and water content in the diluted bitumen. In addition, the formation of a rag layer between diluted bitumen and aqueous phases is an operational challenge. Although the paraffin-based process can produce diluted bitumen with high product quality, the low recovery of solvents is a major drawback. To improve the current processes and/or to develop a more effective process for bitumen froth cleaning in an innovative way, an in-depth understanding of bitumen froth cleaning process needs to focus on the problems described below.

1) Stability of water-in-diluted bitumen emulsions with varying diluent (solvent) composition. The water droplets are stabilized by a protective layer mainly composed of asphaltenes and oil-contaminated fine solid particles (Figure 1.2).<sup>6, 10, 11, 14-17</sup> The emulsified droplets can disperse stably in naphtha-diluted bitumen but flocculate with asphaltenes when paraffinic solvents are used as diluents. In order to get a fundamental understanding of the stability of the water-in-diluted bitumen emulsions, the obstacle preventing the water droplets coalescing and the driving force for their flocculation need to be revealed. For this purpose, quantitative determination of the interaction forces between asphaltene surfaces in organic solvents with varying composition is necessary. However, up to date, little quantitative measurement of interaction forces between asphaltenes-asphaltenes in organic solvents has been reported. The limited reports on the interaction forces of asphaltene surfaces in diluents are rather qualitative and the effect of solvent quality, e.g., aromaticity, on the interaction forces is not clearly addressed.<sup>18, 19</sup>

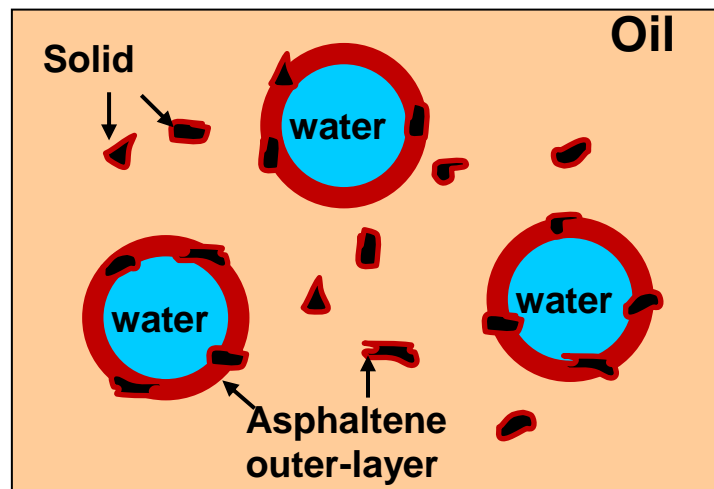


Figure 1.2. Structure of emulsified water droplets and solids in bitumen froth

In studying the interactions between asphaltene surfaces, effect of the factors listed below needs to be investigated.

#### 1-1) Aromaticity of solvents

Aromaticity of the solvents significantly affects asphaltene interactions. Asphaltene molecules are polyaromatic sheets connected by heteroatoms and aliphatic chains.<sup>20</sup> Asphaltenes dissolve in aromatic solvents but precipitate out in alkanes. The interaction forces between asphaltenes-asphaltenes in organic solvent should change significantly when tuning the solvent composition in terms of aromaticity.

#### 1-2) Temperature

Temperature affects the solubility of asphaltenes in the oil phase. From the published studies on this topic, it is indicated that the solubility of asphaltenes increases with temperature.<sup>21</sup> While some researchers found that temperature has a negligible effect on asphaltene precipitation.<sup>12, 22</sup> In the scope of the solubility of asphaltenes in oil phase, a clear and definite conclusion of temperature effect on solubility of asphaltenes in a given solvent needs to be established.

#### 1-3) Water content of solvents

As an inevitable consequence of the water-based bitumen extraction process, there is always certain amount of water in the oil phase. Water is a poor solvent of asphaltenes. The presence of water in the oil phase leads to a less favorable environment for asphaltenes. It is reported that even a trace amount of water can lead to a noticeable change in asphaltene aggregation.<sup>23</sup> Murgich et al. stated that water can enhance the aggregation of asphaltenes by forming bridging hydrogen



bonds between the heteroatoms of asphaltenes.<sup>24</sup> In addition, it is believed that water is involved in hydrogen bonding with asphaltenes at the water/oil interface, enhancing the stability of water-in-oil emulsions.<sup>10, 11</sup> Further studies on the effect of dissolved water in solvents on the interactions between asphaltenes-asphaltenes in oil phase are necessary.

Other factors such as surfactants (naphthenic acids) in bitumen may also affect the interactions between asphaltene surfaces but are not considered in this work.

2) Wettability control of oil-contaminated solids. The oil-contaminated solids contribute significantly to stabilizing water-in-oil emulsions and to formation of rag layers.<sup>4, 5, 15, 25, 26</sup> Most of the residual solids in the oil phase and rag layer are ultra fine clay particles.<sup>7, 8</sup> They are originally hydrophilic but rendered hydrophobic due to adsorption of bitumen/asphaltenes (Figure 1.2).<sup>8, 9, 27</sup> The hydrophobicity of solids has negative effect on the overall bitumen extraction, resulting in poor froth quality and lower bitumen recovery.<sup>7, 8, 28, 29</sup> It is desirable to modify the surface wettability of the oil-contaminated solids to facilitate their partitioning into the water phase. For example, a chemical modifier that can make the solids more water-wet will facilitate solids partition into the water phase, and therefore lower the stability of water-in-oil emulsions and alleviate rag layer formation. However, research on wettability control of solids in oil phase using chemical modifiers is seldom performed.

## **1.3 Objectives and techniques**

### **1.3.1 Objectives**

This research focuses on two main parts:

1) Measure the interactions between asphaltene surfaces in organic solvents in order to provide a fundamental, molecular-level understanding on the stability of water-in-diluted bitumen emulsions.

The measurement of interaction forces between asphaltenes in organic solvent is highly desirable in overall heavy oil processing. For example, it is important to predict and to prevent asphaltene precipitation during crude oil mixing or production.<sup>30, 31</sup>

Force measurement for asphaltenes-in-solvent system, however, is not an easy task. Until now, only few experiments were ever conducted to directly measure the forces between asphaltenes in organic solutions. The major hindrance is the complexity of asphaltenes. As a solubility class, asphaltenes are a mixture of a large number of heavy hydrocarbons. These hydrocarbon compounds tend to self-associate in even good solvents.<sup>32-34</sup> Compounds in asphaltenes can exist in the form of monomers, dimers, ... or multimer-aggregates.<sup>16, 20</sup> The molecular structure of various compounds in asphaltenes remains to be established. Thus it is not practical to determine experimentally the interaction forces between individual components in asphaltene solutions. Theoretically, computer-based computation (e.g., molecular dynamics simulation) provides some information on molecular interactions of model compounds of asphaltenes.<sup>24, 35-38</sup> However, the molecular simulation results cannot represent the real conditions, especially when the structure and molecular weight of asphaltenes remain ill-defined.

In this study, the interaction forces between asphaltenes are measured as a function of their separation distance using an atomic force microscope. The direct

measurement of surface forces between asphaltene surfaces has several advantages. First, the forces between two asphaltene surfaces are a statistical combination of the interactions between various components in asphaltenes. The results thus represent the “general” or “average” asphaltene behavior. Second, it is easy to prepare an asphaltene film that is similar to those adsorbed on solid surface or at water/oil interfaces, e.g., by Langmuir-Blodgett technique. The forces between such prepared asphaltene films or surfaces can be extended to indicate the interactions between the solids or water droplets in diluted bitumen or heavy oil. Finally, the techniques such as surface force apparatus (SFA) and atomic force microscopy (AFM) for direct surface force measurement are now available.

2) Control the wettability of solids in diluted bitumen by chemical modifiers to facilitate solids partition into water phase.

The use of chemical modifiers to control the wettability of solids in diluted bitumen is based on the destabilization of water-in-oil emulsions by chemical demulsifiers. The consideration is based on two premises. First, both the water droplets and solids are covered with asphaltenes (Figure 1.2). Second, the water/oil and hydrophilic solid/oil interfaces are fundamentally similar (Figure 1.3). Both interfaces have a layer of hydroxyl groups facing the oil phase. An amphiphilic demulsifier that works at water/oil interfaces is thus expected to be able to modify the organic-coated solid surface by altering the structure of the organic coatings or displacing them. Moreover, the use of a demulsifier as a modifier for control of solids wettability avoids the possible counter-effect of

multiple chemical additions, especially for avoiding the formation of rag layers which are composed of multiple emulsions, bi-wettable solids and oil.

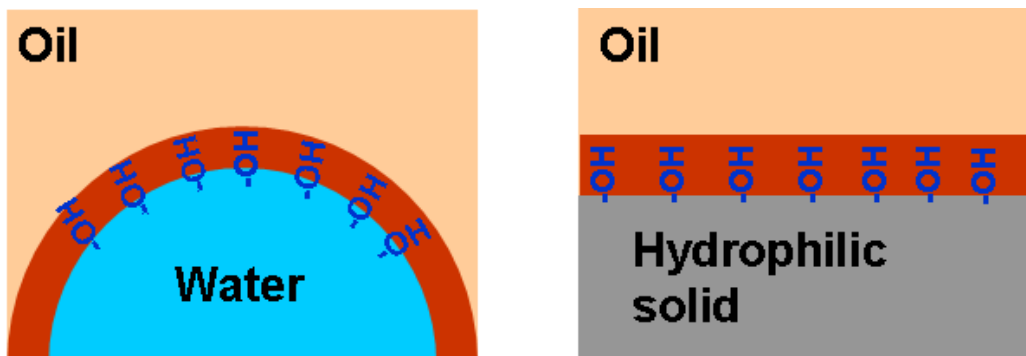


Figure 1.3. Structure of water/oil and hydrophilic solid/oil interfaces

### 1.3.2 AFM force measurements

The two mostly used surface force measurement techniques are surface force apparatus (SFA) and atomic force microscope (AFM).<sup>39</sup> The application of SFA was pioneered by Israelachvili et al. in 1970s.<sup>40</sup> It allows direct measurement of interaction forces between two crossed cylindrical surfaces. The absolute separation distance between the two surfaces is determined through optical interferometry. The colloidal technique of AFM was developed by Ducker et al. in 1991.<sup>41</sup> AFM allows direct measurement of interaction forces between a microspherical surface and a flat surface. Using AFM, the separation distance between two surfaces is derived from the constant compliance region of the force curve. For this reason, the absolute separation distance is not always accessible in AFM colloidal force measurement. Both surface force techniques can detect forces to nano-Newton ( $10^{-9}$  N) resolution at nano-meter resolution ( $10^{-9}$  m) of the separation distance. Due to its convenience in operation, the AFM colloidal technique of force measurement has been widely applied in more complex, less

well-defined systems.<sup>42</sup> In oil sands engineering, for example, AFM has been successfully used to measure colloidal forces for bitumen-bitumen, bitumen-silica and clay-silica systems.<sup>43-48</sup> In this study, the interaction forces between asphaltene surfaces were determined by AFM. AFM force measurements have been mostly applied to aqueous systems. Extending the application of AFM colloidal force measurements to nonaqueous system is necessary for understanding molecular/colloidal phenomena in nonaqueous systems. Issues related to AFM force measurements in organic system will be discussed in detail in Chapter 2.

#### **1.4 Literature review**

To provide a broader and detailed background of this work, the nature of asphaltenes (e.g., composition, molecular structure, molecular weight, etc.) and the properties of asphaltenes in oil sands and more generally in heavy oil engineering are comprehensively reviewed in the following text.

##### **1.4.1 Bitumen and asphaltenes**

Bitumen is an extremely heavy crude oil that contains a large number of hydrocarbon components which are usually fractionated to saturate, aromatic, resins and asphaltenes.<sup>1</sup> This fractionation method is called SARA which is shown in Figure 1.4.<sup>1</sup> Asphaltenes are the fraction of bitumen that is soluble in toluene and insoluble in alkanes such as n-heptane or n-pentane. By this classification, the most polar and highest molecular weight components of bitumen belong to asphaltenes in which the components still vary in composition, structure and molecular weight. In addition, the amount and composition of asphaltene

precipitated when mixing bitumen with an alkane depends on the alkane type and the alkane to bitumen ratio. Lighter alkanes can precipitate more asphaltenes than heavier alkanes for alkanes lighter than C10 and reversed after C10. For each type of alkane, higher alkane to bitumen ratio will precipitate more asphaltenes but there is a threshold at which almost all asphaltenes are precipitated out. Wang et al. found that as the volume ratio of n-heptane to heavy oil reaches 30:1 to 40:1, maximum amount of precipitated asphaltenes were be obtained.<sup>49</sup> This n-heptane to heavy oil ratio is thus generally used in asphaltene preparation and is employed in this study.

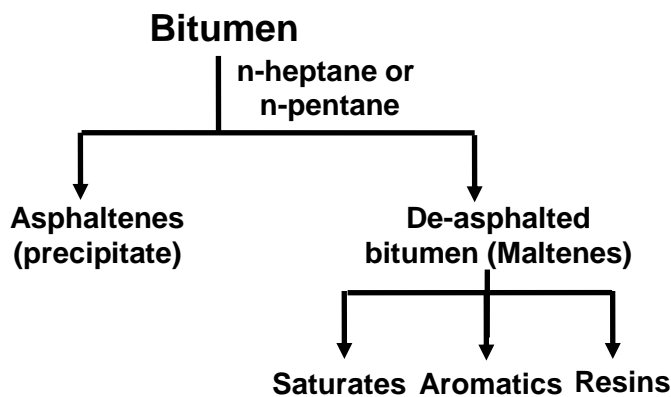


Figure 1.4. Separation of bitumen based on solubility into four classes (SARA fractionation) (Re-plotted according to reference<sup>1</sup>)

### 1.4.2 Characterization of asphaltenes

Because of the complex nature of asphaltenes, it is not practical to characterize each molecule within the asphaltenes. In fact, asphaltenes are usually treated as a pseudo-component and the average properties of all the asphaltene components are used to represent the whole asphaltenes. Although this treatment may obscure the fine differences among the components, it is still a convenient and workable way to deal with asphaltenes. Several techniques have been applied to

characterize asphaltenes and extensive information about asphaltenes has been obtained.<sup>50-56</sup> The following sections will give a brief introduction of asphaltenes in terms of elemental composition, structure and molecular weight.

#### 1.4.2.1 Chemical composition of asphaltenes

Chemically, asphaltenes are a mixture of hydrocarbons which contain heteroatoms (N, S, O, etc.) as well as some transition metals (vanadium and nickel).<sup>20</sup> Table 1.2 lists the elemental composition of Athabasca bitumen and the corresponding asphaltenes used in this study. Asphaltenes contain the heaviest components of bitumen and have a much lower H/C ratio. The aromaticity of Athabasca asphaltenes, for example, is about 0.5.<sup>57</sup> The content of heteroatoms (e.g., N, S, and O) of asphaltenes is also much higher than that of bitumen. These heteroatoms are electron deficient and make asphaltenes more polar. It was also reported extensively that asphaltenes contain most of the transition metals (V and Ni) which exist mainly in the form of porphyrin.<sup>58</sup>

Table 1.2. Elemental composition of bitumen and asphaltenes precipitated with n-heptane

Element	Carbon	Hydrogen	Nitrogen	Sulfur	Oxygen	H/C
Asphaltenes, wt%	80.8	7.8	1.2	8.8	1.4 <sup>57</sup>	1.15
Bitumen, wt%	83.1	10.6	0.4	4.8	1.1	1.53

Note: Bitumen sample was provided by Syncrude. Data of bitumen are from Speight, 1991.<sup>59</sup>

Due to the complex nature of asphaltenes, efforts have been made by some researchers to separate asphaltenes into subfractions and study the compositional and structural differences of these subfractions.<sup>22, 34, 57, 60-66</sup> These studies demonstrated that, depending on the subfractionation methods, the aromaticity, polarity and molecular size might be different for each asphaltene subfraction.

The subfractions can behave differently in terms of interfacial tension reduction and ability to aggregate and to stabilize water/oil emulsions. Therefore, further subfractionation of asphaltenes is necessary to get more details of asphaltene composition.

#### **1.4.2.2 Structure of asphaltene molecules**

The structure and functional groups of asphaltenes have been characterized by various analytical techniques.<sup>50-56</sup> Basically, asphaltenes are multi-hydrocarbons composed of fused aromatic sheets inter-connected by linear or cyclic alkanes and heteroatoms.<sup>50, 67, 68</sup> X-Ray diffraction was used to study the structure of asphaltene in solid state and detected that the aromatic rings could stack in a few layers through  $\pi$ - $\pi$  interaction to form condensed aromatic sheet.<sup>69</sup> However, packing of aromatic sheets was loosened by the aliphatic chains.<sup>50</sup>

Infrared spectroscopy (IR) and other techniques were applied to investigate the functional groups in asphaltenes.<sup>51, 56</sup> It was revealed that the oxygen-contained groups are mainly carbonyl, carboxylic and hydroxylic.<sup>10, 70</sup> It is suggested that the condensed aromatic sheets are interconnected by sulfide, ether, aliphatic chains, or naphthenic ring linkages and heterocyclic atoms (O, N, S); while the transition metals (vanadium, nickel, iron) mainly exist in the form of porphyrin by chelate or coordinate bonds.<sup>20, 58</sup>

Since asphaltenes by definition is a complex mixture of components, these analytical results of asphaltenes only represent the “average” structural characteristics of asphaltenes. Nonetheless, some researchers have tried to establish a model molecular structure of asphaltenes. Basically, two model



structures were proposed: the continental and the archipelago models.<sup>38, 71-78</sup> The continental model assumes asphaltene molecule to be a large condensed poly-aromatic ring with aliphatic chains in the periphery. The archipelago model contains several poly-aromatic rings connected by aliphatic chains or heteroatoms.<sup>72, 79</sup> Both models achieved certain success in explaining some asphaltene properties but neither is an all-around model. For example, as stated by Mullins,<sup>80</sup> the continental model corresponds well to an asphaltene molecular weight of ~750 g/mol while the archipelago model conflicts with this molecular weight. However, the archipelago model is successful in illustrating the polymeric properties of asphaltenes as observed by some researchers.<sup>78</sup>

The molecular weight of asphaltenes has been a controversy for many years.<sup>66, 81-85</sup> Results measured by vapor pressure osmometry (VPO) or gel permeation chromatography (GPC) indicate that the molecular weight of asphaltenes varied from a few hundred Daltons to more than ten thousand Daltons, depending on the analytical techniques, solvent, temperature and the concentration of asphaltene solution.<sup>16, 32</sup> The wide range of the molecular weight of asphaltenes is not unexpected when recognizing the polydispersity of asphaltene components. However, the results were made more obscure when considering the self-association and aggregation of asphaltenes in solvents. The association state of asphaltenes is closely related to the solution condition (e.g., solvency, temperature, pressure) as well as existence of solids and water. The following text will be devoted to the illustration of asphaltene properties in the bulk oil phase and at interfaces.

### **1.4.3 Properties of asphaltenes and effect on oil sands processing**

The characterization of asphaltenes in solid state gives us valuable information about the chemistry and structure of asphaltenes. However, properties of asphaltenes in an organic medium are more relevant to the industrial operations. For asphaltenes in solution, two distinct properties are usually stated: 1) the tendency to self-associate/aggregate in solvents; and 2) the interfacial activity by accumulating at water/oil and solid/oil interfaces. Asphaltenes' tendency to aggregate is closely related to their molecular structure since large fused aromatic sheet can stack together through  $\pi$ - $\pi$  plus acid-base interactions. The amphiphilic nature of asphaltene molecules determined that they are active at interfaces. Due to the close relevance of these properties to industrial operations, many investigations have been carried out to understand the aggregation, flocculation and precipitation of asphaltenes in solution as well as to explore the adsorption of asphaltenes at water-oil interface and on solid surfaces.

#### **1.4.3.1 Self-association and aggregation**

The experimental techniques used to understand the mechanisms of asphaltene self-association and aggregation include surface tension measurements,<sup>82, 86</sup> titration calorimetry,<sup>33, 87</sup> near-infrared spectroscopy,<sup>88</sup> small angle neutron scattering (SANS),<sup>89-92</sup> dynamic light scattering (DLS),<sup>16</sup> conductivity measurement<sup>16</sup> and more complicated techniques.<sup>93</sup> Theoretically, molecular simulation was also employed to explore the aggregation behavior in the molecular level.<sup>24, 35-38</sup> It is generally accepted that asphaltenes associate in solutions through  $\pi$ - $\pi$  stacking, hydrogen bonding and acid-base interactions,

giving rise to more or less extended aggregates. The aggregation depends on solvent, concentration, temperature, pressure, and dispersing and flocculating agents. Good solvents of asphaltenes will reduce aggregate size.<sup>91, 92</sup> In toluene, asphaltenes start to associate at a concentration of about 50 mg/L and form nanoaggregates above 100 mg/L.<sup>94-97</sup> The molecular weight of asphaltenes measured by SANS are therefore affected by asphaltene concentration and solvent quality.<sup>91</sup> Temperature may affect asphaltene aggregation and flocculation. Asphaltene aggregates become larger when temperature decreases,<sup>90</sup> and vice versa.<sup>67, 89, 92</sup> The effect of pressure on asphaltene precipitation/aggregation is much less significant than that of temperature. It was reported that pressure has only minor effect on asphaltene aggregation in toluene.<sup>67, 98</sup> Aggregation of asphaltene also depends on the presence of dispersants and flocculants. Resins are believed to be able to solvate asphaltenes, reduce the aggregate size<sup>99</sup> and stabilize asphaltenes in solvents.<sup>21, 100</sup> Dissolution of resins from the outer-layer of asphaltene aggregates into alkanes enhances asphaltene agglomeration.<sup>101, 102</sup> Natural surfactants in crude oil such as naphthenics were shown to be able to stabilize asphaltenes.<sup>103</sup> Inhibitors and dispersants have been explored to enhance asphaltene stabilization and proved to be effective in various extent.<sup>86, 102, 104</sup> Water can enhance asphaltene aggregation in solution by strengthening hydrogen bonding.<sup>24, 105</sup> Asphaltenes can bind with molecular water by polar groups<sup>106</sup> and even the effect of trace amount of water on asphaltene association can not be neglected.<sup>87</sup>

Despite numerous studies of asphaltene aggregation, there are still no agreement on the aggregation mechanism and process. Various models about aggregation have been suggested. Generally, these models can be classified into two classes: the “colloidal model” and the “polymeric model”. The “colloidal model” originated from the amphiphilic nature of asphaltenes, which suggests that asphaltenes form micelle-like aggregates resembling that of surfactants, with the relative polar parts (aromatic groups, heteroatoms) inside while the apolar parts (aliphatic side chains) outside. Similar to the critical micelle concentration (CMC) of surfactants, it has been suggested that a critical micelle or aggregation concentration (CMC or CAC) also exists for asphaltene solution. Above the CMC or CAC, asphaltenes can be viewed as colloidal particles suspended in the bulk oil phase. The colloidal nanoaggregates agree with Yen’s model<sup>97</sup> in which the fused aromatic sheets of several asphaltene molecules are packed together, and the aliphatic side chains are mostly located at the periphery of the aggregates. The “colloidal model” is in agreement with the observation of CMC or CAC of asphaltene solutions.<sup>34, 86, 101, 107-110</sup> For example, through surface tension measurements, Sheu et al.<sup>111</sup> found a threshold solution concentration above which surface tension does not change. Also using the “colloidal model”, Rogel successfully predicted asphaltene aggregations in different solvents.<sup>109</sup> However, Rogel also pointed out that for asphaltenes with low aromaticity the CMC does not exist, which indicates that the chemistry of asphaltenes affect their aggregation. In fact, some researchers did not find a CMC or CAC for asphaltene solution.<sup>33, 69, 112</sup> For these cases, it was suggested that asphaltene association

occur in a stepwise manner and an aggregation model similar to that of polymerization was suggested.<sup>32, 33, 69, 87, 112-114</sup> For example, Agrawala and Yarranton proposed that asphaltene molecules associate with each other through linear inter-molecular binding.<sup>113</sup> In their work, resins can block the binding sites on asphaltenes and therefore can stop the process of asphaltene aggregation. The authors also showed that the “polymeric model” can be successfully used to explain the apparent molecular weight of asphaltenes with the existence of resins. Using single molecule force spectroscopy, Long et al. detected a chain-like aggregates of Athabasca asphaltenes.<sup>78</sup>

In addition to the discrepancy about the nature of asphaltene aggregation in solvents, the aggregate structure (aggregate shape, size, etc.) is also under debate. Such structures as chain-like aggregates,<sup>78</sup> membrane-like particle to fractal structure,<sup>92</sup> fractal structure<sup>99, 115, 116</sup> and cylindrical aggregate<sup>109</sup> have been reported. For example, using X-ray scattering (SAXR) and X-ray diffraction techniques, Ryuzo Tanaka et al.<sup>69</sup> portrayed aggregates to be a hypothetical hierarchical model. By fractal structure study, Liu et al.<sup>115</sup> stated that asphaltene aggregates are polydisperse fractal objects composed of asphaltene micelles. While atomic force microscopy (AFM) imaging measurements showed that asphaltene aggregates are like discoids or long rods with disk-shape heads.<sup>57, 117</sup> Such controversies are partially due to the complexity of asphaltene components from which multiple aggregate structures might be formed. The high polydispersity of asphaltene aggregates also makes it difficult to determine the

aggregate size.<sup>118</sup> For example, two size regimes of aggregates have been reported.<sup>90, 93</sup>

Asphaltene aggregation makes characterization of asphaltenes in solution difficult since the system might contain both monomers and aggregates. An obvious example is the controversy about the molecular weight of asphaltenes. Data of very broad range of asphaltene molecular weight, from a few hundred to tens of thousands Dalton, have been reported.<sup>66, 81-85</sup>

#### **1.4.3.2 Flocculation and precipitation**

Asphaltene aggregation is the initial step towards precipitation. In unfavorable environment, asphaltene aggregates will flocculate to form larger clusters and precipitate out of the solution. Although asphaltene aggregation is through strong specific interactions such as  $\pi$ - $\pi$  stacking, hydrogen bonding and acid-base interactions, the driving forces for flocculation of asphaltenes are reported to be mostly due to dispersion forces, e.g., van der Waals forces.<sup>86, 119-123</sup> Titration experiment is usually carried out to test the crude oil stability, in which a precipitant, usually n-alkane, is added to the oil until asphaltenes will precipitate out at a certain dilution ratio.<sup>49, 124</sup> To determine the onset of asphaltene precipitate from a solution, techniques of nuclear magnetic resonance (NMR),<sup>125</sup> near-infrared (NIR) spectroscopy,<sup>31</sup> dynamic light scattering (DLS),<sup>67</sup> x-ray (SAXS)<sup>67</sup> and neutron scattering (SANS)<sup>67</sup> are generally employed. Asphaltene precipitation depends on solvent, temperature and pressure. Aromaticity of the solvents directly affects asphaltene stability. Increasing temperature can increase

the solubility of asphaltenes and therefore reduce their amount precipitated.<sup>21, 98</sup> Depressurization of crude oil can also induce asphaltene precipitation.<sup>31, 101</sup> Asphaltene precipitation can cause serious problems during crude oil production, e.g., well bore and pipeline plugging and equipment fouling.<sup>31</sup> Motivated by the impacts on industrial operations, many studies have been devoted to answering these questions: How do asphaltene flocculation and precipitation develop with variation of the organic medium? How to predict the incipient of asphaltene precipitation and the amount precipitated? There are two main approaches that have been developed to theoretically predict asphaltene precipitation. The first approach is through the pressure-volume-temperature (PVT) calculation by equation of state.<sup>126-130</sup> For example, using Peng-Robinson equation of state, Sabbagh et al. successfully predicted the onset point of asphaltene in solution and the amount of asphaltenes precipitated.<sup>128</sup> The second approach is by measuring the refractive index (RI) of the oil mixture.<sup>100, 119, 131, 132</sup> This method is based on the assumption that the dominant driving forces for asphaltene precipitation are the London dispersion forces.<sup>119</sup> Using the RI method, Buckley was able to predict the onset of asphaltene precipitation in solutions with varying concentrations.<sup>132</sup> An variation of the RI approach is based on the solution theory of polymers, e.g., the Flory-Huggins theory.<sup>49, 133-136</sup> For example, by dissolving bitumen in a variety of solvents with solubility parameters from 3.2 to 6.9  $\text{dyn}\cdot\text{mol}^{1/3}\text{cm}^{1/2}$ , Mitchell and Speight found that there is a linear relationship between the solvent solubility parameter with the amount of asphaltene precipitated out, with more asphaltenes precipitated out in solvents with lower

solubility parameter.<sup>137</sup> Through a 2-D mapping of the solubility parameters of heavy oil, Wiehe<sup>138</sup> found that the insolubility of asphaltenes are mainly due to the high aromaticity and high molecular weight of asphaltene molecules, and are less likely dominated by polar and hydrogen bonding interactions. The reported solubility parameter for asphaltenes by different researchers is mostly in the range of 16 to 21 (MPa)<sup>1/2</sup>, depending on the chemistry and source of asphaltenes.<sup>139-141</sup> Other models have been developed and demonstrate some success in predicting asphaltene precipitation.<sup>21, 142</sup> For example, using a solubility model extended from polymer solution, Mannistu et al. were able to predict the precipitation of asphaltene fractions from mixed solvents.<sup>143</sup>

Although the methods mentioned above have achieved certain success in predicting asphaltene precipitation, none of them have provided the quantitative information of the interactions between asphaltenes. In fact, these methods assumed that dispersion forces are the dominant forces for asphaltene precipitation. The quantitative determination of the interactions between asphaltenes is still needed.

#### **1.4.3.3 Interfacial activity**

Many asphaltene molecules are amphiphilic and they tend to accumulate at water/oil and solid/oil interfaces. The stability of the water droplets and the bi-wettability and oil-wettability of the solids are to a large extent due to asphaltene adsorption.<sup>6, 8, 10, 11, 16, 17, 144</sup> The adsorption of asphaltenes at the interface is irreversible.<sup>145</sup> The water droplets and solids having an asphaltene-coated exterior can stably disperse in an organic medium that is a good solvent for asphaltenes.



A thorough understanding of the asphaltene structure at the water/oil and solid/oil interfaces is important for successfully breaking water-in-oil emulsions. It has been accepted that upon adsorption at the water/oil interface, asphaltenes form a cross-linked, viscoelastic network which stabilizes the water-in-oil emulsions by sterically preventing the coalescence of water droplets.<sup>10, 145-147</sup> Polar interactions such as hydrogen bonding and acid-base interactions are believed to involve in the formation of the interfacial net-work structure of asphaltenes.<sup>10, 148</sup> Kinetic studies revealed that asphaltenes adsorbed at the water/oil interfaces have a long process of reorganization which may help the formation of the stable interfacial film structure.<sup>149</sup> Experimental studies<sup>150</sup> and molecular simulation<sup>24</sup> found that water can enhance asphaltene aggregation at water/oil interface by bridging H-bonds, providing additional strength for the interfacial films at water/oil interfaces. The rheological properties of the interfacial film have also been studied by various techniques, such as micropipette technique,<sup>151, 152</sup> Langmuir trough,<sup>150</sup> pendant-drop oscillation,<sup>153, 154</sup> atomic force microscopy (AFM)<sup>150</sup> and surface/interfacial tension measurements.<sup>155-158</sup> It was found that asphaltene molecules form a viscoelastic film of 2 to 9 nm at toluene/water interfaces.<sup>12, 146</sup> AFM imaging revealed the presence of asphaltene nanoaggregates in size of 20-50 nm in the interfacial films.<sup>150</sup>

To break water-in-oil emulsions, a demulsifier must be able to weaken the strength of the interfacial film through interacting with the interfacial materials<sup>158</sup> or by displacing them,<sup>155, 159, 160</sup> Upon weakening of the interfacial film, water

droplets will coalesce. For example, demulsifiers can reduce the rigidity of the interfacial film<sup>161, 162</sup> and lower the interfacial tension.<sup>157, 163</sup>

In heavy oil processing, solids such as clays play an important role in stabilizing water-in-oil emulsions<sup>6, 157, 164, 165</sup> and in the formation of rag layer.<sup>4, 5, 25, 26</sup> These solids are rendered oil-wet or bi-wettable due to adsorption of organic materials.<sup>7, 8, 27, 166</sup> Microbalance adsorption experiments (QCM-D) revealed that asphaltenes have a high affinity to hydrophilic surfaces<sup>167</sup> and the adsorption of asphaltenes on hydrophilic surfaces is almost irreversible.<sup>168</sup> The problematic solids in heavy oil processing are mostly fine aluminosilicate clay particles with a diameter from sub-microns to a few microns.<sup>7, 9</sup> The clay particles are originally hydrophilic but due to adsorption of “asphaltene-like” organic materials their surface become oil-wet or bi-wettable.<sup>8, 9, 27</sup>

The wettability of solids has great effect on bitumen recovery and froth quality in oil sands processing.<sup>28, 166</sup> Due to their extremely small size, the organic rich solids cannot be completely removed by mechanical techniques, e.g., centrifugation. Similar to the demulsification of water-in-oil emulsions by demulsifiers, chemical treatment of the organic-contaminated solids to make their surface more water wet (hydrophilic) is a possible approach to solving the problems caused by these solids. To the best of our knowledge, up to now, few studies have been conducted in this area.

## **1.5 Outline of thesis**

This thesis consists of six chapters.

Chapter 1: This chapter provides the background of this study. The hot-water bitumen extraction and the bitumen froth treatment processes are briefly introduced. By comparing the two froth treatment processes: the naphtha-based and paraffin-based processes, the objectives of this work are introduced. Previous work on asphaltenes in the scope of oil sands and heavy oil processing is reviewed.

Chapter 2: The materials and equipments used in this study are described in this chapter. The fundamentals and operation procedures of the experimental work, especially the atomic force microscopy (AFM) colloidal force measurement are provided.

Chapter 3: In this chapter, the results on interaction forces between asphaltene surfaces in toluene are presented. The effects of temperature, water content in solvent and asphaltene surface preparation methods on measured interaction forces are investigated. The nature of the interaction forces is described.

Chapter 4: This chapter focuses on the effect of solvent aromaticity on interaction forces of asphaltene films. The nature of the force in good and poor solvents is illustrated.

Chapter 5: This chapter explores the possibility of using an effective demulsifier for water-in-oil emulsions, i.e., ethyl cellulose, to modify the surface hydrophobicity of the asphaltene- and bitumen-contaminated solids. This part of work intends to open a way for using chemical modifiers to alleviate the rag layer formation during oil sands processing.

Chapter 6: The overall conclusions, the major contributions of this work and suggestions for future work are outlined in this chapter.

## Chapter 2 Materials and Experimental Techniques

### 2.1 Materials and chemicals

Asphaltenes used in this work were extracted from vacuum distillation feed bitumen (provided by Syncrude Canada Ltd.). First, bitumen was diluted with HPLC-grade toluene at a toluene to bitumen volume ratio of 5 to 1. The toluene-diluted bitumen was centrifuged at 20,000 rpm (35,000 g) for 30 minutes to remove contained fine solids (account for about 0.8 wt% of the vacuum feed bitumen). Toluene was then allowed to evaporate from the diluted-bitumen in a well-ventilated clean fume hood to obtain “solvent-free” bitumen. Subsequently, technical grade *n*-heptane was added to the “solvent-free” bitumen at an *n*-heptane to bitumen volume ratio of 40 to 1. The *n*-heptane and bitumen mixture was shaken for 2 hours on a horizontal shaker (Fisher Scientific Canada) operating at 250 cycles/min with an amplitude of 3.5 cm. The mixture was then left overnight for asphaltenes to precipitate. The precipitated asphaltenes were washed with excess amount (1 L) of *n*-heptane to remove co-precipitated maltenes. To do the washing, the mixture of asphaltenes and heptane was shaken on the shaker for 2 hours and left overnight for asphaltenes precipitation. The washing with *n*-heptane was repeated until the supernatant became colorless. The last two washings were performed using HPLC grade *n*-heptane. After the last wash, the asphaltene precipitate was left in a fume hood for 3 days to ensure a complete evaporation of *n*-heptane. The dried asphaltenes account for about 11 wt% of the original bitumen. The general characteristics of the asphaltenes, such

as chemical composition, molecular weight, density and interfacial property were described in Chapter 1 and more details were reported by Zhang et al.<sup>57</sup>

Ethyl cellulose (EC) purchased from Sigma-Aldrich was used as received. The ethoxyl content of EC used in this study was 48% and the molecular weight, determined by intrinsic viscosity measurement, was 46 kDa.<sup>169</sup>

Milli-Q water with a resistivity of 18.2 M $\Omega$ ·cm, prepared with an Elix 5 system followed by purification with a Millipore-UV plus system, was used throughout the experiments. HPLC grade toluene and *n*-heptane, purchased from Fisher Scientific, were used as the solvent.

Silica microspheres ( $\sim 8 \mu\text{m}$ ), purchased from Duke Scientific Co., USA, were used to prepare asphaltene probes in the AFM force measurements. A two-component epoxy (EP2LV, Master Bound, Hackensack, NJ, USA) was used to glue the silica sphere to the tip of AFM cantilevers. Kalrez o-ring (Cole Parmer) was used during AFM force measurements in solvents.

Silica wafers with one side polished were purchased from NanoFab (University of Alberta, Canada) and used as the substrates for immobilizing asphaltenes used in AFM force measurements and imaging. Prior to their use, the silica wafers were cut into 1.5 by 1.5 cm square pieces and cleaned in a 70 vol% sulfuric acid mixed with 30 vol% hydrogen peroxide solution at 85 °C for 25 minutes followed by a thorough washing with Milli-Q water. Alumina wafers (University wafer, Massachusetts, USA) of C-plane were used as the model solids to represent one of building blocks of clays. For cleaning, the alumina wafers were immersed in the sulphuric acid for 10 minutes to remove organic contaminants, followed by

thorough washing with Milli-Q water and blow-drying with nitrogen. The alumina wafers were then exposed to UV radiation in air (Bioforce Nanosciences, US) for 10 minutes. The silica and alumina surfaces cleaned as such are hydrophilic with contact angle of water drops less than  $10^\circ$  as measured by DSA100 (Krüss, Germany).

## **2.2 Atomic force microscopy (AFM)**

### **2.2.1 Fundamentals of AFM**

AFM is one type of scanning probe microscopes used to image and measure properties of solid surfaces.<sup>170</sup> Its development stemmed from the success of scanning tunneling microscope (STM), which was invented by Gerd Binnig and Heinrich Rohrer in 1982.<sup>171</sup> AFM was developed by Binnig et al. in 1986 to extend the concepts of the scanning tunneling microscopy techniques to the non-conducting materials.<sup>172</sup> The resolution of AFM imaging can go down to nano or sub-nano scale (atomic resolution) and forces in the order of a pico-Newton ( $10^{-12}$  N) can be detected by AFM.

As shown in Figure 2.1, the major components of AFM include a piezo scanner, a probe (a cantilever with a sharp tip), a laser beam source, a split photodiode and a feedback loop system. When the probe is brought to approach the sample surface, the interactions between the tip surface of the probe and the sample surface will cause the cantilever to bend up or down, depending on whether the force is repulsive or attractive. The deflection of the cantilever is monitored by a laser beam focused on the back of the cantilever tip. The reflected laser is directed to split photodiodes where the intensity of light signal is converted to a voltage. The

voltage signal is input to a feedback loop which compares the new input with the setpoint value (a certain voltage value corresponding to a certain deflection of the cantilever) and generates error signals. The error signals are processed by the controller electronics and fed to the scanner. The scanner then adjusts the movement of the sample to remain a constant separation between the tip and the sample.

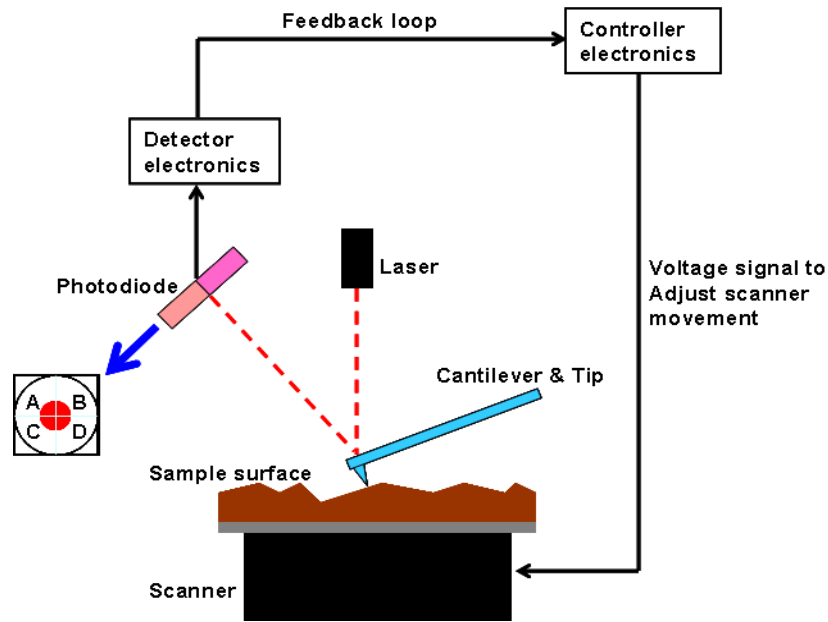


Figure 2.1. Schematic of AFM working mechanisms

A sample surface usually has bumps and depressions. When scanning the sample surface with a sharp tip, the frequent adjustment of the AFM sample surface to maintain a constant tip-sample separation can generate a 3-D mapping of the topography of the sample surface, which is the basic mechanism for AFM imaging.

Since its first development, AFM has been improved continuously to extend its applications to various systems for measuring various physicochemical,



mechanical and electrochemical properties.<sup>170, 173-177</sup> An obvious advantage of AFM imaging is that it can be performed in a liquid environment, which is quite useful for bio-systems. For example, such materials as bio-molecules, bio-membranes and cells can be imaged in their natural medium without denaturing them during sample preparation.<sup>178</sup>

### 2.2.2 Surface force measurement by AFM

By keeping the movement of the tip only in the vertical direction (Figure 2.1), the interactions between the tip surface and the sample surface as a function of the separation distance between them can be obtained (Figure 2.2). Basically, two types of forces can be acquired: the long-range force when the two surfaces approach each other and the adhesion force when they separate after contact. From force measurements by AFM, two types of colloidal behaviors between the interacting bodies can be predicted: the coagulation behavior (long-range force) and the flocculation/coalescence tendency (adhesion force).

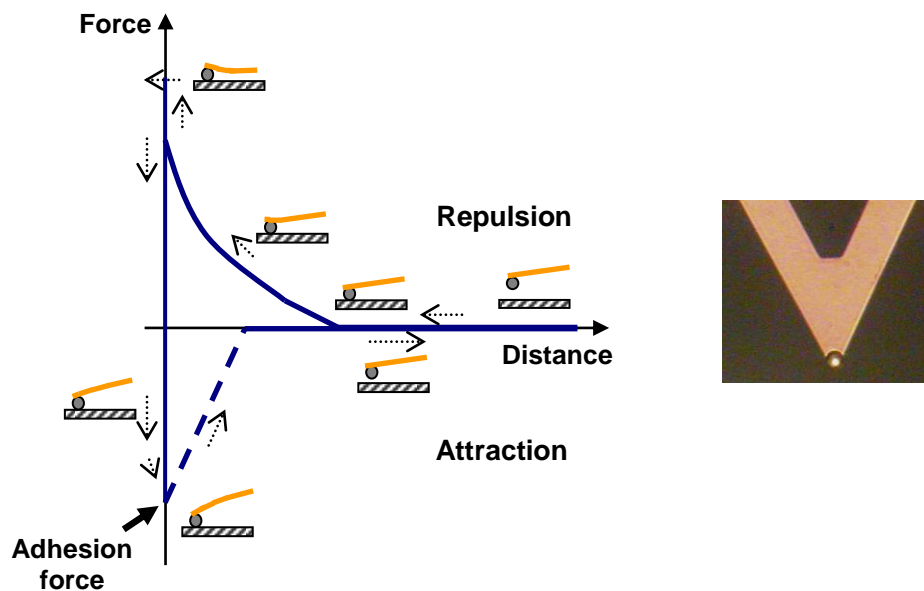


Figure 2.2. AFM force profile and a colloidal probe attached cantilever

Through modifying the sharpness and the chemistry of the tip, AFM offers various possibilities in force measurement. An AFM tip usually has a radius of a few to a few tens of nanometers. Such a small tip scale enables AFM to probe the local interactions between the tip and a sample surface, providing the possibility of differentiating the surface heterogeneity.<sup>179-181</sup> A sharp tip has been used in a technique called single molecular force spectroscopy (SMFS). In a SMFS force measurement event, the tip adheres to and picks up a single macromolecule from the sample surface, during which process the molecule is stretched or unfolded until it detaches from the sample surface. Through the force-distance profile of the stretching process, the structure of the macromolecule can be determined. SMFS has been used in studying the structures of bio-macromolecules or polymers.<sup>78, 182-184</sup> If a tip is chemically modified with a special functional group, it is even possible to detect a specific binding event between the functional group on the tip and that on the sample surface, e.g., antibody-antigen interactions, which provides chemical and structural information of the sample surface.<sup>185-187</sup>

The most general application of AFM force measurement technique is the colloidal technique developed by Ducker et al.,<sup>41</sup> in which the forces between a colloidal particle and a flat surface is determined. Based on this technique, interactions between any materials can be measured if the material of interest can be coated to the colloidal particle and the flat surface. For example, the interactions of two polymer brushes can be measured by grafting the polymer to the particle and the flat surface. During AFM force measurements, the total forces between the colloidal probe and the flat sample surface are obtained when they

approach and retract from each other. However, in separate force measurement events, the radii of the probes are not necessarily the same, giving different total forces for the same system. It is thus necessary to normalize the force obtained at different force measurement events for the purpose of comparison. According to the Derjaguin approximation, the total interaction force between a flat surface and a sphere with radii of  $R$ ,  $F(D')$ , is related to the interaction energy between two parallel flat plates per unit area by the following formula:<sup>188</sup>

$$F(D') = 2\pi R \cdot E(D') \quad (2-1a)$$

where  $E(D')$  is the interaction energy between two parallel flat plates per unit area;  $D'$  is the separation distance between the two solid surfaces.

Equation (2-1a) can be re-written in the following form:

$$\frac{F(D')}{R} = 2\pi \cdot E(D') \quad (2-1b)$$

The right hand side of equation (2-1b) is independent of any geometric effect of the interacting bodies. Therefore forces measured by AFM are normalized by dividing the force with the radius of the colloidal particle,  $R$ .

### **2.2.3 Issues with AFM force measurement in organic solvents**

AFM force measurements are usually carried out in liquid, either aqueous or non-aqueous. In aqueous environment, the measurements have obtained results consistent with the predictions of DLVO theory.<sup>41, 47, 48</sup> However, in nonaqueous environment, or organic medium, the electrostatic double layer cannot be effectively established due to the low dielectric constant of organic solvents. The forces occurred in organic medium are usually attributed to structure forces, such

as steric repulsion between two polymer brushes in good solvents.<sup>189-191</sup> Force measurements in nonaqueous systems are very important for determining the stability of suspensions dispersed in organic solvents with the help of oil-soluble dispersant, especially polymers.

Although there are many studies of AFM force measurements in aqueous systems, less attention has been devoted to nonaqueous system. Most of the reported force measurements in organic system were performed using SFA,<sup>189-191</sup> while the colloidal probe technique of AFM force measurement was seldom used. This is partly because, by and large, the commercial AFM is not specifically designed for nonaqueous system. As shown in Figure 2.3, for force measurement in organic solvents, the accessories such as o-ring, tubing and fluid cell should all be chemically and mechanically resistant to the solvents. However, materials with certain elasticity appropriate to be used as o-rings generally swell in organics and cause leaking problems. Fast evaporation of organics at the leaking point can generate air bubbles inside the fluid cell and disturb the force measurements. From our preliminary AFM measurements of forces between silica surfaces in toluene, we noticed that contamination may lead to very misleading results due to strong solvency of organic solvents (Figure 2.4). In general, AFM force measurements performed in organic system is not as convenient as those in aqueous system; much care should be taken in carrying out the experiments and in explaining the measured forces. Only by using appropriate accessories and taking great care can trust-worthy results be obtained (Figures 2.3 & 2.4).

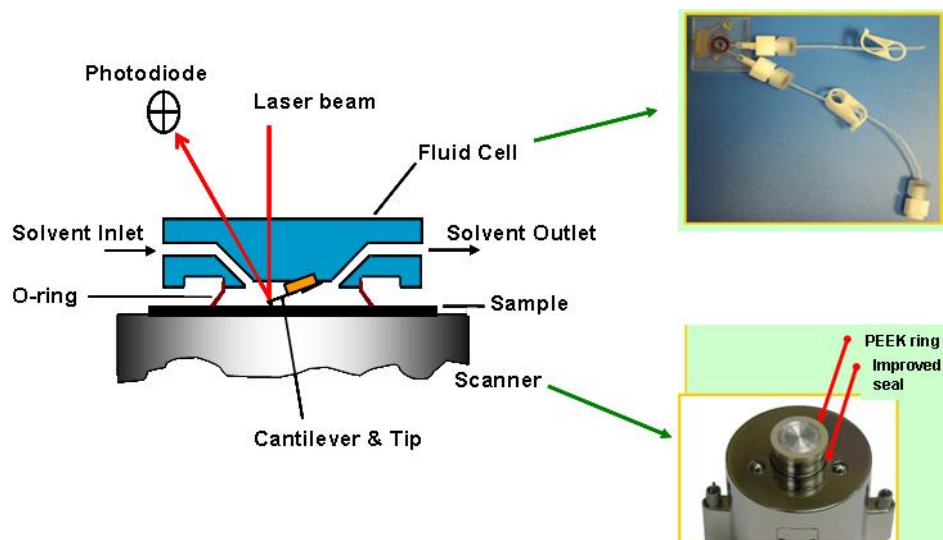


Figure 2.3. AFM force measurement setup (Figure re-plotted from Veeco Co.)

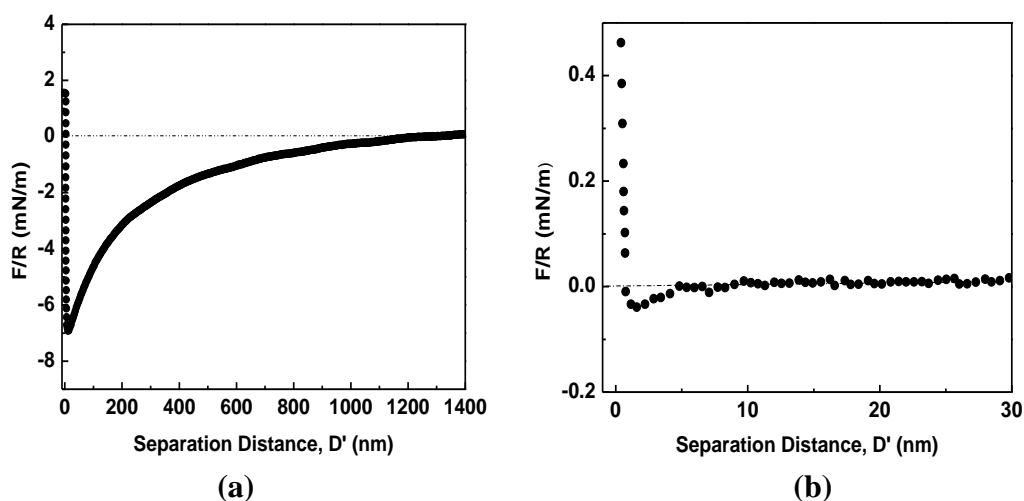


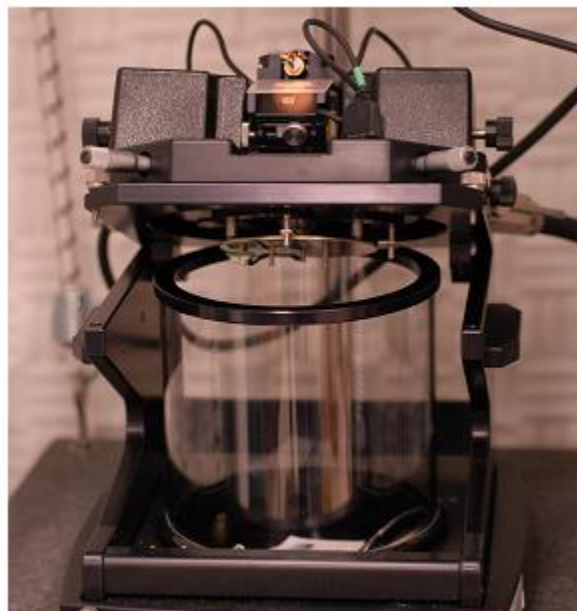
Figure 2.4. Forces between silica surfaces in toluene measured by AFM. (a) Silicone tubing was used (strong attraction is due to contamination caused by dissolution of silicone tubing); (b) Kalrez tubing was used (weak attraction is the van der Waals force in toluene)

## 2.2.4 AFM used in this work

A Nanoscope Multimode AFM (Digital Instrument, Santa Barbara, CA, USA) was used to measure the surface forces between asphaltenes in organic solvents (Figure 2.5a). Agilent 5500 AFM (Agilent Technologies, Inc., Chandler, AZ) was used to obtain the images of any sample surfaces (Figure 2.5b).



(a)



(b)

Figure 2.5. AFMs used in this work. (a) Nanoscope Multimode (Veeco Co.); (b) Agilent 5500 (Agilent Technologies)

### 2.2.5 Typical setup of AFM force measurement

The flat sample, e.g., the asphaltene-coated silica wafer, was glued onto a magnetic puck which was mounted on the piezoelectric translation stage of the AFM scanner. The AFM cantilever substrate with an asphaltene-coated microsphere attached to the short, wide beam spring (nominal spring constant 0.58 mN/m) was mounted on the holder in the liquid cell. The liquid cell was mounted on top of the sample surface and was well sealed with a Kalrez o-ring. Toluene was injected into the liquid cell slowly and the system was allowed to equilibrate for 15 minutes before any force measurement was initiated. To ensure a representative force profile, force measurements were carried out at a number of different locations on the flat asphaltene sample surface for a given pair of asphaltene-coated wafer and asphaltene-coated microsphere, with at least two

independent asphaltene-asphaltene pairs used. All the AFM force measurements were carried out at room temperature ( $20 \pm 0.5$  °C).

### **2.2.6 Typical setup of AFM imaging**

AFM topographical images of the sample surfaces were obtained using an Agilent 5500 AFM (Agilent Technologies, Inc., Chandler, AZ) operated under acoustic AC mode in air. Silica cantilevers (RTESP, Veeco, Santa Barbara, CA) with a nominal resonance frequency of 200-300 kHz were used for imaging. During the imaging, the amplitude setpoint ( $A_s$ ) was set at a value of 98% of the free amplitude ( $A_0$ ). At this ratio of  $A_s/A_0$ , the tapping force between the cantilever tip and the sample surface is small enough to avoid damaging the sample. For each sample, images were obtained at several locations and a representative image was presented. All the AFM imaging was carried out at room temperature ( $20 \pm 0.5$  °C).

### **2.3 Langmuir-Blodgett (LB) trough**

A Langmuir trough is an apparatus used to study a film formed by amphiphilic molecules at a liquid/gas or liquid/liquid interface. An amphiphilic molecule contains both hydrophobic and hydrophilic groups and tends to accumulate at the water/gas or water/oil interface to form a monolayer or multilayers. The interfacial tension of the two phases generally decreases due to the formation of an interfacial film. The LB trough allows quantitative studies of the interfacial film in respect of interfacial pressure and rheological properties.<sup>192, 193</sup> In combination with a microscopic technique, such as Brewster angle microscope, it is possible to directly observe the structure of the monolayer at the interface.<sup>194</sup>

LB trough is also an important tool in preparing and transferring a layer (or multilayers) of an interfacial film onto a solid surface. The transferred interfacial film on a solid substrate can then be analyzed using techniques such as AFM, ellipsometry and contact angle measurement. The interfacial film formed by LB trough has uniform thickness and few flaws due to ordered arrangement of the amphiphilic molecules.

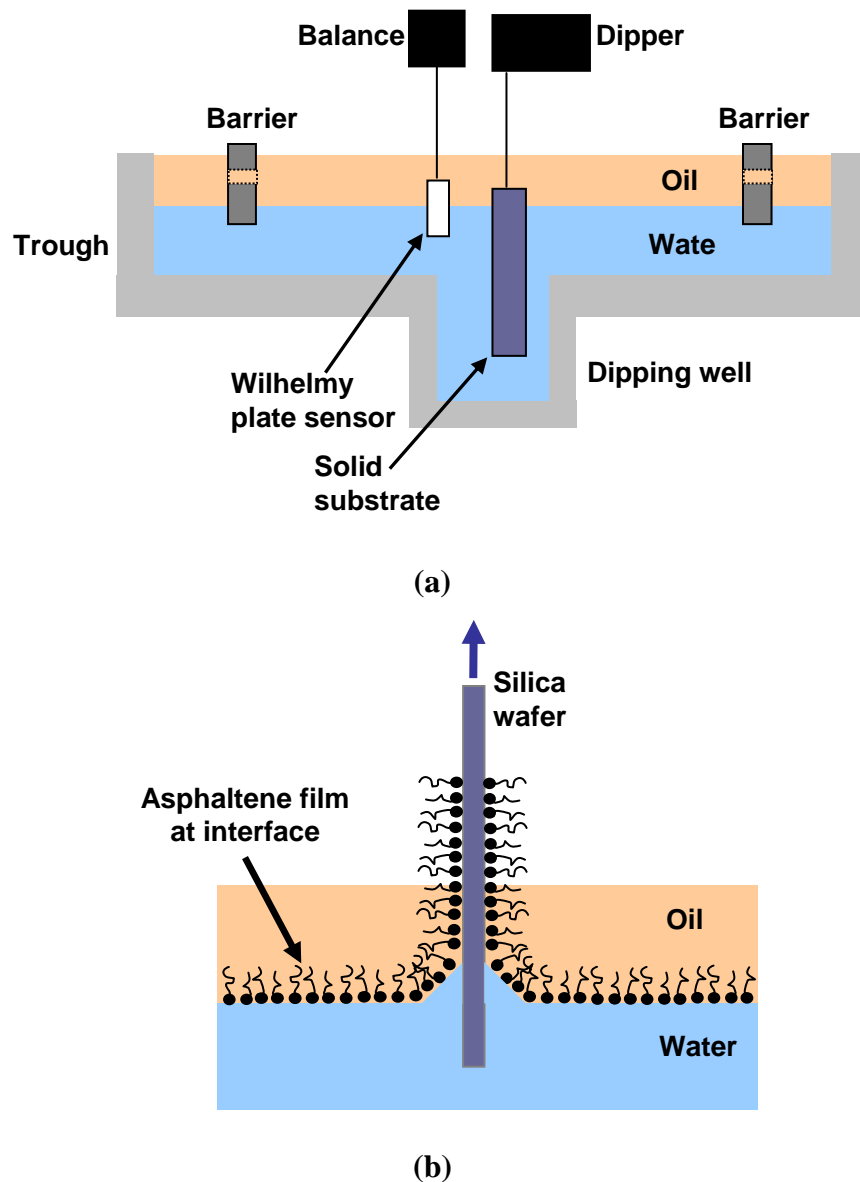


Figure 2.6. (a) Schematic of Langmuir trough; (b) Langmuir-Blodgett upstroke technique to prepare asphaltene surfaces



As shown in Figure 2.6, a LB trough is mainly composed of four parts: 1) A trough made up of Teflon to contain the liquid phase(s), allowing the formation of an interface (and interfacial film); 2) Two barriers used to control the interfacial area by compression or retraction; 3) A microbalance sensor to monitor the change of interfacial pressure due to addition of interfacial materials or change of interfacial area and 4) A dipper to control the vertical movement of a solid substrate when transferring the interfacial film onto the solid surface.

### **2.3.1 Asphaltene deposition onto silica wafer and AFM silica probe**

In this study, an asphaltene film at the toluene/water interface was prepared and transferred to a silica substrate by a KSV Mini trough (Finland). The trough has an effective film area of  $17010 \text{ mm}^2$  with a dipping well in the center. The movement of the two symmetric barriers (Delrin) is controlled by a micro step driven stepping motor. A Wilhelmy plate (made of Whatman 1 CHR filter paper) was used to measure the interfacial pressure. The dipper is controlled by a DC motor and is vibration-free. The detailed operation procedure of transferring asphaltene LB films onto a silica wafer will be explained in the text below and more details can be found in literature.<sup>57, 150</sup>

Detailed operations of preparing and transferring an asphaltene LB film are described below:

The trough and barriers were carefully cleaned; then ~120 mL Milli-Q water was poured into the trough. To test the cleanness of the water surface, the water surface area was compressed while the reading of the surface pressure was monitored. If the water surface is sufficiently clean, the variation of the surface

pressure during compression should not exceed 0.1-0.2 mN/m. Otherwise, the water surface needs to be cleaned by sucking out the contaminants on the water surface with a pipette connected to a vacuum inlet. The compression and cleaning processes were repeated until the change of surface pressure was below 0.1-0.2 mN/m. More water was added to compensate for the reduction due to cleaning. A clean silica wafer (about 25 mm in height and 10 mm in width) was placed vertically onto the holder of the dipper and immersed into the water phase using the motor control of the dipper. The silica wafer was adjusted in a position with its flat surfaces facing the two barriers. An amount of 15  $\mu\text{L}$  of asphaltene-in-toluene solution (2 mg/mL) was carefully added on the water surface by a 50  $\mu\text{L}$  gastight Hamilton syringe (Cole-Parmer). After about 10 minutes, toluene had evaporated and a layer of asphaltenes was formed on the water surface. Then about 100 mL of toluene was carefully added to the top of the water phase. To avoid disturbing the water phase, the toluene was led to flow slowly through an inclined glass rod to the step edge inside the trough. Toluene would flow from the edge and spread slowly over the whole water phase. The interface was allowed to equilibrate for 30 minutes before it was compressed at 5 mm/min to an interfacial pressure of 2 mN/m, at which the LB film was deposited onto the hydrophilic silica substrate through upstroke technique. The surface pressure was zeroed before the compression. The pulling up speed of the dipper was 5 mm/min and a transfer ratio close to 1 was usually achieved. To deposit asphaltene films onto a silica probe that was glued on an AFM cantilever, the cantilever substrate was sandwiched between two hydrophilic silica wafers by a paper clip.<sup>48</sup> Following

the procedure above an asphaltene LB film can also be deposited onto the cantilever probe. In this manner, the transfers of asphaltene films onto the flat silica substrate and onto the silica probe were accomplished in a single LB experiment, which ensured the similarity of the two asphaltene films coated on the silica substrate and silica probe. In this work, all Langmuir trough experiments were performed at a temperature of  $20\pm 0.1$  °C controlled through a circulating water bath. Figure 2.6b schematically demonstrated the process of the transferring an asphaltene film to a silica wafer.

### **2.3.2 Compression isotherms of asphaltene interfacial films**

To obtain the information about the structural change of an asphaltene film with the composition of the organic solvent, the isotherms of the asphaltene films at water-heptol (toluene plus *n*-heptane) interface were obtained by Langmuir trough compression experiments. In this set of experiments, the top phase was heptol of varying volume ratio of toluene to heptane. The procedure of preparing the asphaltene films was the same as that mentioned above. After being equilibrated for 30 minutes at a heptol/water interface, the asphaltene film was compressed with a barrier compression speed of 5 mm/min to obtain the interfacial pressure-area isotherm at each heptol composition.

### **2.4 Quartz crystal microbalance with dissipation (QCM-D)**

QCM-D (Q-sense E4 system, Sweden) is used to measure the adsorption of asphaltenes and EC on quartz crystal sensors coated with silica and alumina. The quartz crystals of 14 mm in diameter used in this study are AT-cut crystals (5 MHz) coated with silica (QSX 303) or alumina (QSX 309). A quartz crystal

sensor is a thin piezoelectric plate with gold electrodes on each side.<sup>168</sup> When an AC voltage is applied to the electrodes, the crystal oscillates at a specific resonance frequency that is highly sensitive to the total mass of the crystal. The mass adsorbed on the surface can be calculated by measuring the reduction of the sensor's resonance frequency,  $\Delta f$  in Hz. If the adsorbed layer is thin and rigid, the Sauerbrey relation is applicable. In this case, the decrease in resonance frequency is proportional to the mass adsorbed:<sup>15, 168, 195</sup>

$$\Delta m = -\frac{C \times \Delta f}{n} \quad (2-2)$$

where  $\Delta m$  is the adsorbed mass on a sensor surface in  $\text{ng}/\text{cm}^2$ ;  $n$  is the number of harmonic overtones of the crystal sensor ( $n = 1, 3, 5, \dots, 13$ ); and  $C$  is a constant of the crystal. For the 5 MHz quartz crystal sensor manufactured by Q-sense (Sweden),  $C = 17.7 \text{ ng}/(\text{Hz} \cdot \text{cm}^2)$ . This type of quartz crystal sensor was used in this study.

In addition to determining the quantity of the adsorbed mass, the QCM-D also monitors the dissipation,  $D_{qcm}$ , which is a result of energy loss due to viscous dissipation when oscillating the crystal with the adsorbed materials (equation (2-3)).

$$D_{qcm} = -\frac{E_{lost}}{2\pi E_{stored}} \quad (2-3)$$

where  $E_{lost}$  is the energy lost (dissipated) and  $E_{stored}$  is the energy stored in the oscillator during one oscillation cycle.

Shifts in  $D_{qcm}$  during adsorption provide an indication of the rigidity of the adsorbed layer. A small dissipation shift indicates a rigid and compact adsorbed

layer.<sup>196</sup> A simple correlation of the shifts in  $f$  and  $D_{qcm}$  in the form of  $\Delta D_{qcm}/\Delta f$  is generally used to determine whether the Sauerbrey relation is valid or not. As a rule of thumb, Sauerbrey relation of equation (2-2) is applicable when  $\Delta D_{qcm}/\Delta f < 0.2 \times 10^{-6}/\text{Hz}$ .<sup>197</sup> Furthermore, a plot of  $\Delta D_{qcm}$  versus  $\Delta f$  provides information about adsorption kinetics and structural changes of adsorbed layers over time, which provides a better interpretation of the frequency shift than simply mass uptake.<sup>195</sup>

Prior to each QCM-D experiment, the quartz crystal sensor is soaked in ethanol and sonicated for 10 minutes, followed by thorough rinsing with Milli-Q water and blow-drying with nitrogen. The sensor is then exposed to UV radiation in ozone for 10 minutes. The treated sensor surface has a layer of hydroxyl groups and a water contact angle of less than  $10^\circ$  as measured by DSA100 (Krüss, Germany). Since the experiments are carried out in toluene, the solvent-resistant Kalrez o-rings and gaskets, and GORE pump tubing (100CR) are used.

#### **2.4.1 Adsorption of asphaltenes and EC on silica surface**

The QCM-D experimental setup is shown in Figure 2.7. At each start of a QCM-D experiment, a clean crystal sensor was carefully inserted in the flow module with the active surface facing the testing solutions. The flow module was mounted on the chamber platform and the toluene solution was pumped through the flow module by an IPC-N peristaltic pump (Ismatec, Switzerland) at a flow rate of 200  $\mu\text{L}/\text{min}$ . This flow rate was chosen as higher flow rates would lead to noticeable noises in frequency (e.g., frequency fluctuation is about 1 Hz), causing difficulties in quantitative analysis of the recorded signals. The temperature of the solution

was controlled to within 0.02 °C by a built-in heating and cooling thermoelectric device under the flow module in the chamber platform.

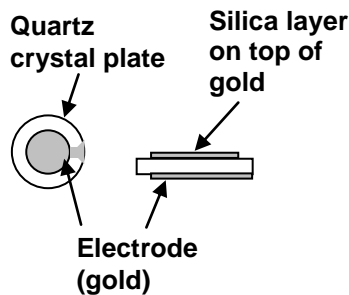
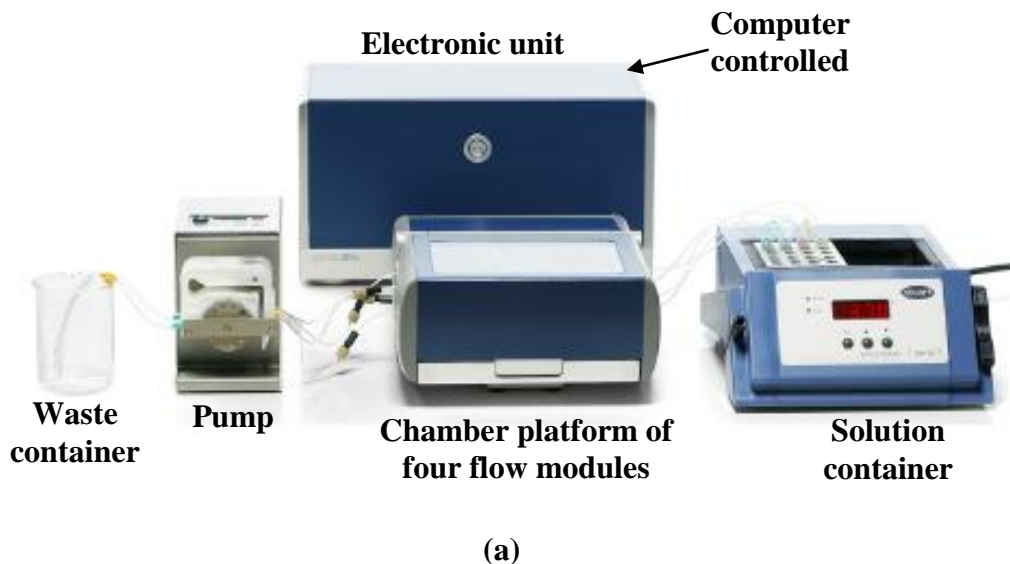


Figure 2.7. (a) QCM-D equipment and experimental setup (Re-plotted from Q-sense); (b) Quartz crystal sensor

For each run of experiment, pure toluene was first pumped through the system until a stable baseline was obtained. Then 50 ppm asphaltene-in-toluene solution was introduced to the flow module. The adsorption of asphaltenes on the sensor surface caused a negative shift in frequency and a positive shift in dissipation. After reaching adsorption equilibrium as judged by a constant frequency over an

extended period, the sensor surface was washed by switching the asphaltenes solution to pure toluene to remove any loosely adsorbed asphaltenes. To study the effect of ethyl cellulose (EC) on the asphaltene pre-adsorbed surface, the EC-in-toluene solution was then pumped through the system. EC was allowed to adsorb on the pre-adsorbed asphaltenes on the sensor surface and/or displace the pre-adsorbed asphaltenes until a new equilibrium was reached. For comparison, EC adsorption from toluene solutions on fresh sensor surfaces, followed by the adsorption of asphaltenes was also measured using reverse injection sequence described above. All QCM-D adsorption experiments were carried out at  $22.0 \pm 0.02$  °C.

## **2.5 Other techniques**

### **2.5.1 Elemental analysis**

Elemental analysis is able to quantitatively determine the weight percent of each element in a compound. For organic materials, the elemental analysis is achieved through a combustion process. First, the sample is burned in an oxygen excess environment. Then the oxidized elements in the form of carbon dioxide, water, sulfur trioxide and nitric oxide are introduced to a reduction tube where these oxides are reduced to certain formulas for analysis.

In this study, an elemental analyzer-vario MICRO (Elementar Analysensysteme GmbH, Germany) was used to analyze elemental composition of asphaltenes. The relative contents of four elements: carbon, hydrogen, nitrogen and sulfur were obtained.

### **2.5.2 Water contact angle measurement**

Static water contact angles on a sample surface were measured with DSA100 (Krüss, Germany) equipped with an optical microscope and illumination system. The sessile drop method with constant drop volumes was employed at room temperature (21 °C). Contact angles from both the left and right edges were considered and the average value was used. For each sample, measurements were performed at three locations with at least six measurements at each location. Standard deviations of the measurements were calculated and shown as error bars in the results.

### **2.5.3 Karl fisher titration**

The water content in toluene was determined by a Karl Fisher titrator (Cou-Lo 2000, GR Scientific Canada). An average value of three measurements was adopted.



## Chapter 3 Colloidal Interactions between Asphaltene Surfaces in Toluene\*

### 3.1 Introduction

Athabasca oil sands of Alberta, Canada are unconsolidated mixtures of bitumen, silica sands, mineral fine solids and water. A water-based extraction process (WBEP) is used to extract bitumen from the oil sands. In this process, the oil sands ore is first mixed with hot or warm water to liberate the bitumen from the sand grains and to aerate the bitumen with entrained air bubbles. The aerated bitumen is enriched by flotation to obtain bitumen froth. The recovered bitumen froth contains about 60% bitumen, 30% water and 10% solids by weight. An appreciable fraction of the water is present as emulsified water droplets. To further separate the water droplets and fine solids prior to bitumen upgrading, the bitumen froth is diluted with a light hydrocarbon solvent (diluent) (e.g., naphtha or alkane). The purpose of adding a diluent is to reduce the density and viscosity of bitumen to facilitate water and solids removal by gravity, cycloning and/or centrifugation. However, small droplets of water (about three to five microns in diameter) still remain in the solvent-diluted bitumen. These droplets contain dissolved salts that are carried along with the bitumen into downstream upgrading processes, where the chloride salts can lead to corrosion issues. Therefore, minimizing the content of the water in the diluted bitumen is essential.<sup>1</sup>

The removal of small water droplets and fine solids from the diluted bitumen depends on two factors: the mobility and the coagulative behavior of water

---

\* Published paper: Wang, S.; Liu, J.; Zhang, L.; Xu, Z.; Masliyah, J., *Energy & Fuels* 2009, 23, 862-869.

droplets and solids in the solvent-diluted bitumen. The mobility of the water droplets in diluted bitumen is highly related to the viscosity of the bulk bitumen, which is determined by the degree of dilution. On the other hand, the coagulative behavior of water droplets in the solvent-diluted bitumen is determined by the interaction forces between the droplets. The nature of the surface active material on the water droplets plays a key role in determining their coagulative behavior in organic solvents.

Bitumen is a complex mixture of asphaltenes, saturates and aromatics. Since asphaltenes are of amphiphilic nature, they can readily adsorb at water/oil interfaces acting as surfactants with their polar groups residing in the aqueous phase and non-polar groups extending into the oil phase. It is commonly recognized that asphaltene macromolecules/aggregates at water/oil interfaces stabilize water droplets in diluted bitumen.<sup>22, 198-200</sup> It is therefore of great importance to measure colloidal forces between asphaltene surfaces in solvents in order to shed light on the stabilization mechanism of water-in-bitumen emulsions, and hence to develop strategies for effective removal of emulsified water droplets from diluted bitumen.

Surface force measurements in aqueous solutions with atomic force microscope (AFM) and surface force apparatus (SFA) were reported extensively in the literature as were a number of quantitative studies on colloidal forces between solids and model oil droplets.<sup>201-204</sup> Reports on surface forces for crude oil systems in aqueous solutions are also available.<sup>19, 205-209</sup> To understand the colloidal interactions between oil sands components in aqueous solutions, using

AFM, a systematic study was conducted to measure surface forces between bitumen-silica,<sup>210</sup> bitumen-clay,<sup>211</sup> bitumen-fine solids,<sup>46</sup> bitumen-bitumen,<sup>47</sup> silica-clay,<sup>212</sup> and asphaltenes-asphaltenes.<sup>48</sup> These studies provided better understanding of bitumen extraction and flotation during oil sands processing.

Many studies show that asphaltenes are macromolecules bearing polymeric properties.<sup>113, 134, 213</sup> To understand the interactions between macromolecules or polymers in organic solvents, a few well-defined polymer systems in organic solvents have been studied using SFA and MASIF (Bimorph SFA).<sup>214-219</sup> It was found in these studies that the solvency conditions (solvent type, temperature, etc.) greatly impact polymer conformation and the nature of interactions. In this study, the interactions between asphaltene surfaces in toluene are considered together with the effect of water content in toluene and temperature. From an industrial point of view, this study will shed light on the mechanism of asphaltene-stabilized water-in-diluted bitumen emulsions under different conditions.

## **3.2 Scaling theory for polymer brushes and force measurements between polymer brushes by AFM**

### **3.2.1 Polymer brushes**

In a good solvent, the polymer exists as a random-walk conformation with a diameter of  $R_F$ .<sup>220, 221</sup> When a polymer solution is in contact with a solid surface, interactions between the polymer and the solid wall will cause the polymer to accumulate at or deplete from the solid surface. For a polymer bearing a polar head group or a diblock polymer containing solvent-philic and solvent-phobic

blocks, the polymer will graft on the solid surface. When the distance between the grafting sites,  $s$ , is smaller than  $R_F$ , the adsorbed or grafted polymer chains will overlap and stretch from the solid surface, forming a dense polymer brush (Figure 3.1). Also, for polymers that uniformly adsorbed on the solid surface but with long tails extending to the solvent, a polymer brush can be envisioned.

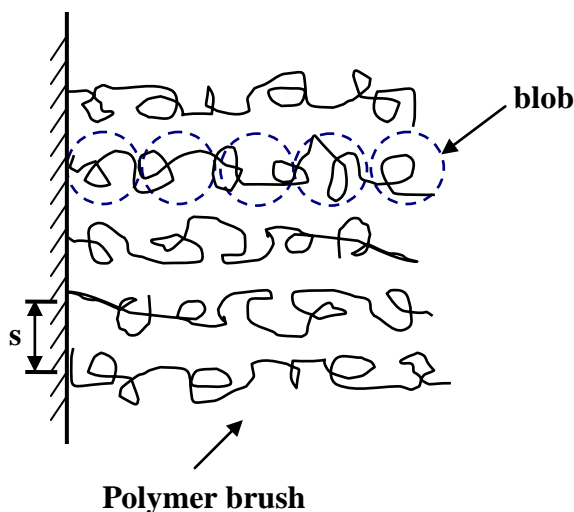


Figure 3.1. Schematic of a polymer brush

Polymer brushes form a screening layer between the solid surface and its surrounding medium, thus altering the surface properties of the solids in many respects, such as wettability, viscosity and interactions with other solids. This ability of polymer brushes is relevant to many practical operations: colloid stabilization, wettability alteration, biocompatibility, and tribology. The properties of the polymer-bearing solid surface are significantly affected by the conformation and profile of the polymer brushes. Thus it is very important to understand the structures and the properties of the polymer brushes.

### **3.2.2 Theoretical modeling of polymer brushes - scaling theory**

Many theories have been established for bulk polymer solutions.<sup>220, 221</sup> It is a natural consideration to check whether these theories of bulk polymer solutions could be applied to polymer brushes, in order to establish a theoretical model to predict the chain configurations and interactions between polymer brushes. The pioneers in this work are Alexander,<sup>222</sup> de Gennes,<sup>223-226</sup> and Milner.<sup>227-229</sup> Two theories were developed to approach this problem: the scaling theory<sup>222-226</sup> and the mean field theory.<sup>227-229</sup> In developing these theories, both approaches started with a simple model polymer brush: the terminally grafted dense polymer brush in a good solvent. The mean-field theory developed by Milner, Witten and Cates predicts more accurately the density profile of the polymer brushes and improves the descriptions of the interactions between the brushes.<sup>17, 228-230</sup> But in general the two theories yield similar results in the layer thickness and the force-distance profile.<sup>189, 231</sup> Due to the simpler equations and its applicability to the adsorbed, diffuse polymer layers, the scaling theory is widely used in estimating the properties of polymer brushes, especially in explaining the force profiles between polymer brushes.<sup>189-191, 223, 232-236</sup>

### **3.2.3 Steric repulsions between polymer brushes described by scaling theory**

Before applying the scaling theory to the description of the steric repulsions between polymer brushes, several assumptions about the scaling theory need to be clarified. 1) The concentration profile of the polymer layer is assumed to be uniform from the solid surface to the free end of the polymer brushes;<sup>220, 222, 223, 226</sup> 2) The monomer density in the polymer brush is sufficiently high that the brush is

in a semi-dilute solution state;<sup>220, 223, 226</sup> and 3) The polymer chain is viewed as a string of “blobs” (Figure 3.1) which interact with each other only through excluded-volume repulsions.<sup>220</sup> Criteria to meet these assumptions have been discussed by a number of researchers.<sup>234, 237</sup> According to these assumptions, the polymer chains in the brush in a good solvent are stretched away from the solid surface while the other end being grafted on the solid surface at the binding site. Two effects are contributed to the energy of a polymer chain: the osmotic effect due to high concentration in the brush and the elastic restoring effect because of stretching of the polymer chains.<sup>220, 222, 223</sup> The osmotic pressure tends to make the brush “swell” while the elastic energy forces the polymer to restore to its random-walk conformation. The brush attains its equilibrium state by balancing the energy between osmotic pressure and elastic free energy. According to the scaling theory by Alexander and de Gennes, the free energy of a polymer chain in the brush can be expressed as:<sup>222, 223</sup>

$$F_C = k_B T N \left[ \phi^{5/4} + \left( \frac{a}{s} \right)^4 \phi^{-7/4} \right] \quad (3-1)$$

where  $T$  is temperature in K;  $k_B$  is Boltzmann constant in J·K<sup>-1</sup>;  $N$  is the number of monomers per chain;  $s$  is the average distance between two polymer grafting sites in m;  $a$  is the effective size of the monomer in m and  $\phi$  is the volume fraction of the polymers in the brush.

In equation (3-1), there is a prefactor of unity omitted. The first term on the r.h.s. of the equation is the osmotic pressure and the second term represents the entropic elastic free energy due to the stretched polymer chains.

In good solvents, the scaling theory predicts that the interactions between two grafted or irreversibly adsorbed dense polymer brushes are repulsive.<sup>224</sup> This repulsion is due to a steric barrier induced by compressing and overlapping of the polymer brushes in good solvents. At the equilibrium state, the osmotic and the elastic energy balance each other and the polymer brush has a thickness of  $L_o$ . When compressing the polymer brushes, the osmotic pressure increases due to increased concentration of monomers in the brush while the elastic energy decreases, leading to an imbalance of energy in the polymer brush and a resultant net osmotic pressure ( $\pi_{os}$ ) given by:<sup>220, 234</sup>

$$\pi_{os} = \frac{\phi^2}{Na^3} \frac{\partial F_C}{\partial \phi} \quad (3-2)$$

In combination of equations (3-1) and (3-2) with expressions of  $\frac{\phi}{\phi_o} = \frac{L_o}{D'/2}$  and

$\phi_o = \left(\frac{a}{s}\right)^{4/3}$ , we obtain the force per unit area of brush:<sup>220, 223, 234</sup>

$$f(D') = \frac{kT}{s^3} \left[ \left(\frac{2L_o}{D'}\right)^{9/4} - \left(\frac{D'}{2L_o}\right)^{3/4} \right] \quad (3-3)$$

where  $D'$  is the separation distance between two solid surfaces in m and  $L_o$  is the length of a polymer brush at the equilibrium state (without compression) in m.

### 3.2.4 Forces between two polymer brushes measured by AFM

Many surface force measurement techniques such as surface force apparatus (SFA)<sup>189-191</sup> and atomic force microscopy (AFM)<sup>232, 233, 235, 236</sup> along with other indirect techniques<sup>231</sup> were applied to measuring the interactions between the end-

grafted polymer brushes. In reality, the interaction surfaces are usually curved in shape and the force measurements were carried out between two curved surfaces. However, equation (3-3) is only applicable to the interactions between two parallel plates. In Chapter 2 we described that for the interactions between a spherical particle and a flat surface, the total force  $F(D')$  normalized by the radius of a sphere can be estimated from interaction energies between two parallel flat plates by the Derjaguin approximation which gives that:<sup>188</sup>

$$\frac{F(D')}{R} = 2\pi \cdot E(D') \quad (2-1b)$$

where  $E(D')$  is the interaction energy between two parallel flat plates per unit area. To get  $E(D')$ , we integrate equation (3-3) from  $2L$  to  $2L_0$ :

$E(D') = \int_{2L}^{2L_0} f(D') dD'$ , and obtain:

$$E(D') = \frac{8kTL_0}{35s^3} \left[ 7 \left( \frac{D'}{2L_0} \right)^{-5/4} + 5 \left( \frac{D'}{2L_0} \right)^{7/4} - 12 \right] \text{ for } D' < 2L_0 \quad (3-4)$$

Substituting equation (3-4) into equation (3-3), we obtain the expression of the force measured by AFM:

$$\frac{F(D')}{R} = \frac{16\pi kTL_0}{35s^3} \left[ 7 \left( \frac{D'}{2L_0} \right)^{-5/4} + 5 \left( \frac{D'}{2L_0} \right)^{7/4} - 12 \right] \text{ for } D' < 2L_0 \quad (3-5)$$

In AFM force measurements, the actual separation distance,  $D'$ , between the two solid surfaces on which polymers grafted can not be determined. What AFM can differentiate is the distance between the outer-layers of the two compressed



polymer layers,  $D$ . Assuming the polymer brushes are compressed ultimately to a thickness of  $\xi$  during AFM force measurements (Figure 3.2), we obtain that  $D' = D + 2\xi$ . Equation (3-5) then becomes:

$$\frac{F(D)}{R} = \frac{16\pi kTL_o}{35s^3} \left[ 7 \left( \frac{D+2\xi}{2L_o} \right)^{-5/4} + 5 \left( \frac{D+2\xi}{2L_o} \right)^{7/4} - 12 \right] \text{ for } D+2\xi < 2L_o \quad (3-6)$$

where  $\xi$  is the thickness of a compressed polymer layer in the compliance range of AFM force profile in m,  $R$  is the radius of the AFM probe in m;  $D$  is the distance between the outer-layers of the two compressed polymer layers in m; and  $L$  is the length of a compressed polymer brush. All other parameters in equation (3-6) are the same as in equation (3-3).

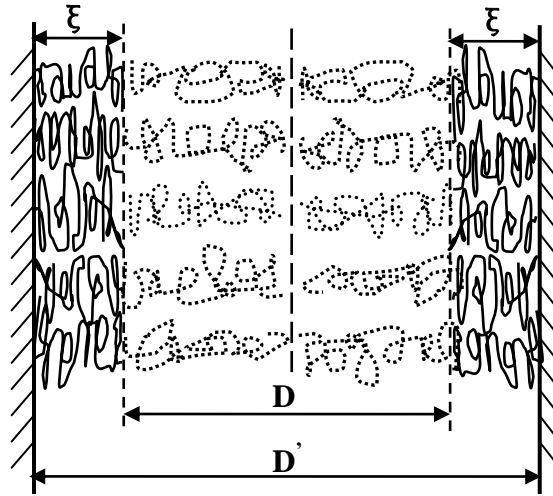


Figure 3.2. Polymer brushes under compression during AFM force measurements

The parameter  $\xi$  is introduced here to offset the zero separation distance from the solid surface to the perimeter of the compressed asphaltene layer. The introduction of  $\xi$  is necessary as the separation distance between the two solid silica surfaces is undeterminable by AFM.

### 3.3 Experimental

#### 3.3.1 Materials

Asphaltenes were prepared from vacuum distillation feed bitumen according to methods described in Chapter 2. Silica microspheres ( $\sim 8 \mu\text{m}$ , Duke Scientific Co., USA) and silica wafers (NanoFab, University of Alberta) were used to prepare asphaltene probes and asphaltene flat surfaces. HPLC grade toluene (Fischer Scientific) was used. To prepare “dry” and “water-saturated” toluene, treat the HPLC toluene with 8-12 mesh molecular sieves (sodium aluminum silicate, Fisher) and de-ionized water, respectively. About 100 mL toluene and 20 g molecular sieves or de-ionized water were mixed in a 150 mL glass bottle. The bottle was gently shaken on the horizontal shaker for 2 days. After settling for 4 days, the solvent was removed and sealed in a separate glass bottle. Toluene without any treatment prior to its use was termed as “as-received” toluene. The water content of dry, as-received and water-saturated toluene was analyzed using a Karl-Fisher titrator with results given in Table 3.1.

Table 3.1. Water content in toluene

Toluene	Dry	As-received	Water-saturated
Water content (ppm)	16	68	365

#### 3.3.2 Preparation of asphaltene films

Two methods were used to coat an asphaltene film onto the silica substrate or probe, the Langmuir-Blodgett (LB) and dip-coating methods. In the LB method, asphaltenes were formed at water/toluene interfaces to mimic asphaltene surfaces exposed to solvents in the bitumen froth treatment process. To compare with an

asphaltene film formed at water/solvent interface, a dip-coating method was also used to make a physically-adsorbed asphaltene film on a hydrophilic silica wafer.

The LB method was described in detail in Chapter 2.3 and asphaltene films were prepared accordingly. For the dip-coating, the treated silica wafer and the AFM probe were immersed in 2 mg/mL asphaltene-in-toluene solution for 30 minutes. The samples were taken out of the solution and gently blown-dried immediately with nitrogen gas to remove any entrained solution. The asphaltene-coated silica wafer and probe were then used for AFM force and image measurements. For the preparation of all the asphaltene films, the as-received toluene was used.

Using the two coating methods, the good deposition of asphaltene films on the silica wafer as well as on the probe was demonstrated by a transfer ratio close to unity (LB film only), AFM imaging, contact angle measurements, and surface force measurements between asphaltene and silica surface, as will be discussed later.

To allow for the influence caused by asphaltene-coating on the probe cantilever, the spring constant of the cantilever was calibrated using the thermal tune function of AFM after the force measurements. For force normalization with the probe radius, the exact curvature of the asphaltene probes used in each set of experiments was determined from scanning electron micrographs after the force measurements were completed.

### **3.3.3 Surface force measurement (AFM technique)**

Interaction forces between asphaltene films were measured using a Nanoscope E AFM (Digital Instrument, Santa Barbara, CA, USA). The AFM setup was shown

in Chapter 2 and experimental procedures of force measurements described there were followed. In general, the force profiles were found to be fairly reproducible, with long-range forces varied within 15% (as will be shown later in Figure 3.10). For the convenience of illustration, only one typical (most repeatable) force profile was reported under a given condition. All of the experiments were conducted at room temperature ( $20\pm 0.1$  °C), unless otherwise specified.

### **3.4 Results**

#### **3.4.1 Characteristics of asphaltene films**

For the LB method, the interfacial pressure-area isotherm of asphaltene monolayer at toluene/water interface is shown in Figure 3.3. The interfacial pressure-area isotherm of an asphaltene monolayer at toluene/water interface is widely expanded and the interfacial film can be compressed to an interfacial pressure of  $\sim 30$  mN/m.<sup>57</sup> In this study, asphaltene films at toluene/water interfaces were deposited onto a silica substrate and silica probe at an interfacial pressure of 10 mN/m. This interfacial pressure was chosen to ensure that the area between the two compressing barriers is sufficiently large to cover both sides of a solid substrate. The transfer ratio was found to be close to unity, indicating a successful transfer of interfacial materials to the substrate.<sup>238</sup>

The prepared asphaltene films were imaged with a Nanoscope IIIa (Digital Instrument, Santa Barbara, CA) AFM operated in tapping mode in air at room temperature. The AFM image is shown in Figure 3.4. It can be clearly seen that asphaltene was successfully deposited on the silica substrate and the asphaltene film is composed of aggregates in size of  $\sim 25$  nm. For both deposition methods,

the surface roughness of the asphaltene films is less than 1nm, indicating that the surface is sufficiently smooth for carrying out AFM force measurements.

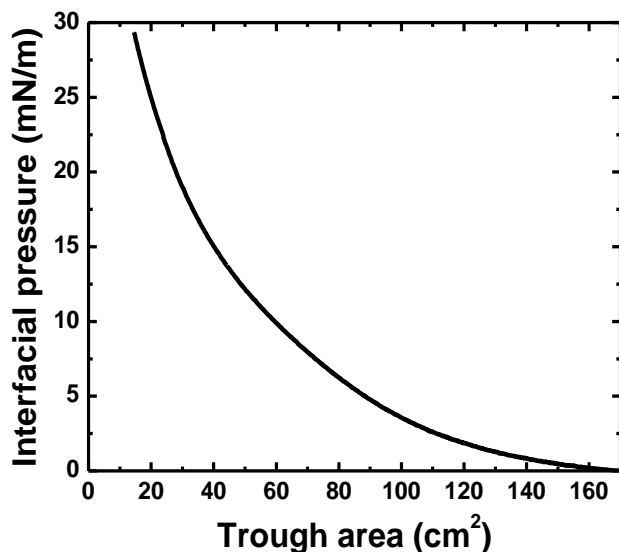
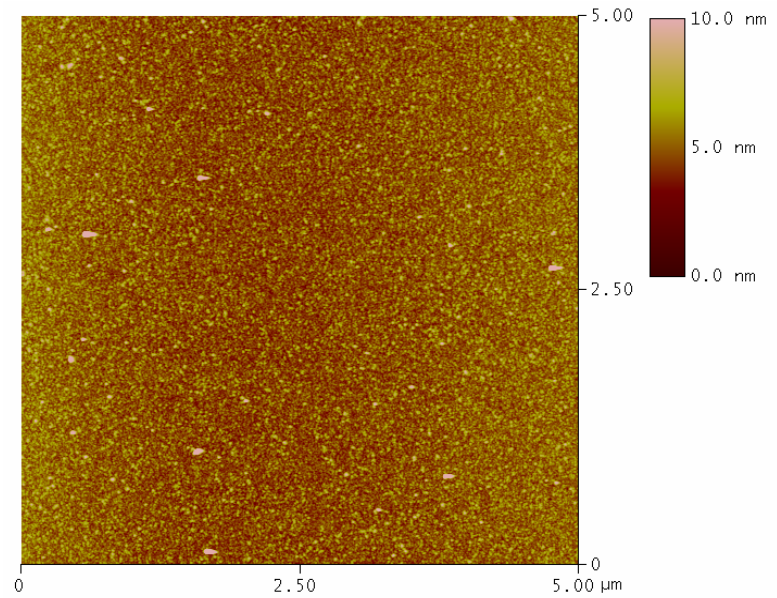


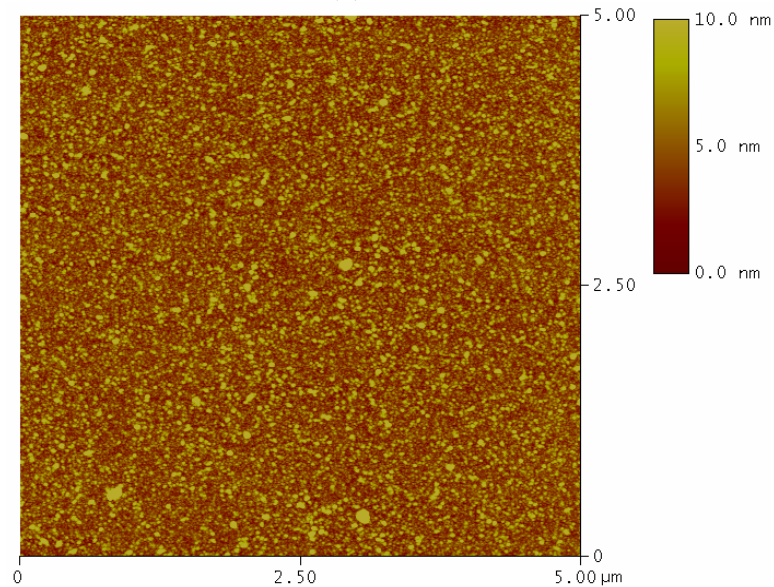
Figure 3.3. Interfacial pressure-area isotherm for asphaltene interfacial film at toluene/water interfaces at 20 °C

The water contact angle as measured with a drop shape analyzer (Krüss, DSA10) confirmed the successful deposition of asphaltene films. In contrast to a contact angle of 10° for the fresh silica wafer, the water contact angle on asphaltene-coated wafer increased to 90°, further confirming a successful deposition of asphaltene film on the silica substrate. For the LB film, we found that once an asphaltene monolayer was transferred from a toluene/water interface onto a silica wafer, the deposited asphaltene film could not be washed off with fresh toluene. For example, when a deposited asphaltene film was soaked in toluene for 2 hours, the contact angle measured on the asphaltene film remained the same as that prior to soaking. While for the dip-coated asphaltene film (Figure 3.4b), after soaking in toluene, the contact angle decreased from 90° to about 75° and remained at 75° with further soaking. This finding would indicate that part of the adsorbed

asphaltenes dissolved in toluene while the layer of asphaltenes immediately in contact with the silica surface was irreversibly adsorbed on the hydrophilic silica substrate.



**(a)**



**(b)**

Figure 3.4. AFM images of asphaltene films. (a) LB asphaltene film from toluene/water interface; (b) Dip-coated asphaltene film from toluene/silicon interface

To further validate this hypothesis, the thickness of the asphaltene film was measured in air by ellipsometry. The thickness of the LB asphaltene film is about 4nm which remained unchanged after soaking in toluene, demonstrating that a monolayer of asphaltene films were irreversibly adsorbed on the silica surface. While for the dip-coated asphaltene film, the film thickness reduced from 10 nm to 3.5 nm after initial soaking in toluene for several minutes. The film thickness remained at 3.5 nm with further soaking for prolonged time. These findings confirm that the adsorption of asphaltenes from asphaltene-in-toluene solution on silica particles is irreversible as reported by Acevedo et al.<sup>239</sup>

The satisfactory deposition of the asphaltene film on the silica sphere was confirmed by measuring the interaction forces between pairs of an asphaltene substrate - silica probe, and a silica wafer - asphaltene probe, where asphaltene films were prepared using the same method. As shown in Figures 3.5 and 3.6, the force profile (approaching force curve) between an asphaltene substrate and silica sphere (triangles) in toluene is almost identical to that between an asphaltene sphere and silica substrate (circles) for both methods, indicating that the asphaltene films on a silica sphere (or silica probe) exhibited the same surface features as the asphaltene films on a silica wafer. However, as shown in Figure 3.6, the force curve obtained using LB methods shows a longer range and stronger repulsive force than that obtained using dip-coating method. This difference will be discussed later.

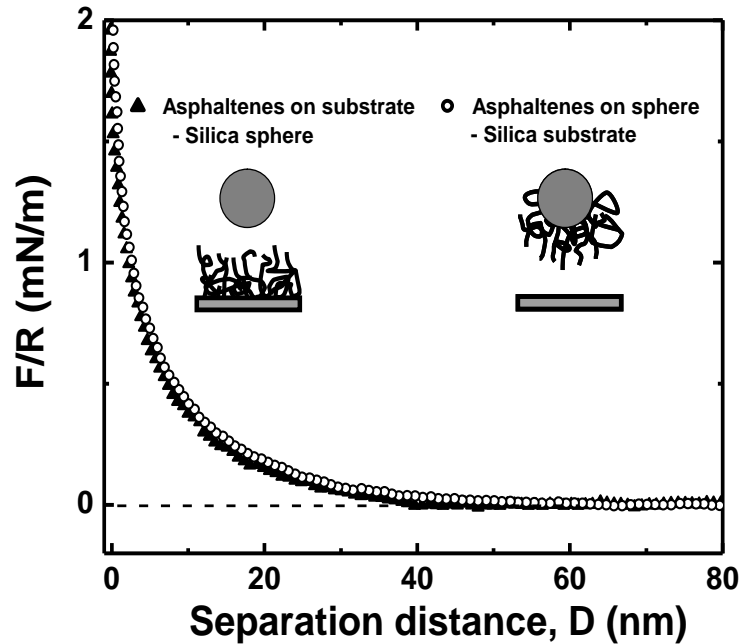


Figure 3.5. Normalized interaction forces between LB asphaltene films and silica surface in toluene at 20 °C

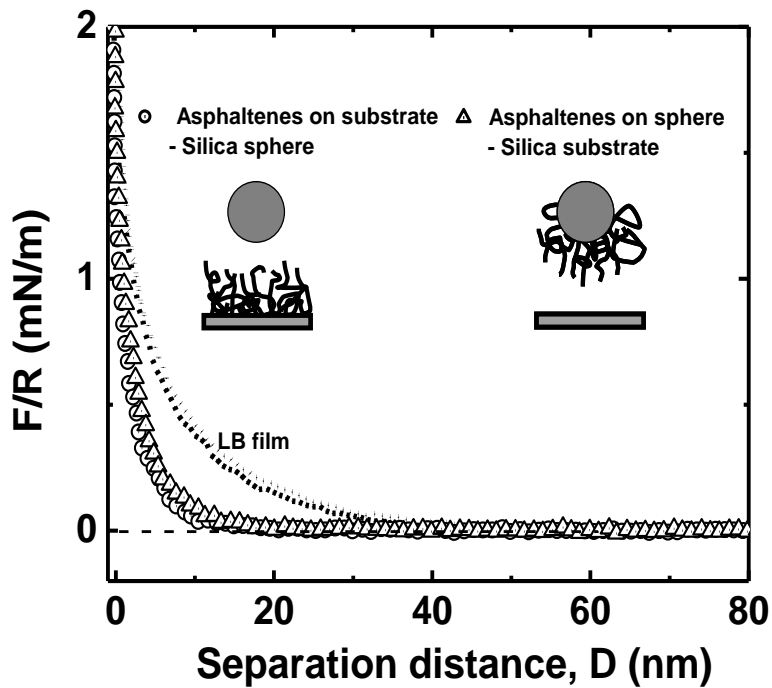


Figure 3.6. Normalized interaction forces between dip-coated asphaltene films and silica surface in toluene at 20 °C. (Data for LB asphaltene films from Figure 3.5 are plotted for reference (dotted lines))



### 3.4.2 Interaction forces in toluene

Bulk asphaltenes are known to be soluble in toluene (“good solvent”). Toluene can significantly mediate the configuration of asphaltene molecules on a substrate and hence affect the interaction forces.

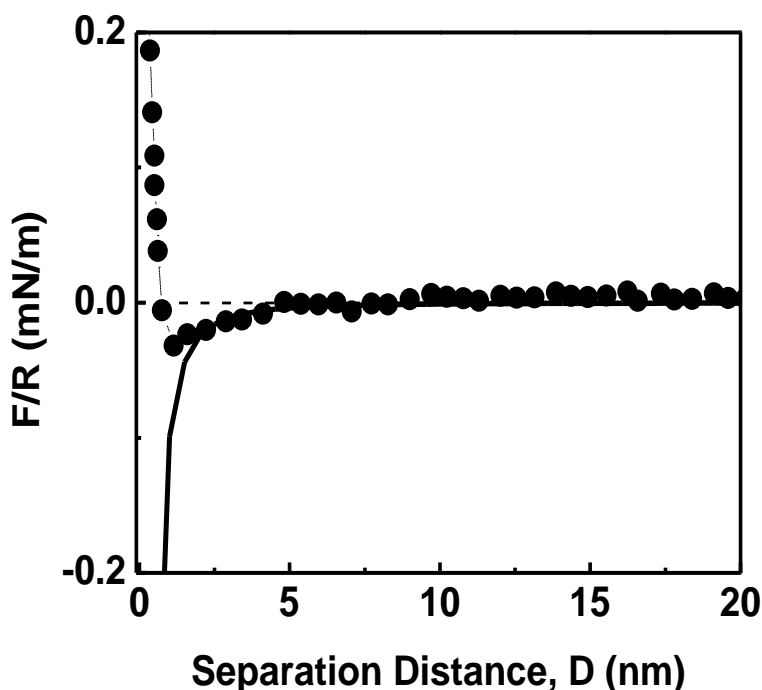


Figure 3.7. Normalized interaction forces between silica-silica in toluene at 20 °C. Solid line: theoretical van der Waals interactions calculated with an effective Hamaker constant of  $6.0 \times 10^{-22}$  J

Since the electric double layer is less well established in a low dielectric constant medium such as aromatic organic solvents, it is interesting to measure the long range electric double layer forces in such solvents. For this purpose, the force profile of a silica probe interacting with a silica substrate in dry toluene was first determined. As shown in Figure 3.7, a weak attractive interaction force was observed as two bare silica surfaces approach each other. The solid line in Figure 3.7 is the van der Waals forces between the silica surfaces in toluene with an

effective Hamaker constant of  $6.0 \times 10^{-22}$  J.<sup>188, 240</sup> The well fitting of the force profile by only van der Waals forces indicates that the electric double layer forces in toluene are negligible and can be ignored in subsequent analysis.

It is interesting to note that when only one surface is coated with asphaltenes, the measured force in toluene becomes repulsive as shown was in Figures 3.5 and 3.6. Analysis to be discussed later in text shows that the repulsion mainly arises from a steric force caused by the asphaltene tails and loops extended from the substrate into toluene. The steric force is sufficient to overcome the attractive van der Waals forces. The nature of the steric force is explained in more detail in the following discussion on the interaction between asphaltene surfaces in toluene.

The interaction force between asphaltene surfaces in dry toluene is shown in Figures 3.8 and 3.9 for LB and dip-coated asphaltene films, respectively. For the asphaltene film prepared by LB method (Figure 3.8), a monotonically repulsive force starting at a separation distance of about 70 nm (between compressed asphaltene layers) was observed as the two surfaces approached each other. The retracting force profile exactly overlapped with the approaching force profile, indicating no adhesion between asphaltene surfaces in toluene. Such a force profile is clearly different from that between the silica pair (Figure 3.7). Since the electrostatic interactions are negligible in toluene, the observed repulsion mainly originated from steric force. Asphaltenes are macromolecules bearing polar functional groups. When asphaltenes adsorbed onto hydrophilic silica surface, the polar functional groups are likely anchored on the silica surface, with the other part of molecules extending into the toluene which is a good solvent for

asphaltenes. In this manner, the tails and loops of asphaltene macromolecules on the silica surface formed a swollen brush and would repel each other when they were compressed, as schematically shown in the insert of Figure 3.8. The scaling theory described earlier can be used to explain the forces between two asphaltene surfaces.

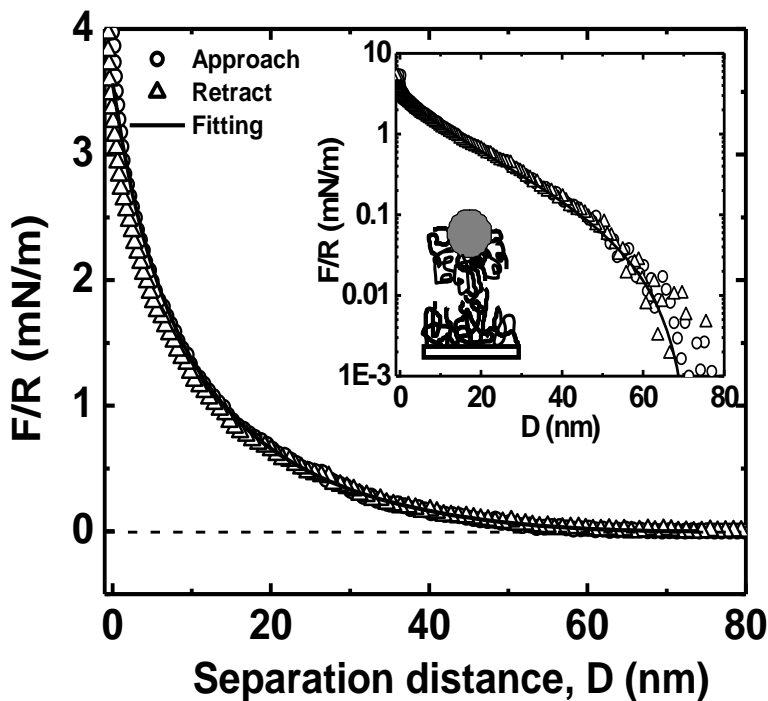


Figure 3.8. Normalized interaction forces between LB asphaltene films in dry toluene as a function of separation distance at 20 °C. Solid line: fitting with scaling theory,  $L_o=43$  nm,  $s=17$  nm and  $\delta =6$  nm

As shown by the solid line in the insert of Figure 3.8, the interaction force profile could be well fitted by equation (3-6). According to the fitting parameters, the swollen brush length of asphaltene in dry toluene is about 43 nm. The good fit would indicate that the repulsion between asphaltenes in toluene at room temperature most likely originates from steric forces.

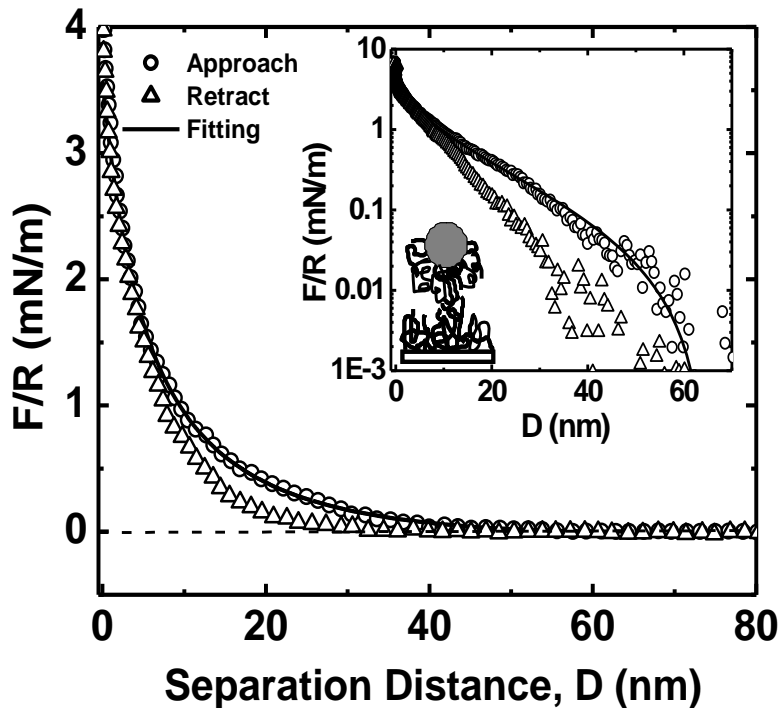


Figure 3.9. Normalized interaction forces between dip-coated asphaltene films in dry toluene as a function of separation distance at 20 °C. Solid line: fitting with scaling theory,  $L_o=36$  nm,  $s=19$  nm and  $\delta=3.5$  nm

For the dip-coated asphaltene films (Figure 3.9), the repulsive interactions are quite similar to that for LB asphaltene films. However, two differences were noted. First, a hysteresis occurred in the approach/retract force cycle; second, there is a considerable reduction in the magnitude and range of the repulsive force. Asphaltenes are a mixture of macromolecules with multi-polar functional groups. When asphaltenes adsorb onto silica surfaces from toluene, the freedom of the macromolecules to maneuver is reduced at the liquid-solid interface, hence it is possible that the molecules anchored themselves by part of the polar functional groups, while leaving other parts of polar functional groups extending into the solvent and thus enhancing the possibility of bridging between the two silica surfaces. A similar phenomenon has been noted in the interactions between

adsorbed homopolymers,<sup>189</sup> in which Luckham also attributed the hysteresis to the bridging of homopolymers attached to two opposing solid surfaces. When the surfaces approach each other under the compression of AFM cantilever force, the two asphaltene layers are easily compressed and bridged between the two solid surfaces, leading to a reduction in the magnitude and range of the repulsive forces as well as a hysteresis in the approach/retract force cycle. While for the LB asphaltene films formed at toluene/water interface (liquid-liquid), asphaltene molecules had more flexibility to organize into an oriented layer, especially by applying a surface pressure to restrict the areas occupied by molecules. Therefore, it is not as easy to compress the more compact asphaltene LB film, and usually a reversible force profile was observed for the approach/retract force cycle (Figure 3.8). The interactions between dip-coated asphaltene films can also be well fitted by equation (3-1). The fitted compressible length of asphaltene brush reduced from 43 nm for LB films to about 36 nm. The fitting parameters are summarized in Table 3.2.

Table 3.2. Interaction force curve fitting parameters by scaling theory

	$\xi$ , nm	$s$ , nm	$L_o$ , nm
Dip-coated film	3.5	19	36
LB film	6	17	43

From Table 3.2, we can note that the compressed thickness,  $\xi$ , for the dip-coated asphaltene film is much smaller than that of LB film. At the same time, the spacing between grafting points of asphaltene molecules in the dip-coated film is larger than that of LB film. Although both sets of data are fitted values from

equation (3-6), the difference qualitatively shows that the asphaltene molecules are more compact and better organized in LB films than that in dip-coated films. We should also note that the value of  $\xi$ , representing the thickness of the compressed asphaltene layer during the AFM force measurement, is dependent on the loading force applied on the asphaltene films when compressing the two asphaltene surfaces during the force measurements. In this regard, all the loading forces were adjusted to the same level (~11 nN) during the AFM force measurements.

It is important to note that, although the concepts applied to polymers (e.g., the tail length) were used to explain the steric nature of the repulsive forces between asphaltenes in toluene, asphaltenes are not conventional polymers. Indeed, to date, the exact structure of asphaltenes is not clear due to its polydispersity and complex nature. Some researchers stated that asphaltenes bear some polymeric properties,<sup>78, 112, 113</sup> while others argued about the colloidal nature of asphaltenes.<sup>20, 241</sup> Our AFM images (Figure 3.4) showed the presence of asphaltenes on the substrates as aggregates in size of nanometers. Nevertheless, our AFM force measurements showed that the repulsive interactions between asphaltenes in a good solvent can be reasonably described by the classic theory used for polymer brushes, indicating dangling side chains, loops and tails extending out from asphaltene aggregates. This can partly explain the stabilization mechanisms of water-in-oil emulsion by asphaltenes which form a steric layer covering the water/oil interface. This behavior of asphaltenes is quite similar to that of polymers as it is well known that in industrial practice polymer adsorption

is used to stabilize nonaqueous colloidal suspensions. From the onset of the repulsion force, we can estimate a 40 nm tail length of the adsorbed asphaltene layers in good solvents like toluene. This estimated value suggests that the tails and loops of asphaltene molecules are sufficient to overcome the van der Waals attractive forces, and to stabilize w/o emulsions, akin to polymer brushes stabilizing nonaqueous suspensions of inorganic pigments by adsorption of polymers on particle surfaces.

As mentioned earlier, the magnitude of the long-range forces varied in the range of about 15% (Figure 3.10). At a given separation distance of 10 nm for example, the forces measured with LB films were  $1.26 \pm 0.15$  mN/m; while for dip-coated films, they were  $0.93 \pm 0.14$  mN/m. For the fitting purposes, only the most repeatable force profile was attempted.

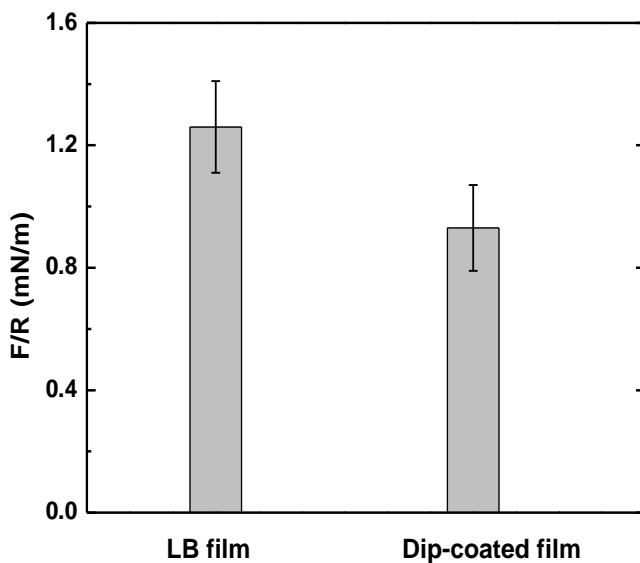


Figure 3.10. Normalized interaction forces in toluene at separation distance of 10 nm to demonstrate the variation of long-range forces. The results are derived from 30 force profiles at a separation distance of 10nm. For LB films,  $F/R = 1.26 \pm 0.15$  mN/m; for dip-coated films,  $F/R = 0.93 \pm 0.14$  mN/m

### 3.4.3 Effect of water content in solvents on interaction forces

A trace amount of water is always present in commercial organic solvents unless they are specifically treated for its removal. The water molecules in the solvents can interact with the polar groups of asphaltene macromolecules and can also change the solvent properties such as its dielectric permittivity and polarity.

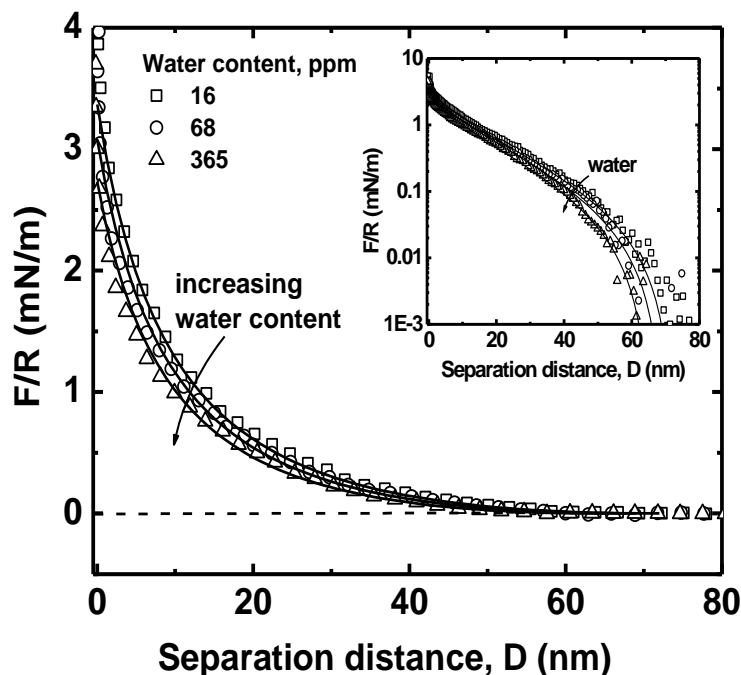


Figure 3.11. Effect of water content on the interactions between LB asphaltene films in toluene at 20 °C. Solid line: fitting with scaling theory,  $L_o=43$  nm (16 ppm water), 40.5 nm (68 ppm water) and 38.6 nm (365 ppm water)

The interaction forces between LB-deposited asphaltene surfaces in solvents with different trace amounts of water at room temperature are shown in Figure 3.11. In toluene, the presence of a trace amount of water in toluene reduced slightly the repulsive forces between asphaltene surfaces. Asphaltenes are insoluble in water, thus it is likely that the presence of water makes toluene a less good solvent for asphaltenes. Water molecules may also enrich at the hydrophilic solid surface.



Through their interactions with the neighboring polar groups of asphaltenes, these water molecules attract asphaltene molecules closer to the solid surface to make them more densely packed. Both effects can lead to reduced extension of asphaltene tails or loops. As shown in Figure 3.11, the fitted asphaltene brush length reduced gradually with increasing water content. Since the amount of water is very small even in water-saturated toluene (<400 ppm), the effect of water is not prominent. Similar reduction in repulsive forces between dip-coated asphaltene films in toluene upon water addition was also observed, but to a much less extent.

#### **3.4.4 Effect of temperature on interaction forces**

At moderate range (without exceeding the critical point of the oil components), temperature can affect the interactions from two perspectives. First, asphaltene solubility increases with temperature as an indication that the solvent quality becomes better at higher temperatures.<sup>21, 242</sup> This effect exhibits itself as an increase in osmotic pressure between the two asphaltene layers during compression. Second, it is known that molecules could possess higher thermo energy at higher temperatures and extrude more into the solvent, leading to longer range repulsion. Therefore, one would expect an increase in repulsion between asphaltene surfaces with increasing the temperature.

As shown in Figure 3.12 for LB asphaltene films, increasing the temperature from 20 °C to 40 °C did lead to a slight increase in the repulsive forces between asphaltene surfaces in toluene. However, for dip-coated asphaltene films, no visible change in the interaction force was observed with temperature (Figure

3.13). Such observation is unexpected should asphaltenes behave like typical polymers. In this regard, the aggregation state of asphaltenes on the substrate and probe, as shown in AFM image, could be a major factor. It is also possible that over the temperature range studied, the thermal effect of solvent on molecule/aggregate state is negligible. Further studies for higher temperature are desirable.

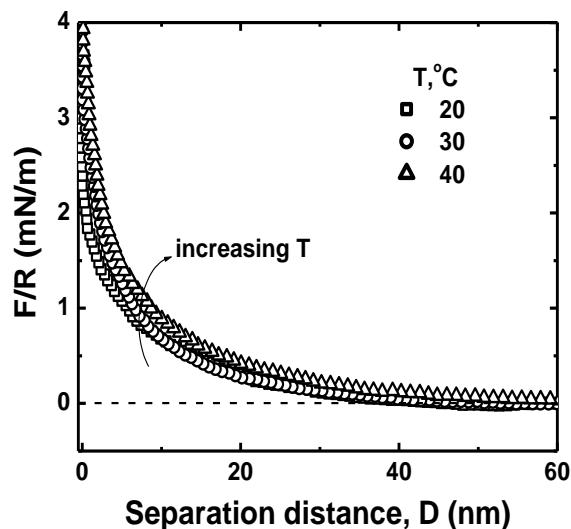


Figure 3.12. Effect of temperature on the interactions between LB asphaltene films in toluene

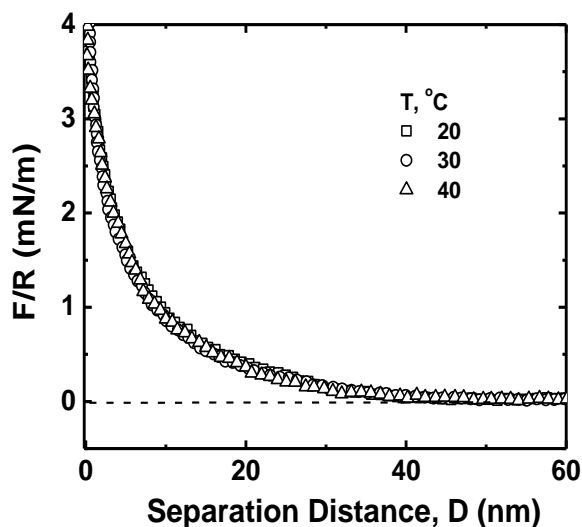


Figure 3.13. Effect of temperature on the interactions between dip-coated asphaltene films in toluene

### 3.4.5 Nature of interaction forces

The interaction forces between macromolecules in organic solvents are complex. The origin can be DLVO forces including electric double layer force and van der Waals forces and non-DLVO forces including inter-segment interactions.<sup>37</sup> Since the electric double layer is less well established in low dielectric constant medium such as toluene ( $\epsilon_r = 2.4$  at 20 °C), the electric double layer forces in the tested organic solvent were found to be negligible. In the present system, the segment interaction between asphaltenes was found to be the dominant component in the detected force profiles. This type of interaction in the organic solvent can be attractive or repulsive, depending on the quality of the solvent. The quality of solvent can be tuned by adjusting solvent solvency or changing temperature.

In good solvents such as toluene, the asphaltene surfaces become brush-like, and the resultant interaction force between asphaltenes is contact steric repulsion. In this case, the force profiles can be reasonably fitted with the polymer scaling theory, as shown by the solid lines in Figures 3.8 and 3.9. The excellent fitting confirms that the repulsion between asphaltenes in toluene most likely originates from a steric force. The steric nature of repulsive forces is further supported by the absence of adhesion forces for all the cases. Other factors that can affect the solvent quality include temperature and water content. However, these two factors were found to marginally impact the interaction forces between asphaltene surfaces, possibly due to the presence of asphaltenes as aggregates on silica substrate and probes.

### **3.4.6 Colloidal forces and stability of water-in-oil emulsions**

Emulsion stability can be evaluated by the nature of long-range colloidal forces between emulsified droplets. Stronger repulsive forces, coupled with the absence of adhesion usually correspond to higher emulsion stability, while a weaker repulsion or attraction with a strong adhesion can lead to flocculation and instability of emulsions.

For water-in-oil emulsions as encountered for example in bitumen recovery from oil sands, a steric layer mainly composed of asphaltenes exists at the water/oil interface. In this scenario, the stability of the water droplets is ultimately determined by the forces between asphaltene surfaces in the oil phase. In this study, the interactions between asphaltene surfaces in toluene were measured by the colloidal probe technique of AFM and the presence of a steric repulsive force was revealed. It is thus expected that water droplets with adsorbed asphaltenes are stable in toluene or in other good solvents for asphaltenes. This is the commercial process for the naphtha-based bitumen froth treatment (cleaning) process in oil sands industry. Since naphtha is a mixture of aromatic and aliphatic/naphthenic hydrocarbons, which is a relatively good solvent for asphaltenes (no asphaltene precipitation occurs at the industrial dilution ratio), 1-2 wt% residual emulsified water droplets are always present in the final diluted bitumen product. The measured colloidal forces between asphaltene surfaces in the current study partly justify the presence of stable emulsified water in naphtha-diluted bitumen.

By far, it is demonstrated that the stability of asphaltene-covered water droplets in toluene is due to the presence of a repulsive force. To break the asphaltene-

stabilized water in oil emulsions, demulsifiers are needed to eliminate the repulsive forces by destroying the asphaltene films adsorbed on the water surface. Besides, the interactions between asphaltenes in organic solvents can be tuned by adjusting the solvent solvency. This implies that it is possible to tune the emulsion stability by changing the solvent solvency. This part of discussion will be illustrated in a subsequent communication.

### **3.5. Conclusions**

We have measured the colloidal forces between asphaltene surfaces in toluene using AFM to gain better understanding on the stabilization mechanism of water-in-oil emulsions as encountered in the naphtha bitumen froth treatment process in the oil sands industry. The following conclusions can be drawn from this study.

1. The repulsion between asphaltene surfaces in toluene originates from a steric force. The force profiles can be well described by the polymer scaling theory developed for non-charged polymers.

2. The preparation method of asphaltene surfaces/films can affect the magnitude and the range of the repulsive forces. Asphaltenes are less organized when formed by dip-coating method than by LB method. The more compact and organized the surface/film is, the higher and longer range is the repulsive force.

3. The presence of trace water slightly reduces the repulsive force between asphaltene surfaces in toluene. The effect of increasing the temperature from 25 °C to 40 °C on the repulsive forces is negligible.

4. It is feasible to evaluate the stability of water in oil emulsions by measuring the colloidal forces between asphaltene surfaces. The colloidal forces measured

between asphaltenes in toluene indicate that the water droplets in naphtha-diluted bitumen are stable due to the steric repulsive forces between the adsorbed asphaltenes on water droplets in good solvent of toluene or naphtha.

## Chapter 4 Interaction Forces between Asphaltene Films in Organic Solvents\*

### 4.1 Introduction

Asphaltenes are the most problematic fraction of crude oils. As defined in the heavy oil industry, the molecular fraction of crude oils that is soluble in toluene but insoluble in n-heptane is classified as asphaltenes. This definition implies that the molecular behavior of asphaltenes is sensitive to the composition of crude oils. Chemically, asphaltenes are composed of poly-condensed aromatic sheets and aliphatic chains, doped with transition metals (vanadium, nickel, iron) and heteroatoms (O, N, S), thereby making asphaltenes amphiphilic by forming polar functional groups such as hydroxyl, carbonyl and carboxyl.<sup>20</sup> Many industrial problems such as wellbore or pipeline plugging, formation of stable water-in-oil emulsions, alteration of wettability of solids and sedimentation during crude blending, are all attributed, at least partly, to molecular aggregation of asphaltenes upon exposure to an unfavorable liquid environment or to an oil/water interface or hydrophilic surface. Motivated by such problems encountered in heavy oil processing, interactions between asphaltene molecules and the related problems of asphaltene precipitation and emulsion stability have been intensively studied during the past several decades. The following is a summary on the current state of understanding of asphaltene interactions in organic medium in the context of asphaltene aggregation,<sup>34, 86, 107, 243</sup> flocculation<sup>244</sup> and solubility<sup>137, 245, 246</sup> in various organic solvents, to set the tone for this study.

---

\* Published paper: Wang, S.; Liu, J.; Zhang, L.; Masliyah, J.; Xu, Z. *Langmuir* 2010, 26 (1), pp 183–190

It is believed that the first step of asphaltene precipitation is aggregation, the mechanism of which is still under investigation. Due to the amphiphilic nature of asphaltenes, some researchers stated that asphaltene molecules would aggregate like surfactants and form micelles above a certain concentration (critical micelle concentration, CMC, or as other researches refer it as critical aggregation concentration, CAC).<sup>91, 97, 107, 108, 111, 247</sup> For example, although asphaltenes have a wide distribution in molecular weight, through surface tension measurements, Rogel et al. estimated the CMC of asphaltene solutions and found that the structural and chemical characteristics of asphaltenes affect their self-aggregation behavior.<sup>86</sup> In other studies, however, the researchers did not observe a CMC or CAC of asphaltene in organic solutions.<sup>112, 113</sup> Instead, a polymeric association was suggested for asphaltene aggregation to account for the polymeric properties observed in asphaltene solutions.<sup>78, 113</sup> For example, using X-ray diffraction technique, Mitchell and Speight showed that the sub-fractions of asphaltenes with higher apparent molecular weight are polymeric analogues of the sub-fractions with lower-molecular weight.<sup>137</sup> In addition to the different suggestions on asphaltene aggregation model, the nature of interactions involved in asphaltene aggregation also remains controversial. Some researchers believe that it is due to a strong specific interaction<sup>121</sup> while others believe that it is due to van der Waals attraction.<sup>119</sup> There is no conclusive agreement on the mechanism of asphaltene aggregation.

Asphaltene flocculation is the step following aggregation, which leads to final asphaltene precipitation. With regard to the mechanism of asphaltene flocculation,



relatively unanimous statement was made that flocculation is caused by van der Waals interactions between the “primary” asphaltene aggregates,<sup>80</sup> or between asphaltene side chains and n-alkanes.<sup>120</sup> Such conclusions were also reached from the results of molecular dynamics simulation by Takanohashi et al.<sup>89</sup>

A direct approach to probing the state of asphaltenes in crude oil is to study their solubility parameter since asphaltenes are a solubility class.<sup>121, 134, 137, 245, 248, 249</sup>

The solubility parameter is directly related to the cohesive energy of molecules as well as their interactions with surrounding solvent molecules. The solubility parameter data and the asphaltene-solvent interaction parameter have been widely used in an effort to describe the phase behavior of asphaltenes and to predict asphaltene precipitation. Among the theories used to evaluate asphaltene solubility, the Flory-Huggins model (referred to as F-H model in the following text), which is a classical theory developed for describing the behavior of polymer solutions, is the one most frequently used. This approach has its legitimate basis as asphaltenes do bear polymeric properties.<sup>113</sup> To apply the F-H model to an asphaltene solution, dispersion forces are considered as the driving force for phase separation.<sup>221</sup> However, asphaltenes of aromatic backbones are known to bear polar functional groups like carboxyl and hydroxyl groups<sup>51, 250</sup> while toluene is a relatively weak polar solvent. As a result, non-dispersion forces, such as  $\pi$ -electron coupling and/or hydrogen bonding, are inevitable. Despite these facts, many researchers reported that the dispersion forces remain the dominant driving force for asphaltene precipitation,<sup>119, 120</sup> which provides a legitimate basis for applying F-H model to asphaltene interactions in solvent solutions. Based on

these discussions, it remains a good approach to understanding asphaltene interactions in heptol (mixture of heptane and toluene) of varying solvency using F-H model.

With the assumption that London dispersion forces are the dominant forces driving asphaltene precipitation, Buckley et al.<sup>119, 139</sup> suggested the refractive index of the oil as an indicator of phase separation. By measuring the refractive index of the crude oil diluted with n-alkanes, they established that the onset of asphaltene precipitation occurred at an almost constant value of refractive index of solutions, and successfully predicted the asphaltene precipitation yield by adding n-alkanes to crude oils.<sup>139</sup> The authors also reported the effect of dilution ratio on asphaltene precipitation and stated that asphaltene precipitation is on a continuum basis. With increasing dilution ratio of crude oil, the amount of asphaltenes precipitated will initially increase, reach a maximum and then decrease. The maximum yield of asphaltene precipitation was reached at about 1/40 crude oil/n-alkane ratio by volume. The polydispersity of asphaltenes is believed to account for continuum asphaltene precipitation.<sup>49</sup>

Based on the above discussion, it is evident that the behavior of asphaltenes in crude oil depends largely on the oil composition and the molecular interactions between asphaltenes and asphaltenes with surrounding solvent medium. The ultimate understanding of asphaltene behavior in crude oil lies on elucidating the interactions between asphaltene molecules/aggregates in an organic solvent. Although many studies and statements have been made on the mechanisms of asphaltene precipitation based on certain assumptions of the forces involved in the

process, there is no direct measurement of the forces between asphaltene surfaces in any oil system of varying solvent aromaticity, although aromaticity of the solvent is a key indicator of the stability of asphaltene in solution. The current study is to determine interactions between asphaltene films in organic solvents of varying aromaticity. The colloidal probe technique of atomic force microscopy (AFM) was used to directly measure the colloidal forces between asphaltene films in heptol (heptane and toluene mixture). This study is based on our previous work of colloidal forces between asphaltene films in toluene alone.<sup>251</sup>

In this study, the aromaticity or quality of the solvent was gradually tuned by varying the composition of heptol from good solvent (pure toluene) to poor solvent (pure heptane). By measuring the interactions between asphaltene surfaces in solvents of finely tuned solvent quality, not only can the forces involved be differentiated, but also the phase separation process can be detected. Through the present study, we hope to provide a molecular level understanding of asphaltene precipitation mechanism in an organic medium, which will shed light on developing techniques in dealing with the problems associated with asphaltene aggregation/precipitation and/or emulsion stability encountered in heavy oil industries.

## **4.2 Experimental**

### **4.2.1 Materials**

Asphaltenes prepared from vacuum distillation feed bitumen were used to prepare LB asphaltene coatings on silica wafers and silica probes used in AFM force measurements.

#### **4.2.2 LB asphaltene films and compression isotherms**

Asphaltenes were prepared at toluene/water interfaces and transferred to silica probes and silica wafers by LB upstroke technique at an interfacial pressure of 2 mN/m. Detailed procedures can be found in Chapter 2.

To obtain the information on the structural change of the asphaltene film with the organic solvent composition, the isotherms of the asphaltene films at heptol-water interface were obtained by Langmuir trough compression experiments. In this set of experiments, the top phase was heptol of varying composition. The composition of heptol was denoted by the volume fraction of toluene with symbol  $\Phi_T$ , e.g.,  $\Phi_T = 1$  for pure toluene and  $\Phi_T = 0$  for pure n-heptane. The heptol composition varied with  $\Phi_T = 0, 0.1, 0.25, 0.8$  and 1. The procedure of preparing the asphaltene films was the same as above stated. After equilibrated for 30min at a heptol/water interface, the asphaltene film was compressed with a barrier compression speed of 5 mm/min to obtain the interfacial pressure-area isotherm at each heptol composition.

#### **4.2.3 Surface force measurements (AFM technique)**

A Nanoscope IIIa AFM was used for the force measurements. For each set of experiments using one pair of asphaltene substrate and asphaltene probe, the solvent was injected in a sequence of decreasing toluene volume fraction in heptol. For example, pure toluene ( $\Phi_T = 1$ ) was first injected into the liquid cell and the asphaltene films were incubated for 10 minutes prior to colloidal force measurements. After a number of force measurements, an ample amount of heptol with  $\Phi_T = 0.7$  was injected into the liquid cell to replace the previous solvent

mixture. The system was allowed to be incubated in the new liquid for additional 10 minutes prior to the next set of force measurements. This procedure was repeated for all the heptol solutions of decreasing toluene volume fractions ( $\Phi_T = 1, 0.7, 0.5, 0.3, 0.2$  and  $0$ ). All of the experiments were conducted at room temperature ( $20 \pm 0.1$  °C). In general, the long range force varied within 15%.<sup>251</sup> The adhesion forces were observed to vary in the range of ~50%. An average value or a distribution of adhesion force was reported.

## **4.3 Results**

### **4.3.1 Characteristics of asphaltene films**

The thickness of the film was measured by ellipsometry to be  $4 \pm 1$  nm. As observed previously,<sup>160, 251</sup> once an asphaltene film was transferred from a toluene/water interface onto a silica wafer, the deposited asphaltene film could not be washed off with fresh toluene. The water contact angle of the asphaltene films is  $90 \pm 2^\circ$ .

The topographical features of the deposited asphaltene films were obtained by AFM Tapping mode imaging. For comparison, AFM image of a bare hydrophilic silica wafer prior to asphaltene film deposition showed a featureless flat surface, as shown in Figure 4.1. In contrast, the AFM imaging revealed that the asphaltenes deposited on silica wafer are in the form of aggregates with sizes in tens of nanometers. The roughness of the deposited asphaltene film calculated by the root mean square average of height deviations is less than 1 nm, indicating that the surface is sufficiently smooth for AFM colloidal force measurement.

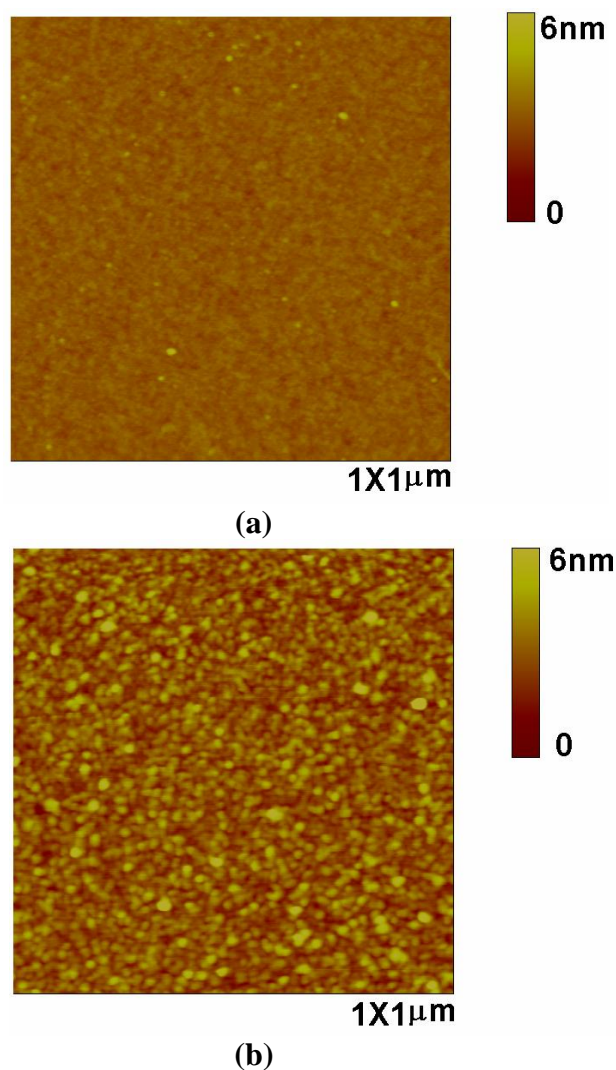


Figure 4.1. AFM image of (a) bare silica surface and (b) asphaltene film

#### 4.3.2 Interaction forces in toluene (good solvent)

Figure 4.2 shows the interaction forces upon approach measured between an asphaltene substrate and a bare silica probe (open circles) or a bare silica substrate and an asphaltene probe (filled triangles) in toluene. The two force profiles are almost identical, exhibiting long range repulsion. In contrast, a purely attractive force profile attributable to van der Waals forces was obtained between silica substrate and silica probe (filled circles). This finding indicates successful and

similar coatings of asphaltene films on the silica probe as well as on silica substrate.

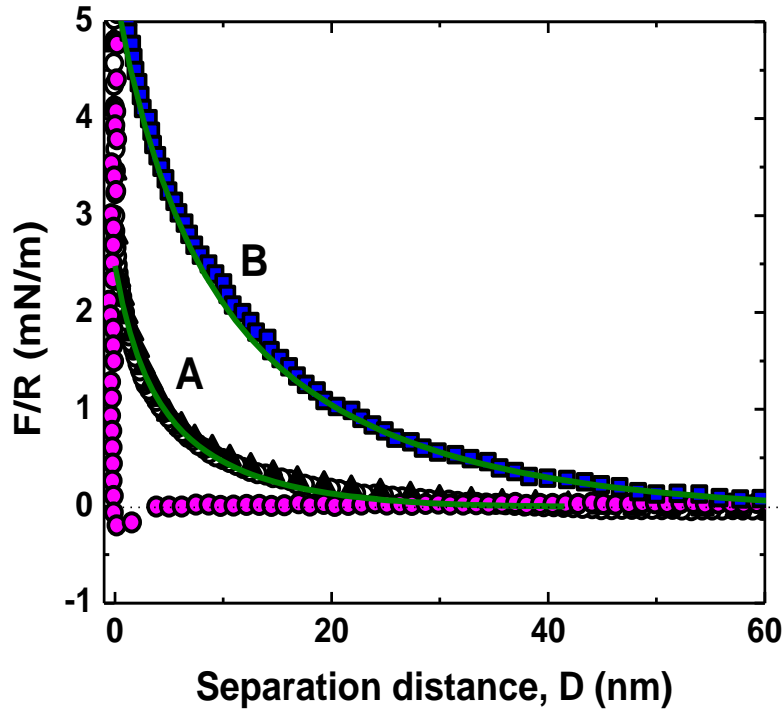


Figure 4.2. Interaction forces upon approach between two asphaltene surfaces as well as an asphaltene surface and a bare silica surface in toluene. ■: Interactions between two asphaltene surfaces; ●: Interactions between two bare silica surfaces; ▲: Interactions between a silica substrate – an asphaltene probe; ○: Interactions between an asphaltene substrate – a silica probe; Green solid lines: scaling theory fitted curves

Since asphaltene molecules are highly soluble in toluene, the tails and loops of immobilized asphaltene molecules on the hydrophilic silica surface tend to stretch and repel each other to form a swollen brush, leading to a steric repulsive force when a brush-like surface approaches a bare silica surface. As illustrated in Chapter 3, the steric repulsive force between two asphaltene coated silica surfaces can be analyzed by the scaling theory expressed in equation (3-6). For the situation of an asphaltene coated surface and a bare silica surface, we simply substituted  $(D + \xi)/L_o$  for  $(D + 2\xi)/2L_o$  in equation (3-6).

$$\frac{F(D)}{R} = \frac{16\pi kTL_o}{35s^3} \left[ 7 \left( \frac{D+\xi}{L_o} \right)^{-5/4} + 5 \left( \frac{D+\xi}{L_o} \right)^{7/4} - 12 \right] \quad \text{for } (D+\xi) < L_o \quad (4-1)$$

where the symbols are the same as equation (3-6).

As can be seen in Figure 4.2, a very good fit (solid curve A) was obtained with a tail length,  $L_o$ , of about 47 nm as listed in Table 4.1.

Table 4.1. Fitting parameters by scaling theory of repulsive force profiles in Figure 4.2

	Asphaltene surface and bare silica surface, (A)	Two asphaltene surfaces, (B)
$\xi$ , nm	6	5.5
$s$ , nm	16	21
$L_o$ , nm	47	47

The interaction forces upon approach between two asphaltene surfaces in toluene have been well characterized in Chapter 3.<sup>251</sup> For comparison, the force profile between two asphaltene surfaces in toluene was also plotted in Figure 4.2 (filled squares). With two asphaltene surfaces, the repulsive force was further extended to a much larger separation distance, which can be well fitted by equation (4-1) (solid curve B) with the fitting parameters listed in Table 4.1. The best fitted values of physical parameters in Table 4.1 show that the fitted tail lengths in two cases of an asphaltene surface against a bare silica surface or another asphaltene surface are identical, although there are slight differences in  $\xi$  and  $s$  values.

### 4.3.3 Interaction forces in heptane (poor solvent)

Since asphaltenes (amphiphilic) and heptane (apolar) are significantly different in molecular structure (highly aromatic of hetero-atoms vs aliphatic), the asphaltene molecules tend to self-associate, aggregate and precipitate in n-heptane.



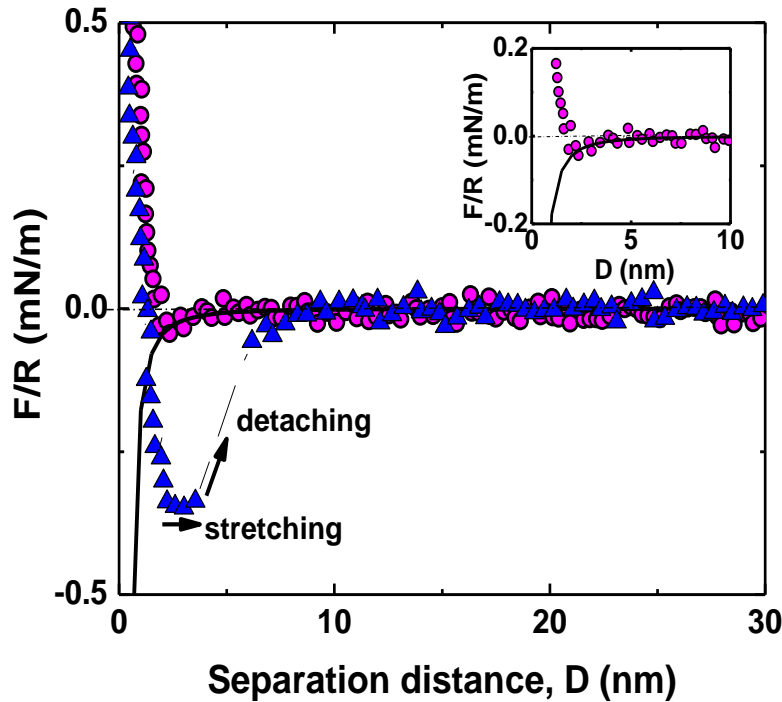


Figure 4.3. Interactions between asphaltene surfaces in *n*-heptane. ●: Approach force; ▲: Retraction force/adhesion force; Solid lines: calculated van der Waals forces between asphaltene surfaces in heptane with a Hamaker constant  $A_{eff}=1.1\times 10^{-21}$  J

As shown in Figure 4.3, the force profile of two asphaltene layers in heptane exhibited a weak long range attraction force when approaching each other and a weak adhesion force when separating the two surfaces. Since heptane is an apolar solvent, the electric double layer forces in heptane, similar to toluene,<sup>251</sup> are negligible. It is also unlikely that the depletion effect causes the attraction, which occurs in a system with suspended, nonadsorbing species in a liquid,<sup>252</sup> while in this study, the force measurement was carried out in pure heptols and asphaltenes do not partition in heptol. As state previously, the dominant forces between asphaltenes in heptane arose from van der Waals forces.<sup>80, 89, 119, 120</sup> The van der Waals forces between a sphere and flat surface can be calculated using Derjaguin's approximation:<sup>188</sup>

$$\frac{F_{vdW}}{R} = \frac{A_{eff}}{6D^2} \quad (4-2)$$

where  $R$  is the radius of the sphere in m,  $D$  is the closest separation distance between the sphere and the flat surface in m, and  $A_{eff}$  is the effective Hamaker constant of the system calculated by:  $A_{eff} = \sqrt{A_{heptane}} - \sqrt{A_{asphaltene}}$ .<sup>2</sup> In fact, the measured attractive force can be well fitted by van der Waals forces with an effective Hamaker constant ( $A_{eff}$ ) of  $1.1 \times 10^{-21}$  J,<sup>188, 241, 253</sup> as shown by the solid curve in Figure 4.3. This observation indicates that the van der Waals forces are indeed the dominant forces leading to asphaltene flocculation in paraffinic solvents. It is therefore not surprising to observe a weak adhesion force of the origin of van der Waals forces between the two asphaltene layers in n-heptane. It is interesting to note a short range stretching before detaching the two surfaces (as indicated by arrows in Figure 4.3) when separating them, indicating some degree of association between the side-chains on the two surfaces in contact.

#### 4.3.4 Interaction forces in heptol

The interaction forces between asphaltene surfaces in a mixture of toluene and heptane (heptol) were measured at different toluene volume fractions ( $\Phi_T = 0$  (heptane), 0.2, 0.3, 0.5, 0.7, and 1 (toluene)). As shown in Figure 4.4, the approach force profiles are highly sensitive to the composition of the solvent and the transition of force profiles from repulsive to attractive occurred at  $\Phi_T \leq 0.2$ . With  $\Phi_T \leq 0.2$ , a weak attraction as shown in the insert of Figure 4.4 was detected. When  $\Phi_T > 0.2$ , repulsive forces appeared. The range and magnitude of the repulsive forces increased with toluene volume fraction. It is interesting to note

that the repulsive forces can be well fitted with the scaling theory, as shown by the solid lines in Figure 4.4.

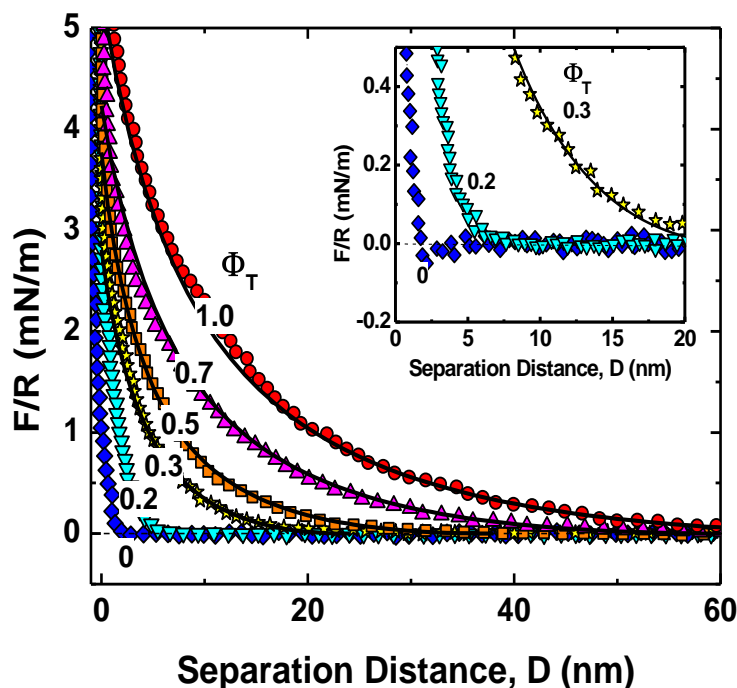


Figure 4.4. Interactions between asphaltene surfaces upon approach in heptol. Symbols: AFM experimental data for different  $\Phi_T$ ; Solid lines: scaling theory fitting of force curve ( $\Phi_T$  in the range of 0.3 to 1.0)

The adhesion force measured by AFM as a function of toluene volume fraction  $\Phi_T$  is shown in Figure 4.5. In pure heptane ( $\Phi_T = 0$ ), the adhesion force is about 0.3 mN/m and decreased sharply to about 0.13 mN/m for  $\Phi_T = 0.2$ . Above a value of 0.2, the adhesion force remained relatively constant for  $\Phi_T = 0.2$  to 0.7 and finally decreased to almost zero in pure toluene. The change of adhesion force with heptol composition agrees well with the long range force profiles. For  $\Phi_T < 0.2$ , heptol is a poor solvent and there was stronger adhesion between asphaltenes. While in a good solvent of pure toluene, the adhesion force was almost zero. For heptol with toluene fraction from  $\Phi_T = 0.2$  to 0.7, the solvency of

heptol gradually increased exhibiting relatively constant adhesion force. It appears that in poor solvents, asphaltenes-asphaltenes interactions are stronger than asphaltenes-heptol interactions, leading to stronger adhesion between asphaltene surfaces. Our study clearly shows that tuning the composition of heptol allows fine control of colloidal forces between asphaltene surfaces in an organic solvent.

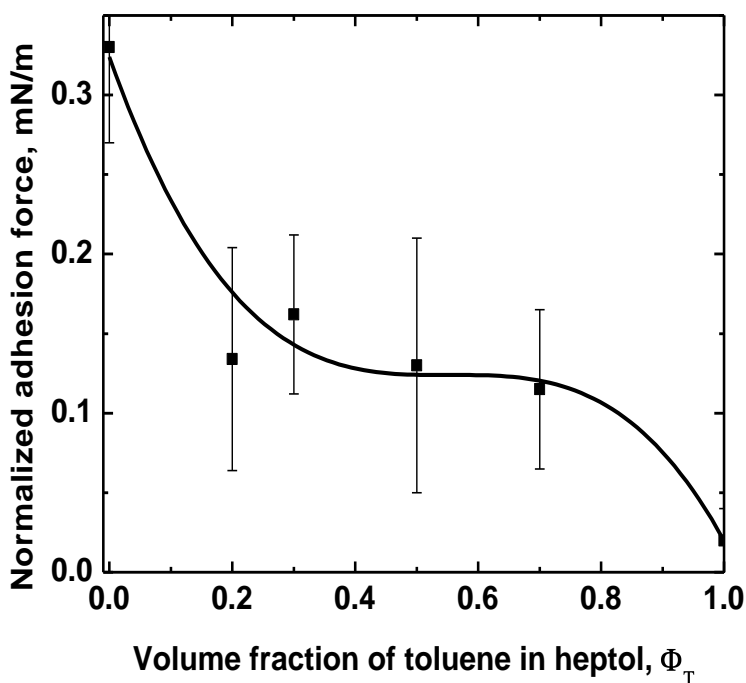


Figure 4.5. Adhesion force as a function of  $\Phi_T$ . Symbols: experimental data; Solid line: fitted trend line

#### 4.3.5 Langmuir compression isotherms of asphaltene interfacial films

To better understand the measured force profiles of asphaltenes in heptol of varying composition, the interfacial pressure-area isotherms of asphaltene monolayers (at heptol compositions of  $\Phi_T = 0, 0.1, 0.25, 0.8$  and 1) were determined. The results in Figure 4.6 showed that the behavior of asphaltene monolayer at the heptol/water interface changed with changing heptol composition. At a toluene volume fraction of  $\Phi_T < 0.25$ , the asphaltene

monolayers buckled under a high degree of compression brought by the two symmetric barriers. After a critical point ( $A_c, \pi_c$ ) as indicated in Figure 4.6, the asphaltene monolayers began to fold at the heptol/water interface for  $\Phi_T < 0.25$ . The critical point ( $A_c, \pi_c$ ) at which an asphaltene monolayer begins to buckle was found to be a function of the toluene volume fraction ( $\Phi_T$ ). At a higher toluene volume fraction of  $\Phi_T \geq 0.8$ , no buckling of asphaltene monolayers was observed. These results show that the rigidity of an asphaltene monolayer increases with decreasing toluene volume fraction in heptol, i.e. an asphaltene monolayer is more rigid and compact at a heptol/water interface with a higher content of heptane. The observed variation in rigidity and buckling of the asphaltene monolayers at heptol-water interface is consistent with that observed by Zhang et al.<sup>161</sup>

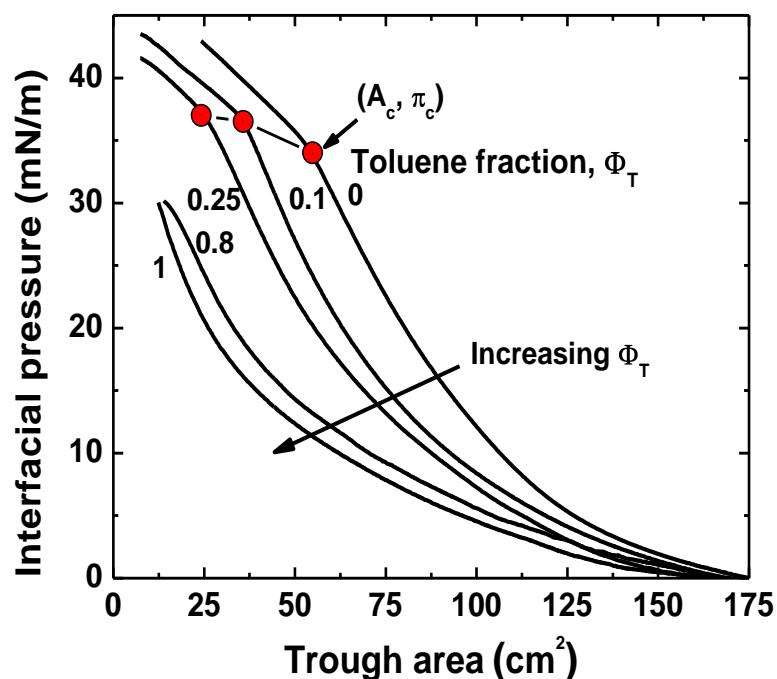


Figure 4.6. Interfacial pressure-area isotherms for asphaltene monolayers at various heptol/water interfaces with a toluene volume fraction ( $\Phi_T$ ) of 0, 0.1, 0.25, 0.8, and 1

## 4.4 Discussion

### 4.4.1 Nature of forces between asphaltene surfaces in heptol

We showed that the interactions between asphaltene surfaces upon approach can be attractive or repulsive, depending on the quality of the solvent (Figure 4.4). The repulsive forces between asphaltenes in heptol of  $\Phi_T > 0.2$  are of steric nature and the electrical double layer force is negligible. The attractive force measured in heptane can be well fitted with only van der Waals forces (Figure 4.3). These observations indicate that heptol of  $\Phi_T > 0.2$  is a good solvent, whereas heptol of  $\Phi_T < 0.2$  is a poor solvent for asphaltenes. In good solvents, the immobilized asphaltenes repel each other due to steric repulsion caused by the swelling side-chains. In poor solvents, on the other hand, the immobilized asphaltenes attract to each other by van der Waals forces, leading to asphaltene aggregation and precipitation. It should be noted that in this study, the attraction between asphaltene surfaces was observed at  $\Phi_T < 0.2$ , which does not mean that only at  $\Phi_T < 0.2$  can asphaltenes precipitate in heptol. At  $\Phi_T < 0.5$ , the generally accepted heptol composition at which onset of asphaltenes was observed, it is possible that some asphaltene molecules in the asphaltene films have already been in a “precipitated” or compact state, but there are still some asphaltene molecules in the asphaltene films soluble in heptol. The latter part of asphaltenes generates a repulsive force until at  $\Phi_T < 0.2$  the overall interactions between asphaltenes are attractive.

Since attractive van der Waals forces are omnipresent in asphaltene/heptol system, it would be interesting to investigate the variation of van der Waals forces with

the solvent composition. From equation (4-2), we know that  $F_{vdW}$  is directly proportional to  $A_{eff}$ . For the purpose of simplicity, only  $A_{eff}$  is calculated and compared in this study. By definition,

$$A_{eff} = \sqrt{A_{heptol}} - \sqrt{A_{asphaltene}}^2 \quad (4-3)$$

in which the Hamaker constant of heptol is calculated on a volume average basis:

$$A_{heptol} = \sum \Phi_i A_{ii}, \text{ with } i = T \text{ for toluene and } i = H \text{ for heptane. The Hamaker}$$

constants of n-heptane and toluene in air are well documented to be

$$A_{heptane} = 4.5 \times 10^{-20} \text{ J and } A_{toluene} = 5.4 \times 10^{-20} \text{ J.}^{188} \text{ As reported by Fotland et al., the}$$

Hamaker constant of asphaltenes in air is about  $6.0 \times 10^{-20} \text{ J.}^{253}$

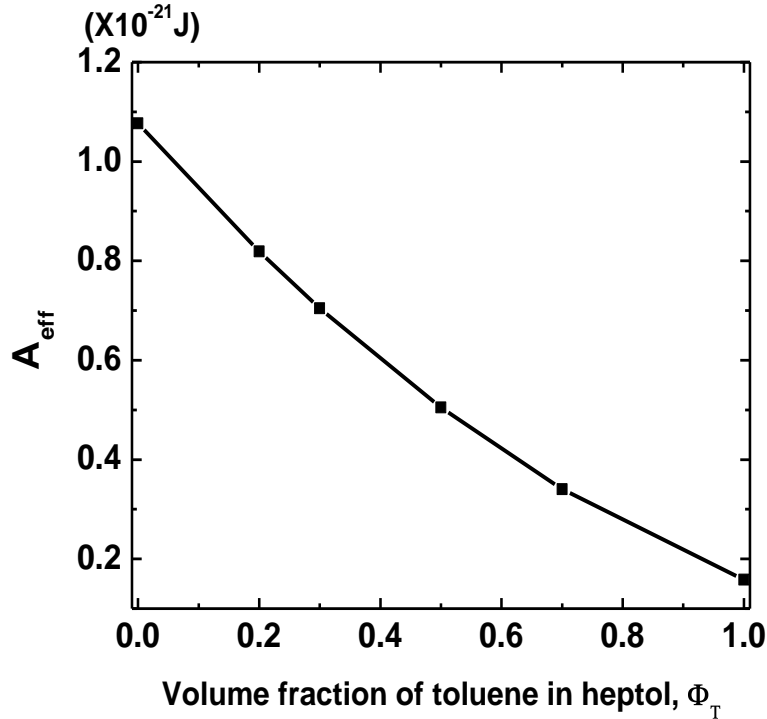


Figure 4.7. Effective Hamaker constant of asphaltenes-heptol-asphaltenes system, as a function of toluene fraction in heptol ( $\Phi_T$ )

The calculated results of  $A_{eff}$  in Figure 4.7 showed a gradual decrease in  $A_{eff}$  of asphaltenes-heptol-asphaltenes system with increasing toluene volume fraction in

heptol ( $\Phi_T$ ), demonstrating a decreased van der Waals attraction with increasing  $\Phi_T$ . The reduction of van der Waals forces with increasing  $\Phi_T$  would contribute to reduced adhesion and hence less aggregation/flocculation of asphaltenes in toluene-rich heptol (Figure 4.5).

However, it is clear from Figures 4.4 and 4.7 that the contribution of van der Waals forces to the total force when  $\Phi_T > 0.2$  is negligible. The dominant force between the asphaltene surfaces in heptol with  $\Phi_T > 0.2$  is steric repulsion which was well fitted with scaling theory of polymer brushes as was shown in Figures 4.2 and 4.4. The fitted parameters of the repulsive forces changed gradually with heptol composition, as shown in Figure 4.8. It is evident that the fitted tail length  $L_o$  of asphaltenes increased with increasing  $\Phi_T$ . The results in Figure 4.8 indicate that asphaltene tails would be collapsed at a  $\Phi_T < 0.2$ , around which the force profiles changed from repulsive to attractive. Figure 4.8 also shows an increase in the apparent average spacing between two grafted points with increasing  $\Phi_T$ , while the thickness of the compressed asphaltene layer increased for a given loading force of the AFM probe. This observation would indicate that in heptols with high  $\Phi_T$ , the asphaltene would swell and extend outwards away from the solid surface, while still being anchored on the silica surface by the polar functional groups of asphaltene molecules. Moving towards poor solvent with decreasing toluene volume fraction in heptol would make the environment less favorable for asphaltene molecules to stretch. Rather, the asphaltenes tend to condense to form a more compact layer. This conformational change of the



immobilized asphaltene with changing the quality of heptol is shown schematically in Figure 4.9.

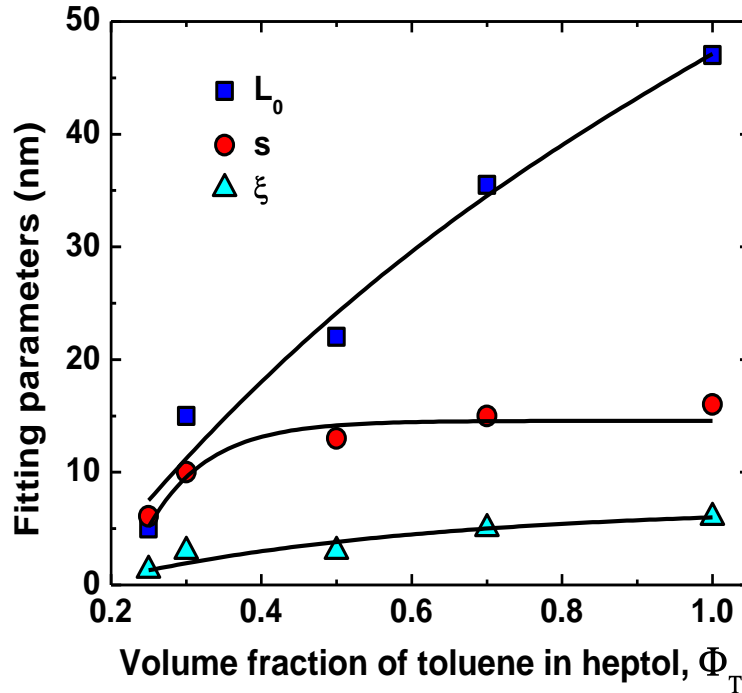


Figure 4.8. Fitting parameters in equation (4-1) as a function of toluene fraction in heptol ( $\Phi_T$ ). Symbols: experimental data; Solid lines: trend lines

Figure 4.8 also shows that in heptol with  $\Phi_T < 0.5$ , the fitted thickness  $\xi$  of an immobilized asphaltene layer is less than 4nm which is the asphaltene thickness value measured by ellipsometry in air. Recalling the definition of  $\xi$  mentioned above, the  $\xi$  value in Figure 4.8 does not represent the overall thickness of the immobilized asphaltene layers, but only that of the compressible side-chains. With decreasing the volume fraction of toluene in heptol, the solvent becomes less favorable for the stretching of asphaltene molecules. Parts of asphaltenes have aggregated with the polar segments shielded inside the aggregates. As a result, part of the asphaltene layer could be rigid and the others flexible (Figure 4.9). Only the flexible parts such as the side-chains can be compressed, while the

rigid parts do not contribute to the measured thickness of compression but behave like a solid substrate. The reduced flexibility of the asphaltene layers with decreasing  $\Phi_T$  was confirmed by the isotherms of the Langmuir trough compression experiments shown in Figure 4.6.

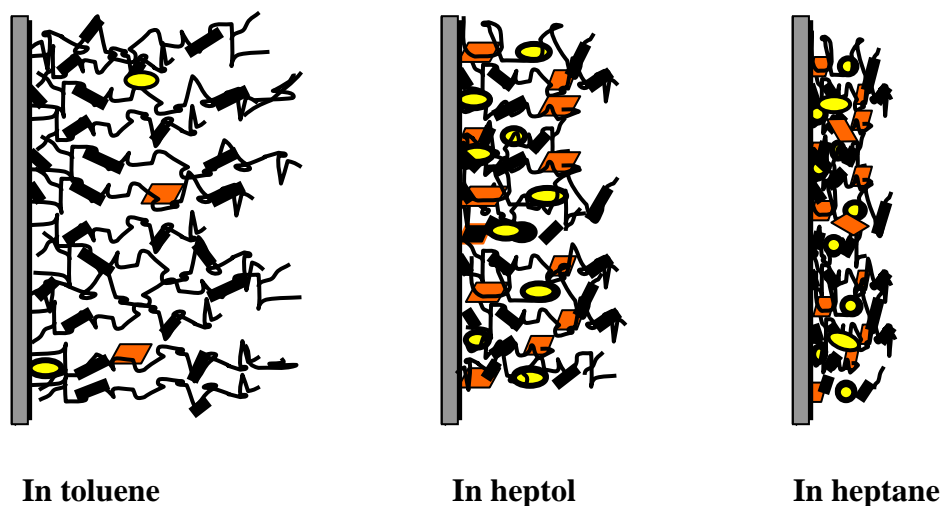


Figure 4.9. Schematic plot of conformational transition of asphaltene layers with  $\Phi_T$  of heptol ( represent the fused aromatic ring sheet or consolidated part of asphaltenes)

As shown above, the composition of the organic phase in terms of its aromaticity can significantly affect the interactions between immobilized asphaltene surfaces. This finding suggests that the interactions between asphaltenes in an organic solvent are linked to the quality of the solvent. In the following text, we will attempt to make use of interaction parameters between asphaltenes and heptols to elucidate the results of the AFM force measurements.

#### 4.4.2 Relation between solution quality and interaction forces

Since asphaltenes are a solubility class, the variation of the measured interaction forces between asphaltenes in heptol of varying solvent quality can be interpreted

in the context of solubility compatibility of the system. The interaction parameter  $\chi$ , a parameter describing the stability behavior of polymer solutions, can be applied to the asphaltene-heptol system. Although  $\chi$  is defined for polymer solutions, its application to the asphaltene-heptol system has its legitimate basis as described in previous text. In this work, the  $\chi$  value between asphaltenes and heptol is calculated to help interpret the effect of solvent quality on the interaction forces between asphaltene surfaces in heptol. By combining the solubility parameter  $\delta$  and F-H model,  $\chi$  can be calculated (using  $\delta_{heptol}$  of the components made up of a binary mixture):

$$\chi = V_{heptol} (\delta_{asp} - \delta_{heptol})^2 / R_{gas} T \quad (4-4)$$

where  $V_{heptol}$  in  $\text{m}^3/\text{mol}$  is the molar volume of the solvent heptol,  $\delta_{asp}$  and  $\delta_{heptol}$  are the Hildebrand solubility parameters in  $\text{MPa}^{1/2}$  of asphaltenes and heptol, respectively,  $T$  is temperature in degrees Kelvin, and  $R_{gas}$  is universal gas constant in  $\text{J}\cdot\text{mol}^{-1}\cdot\text{K}^{-1}$ .  $\chi$  is a dimensionless parameter which characterizes the differences of interaction energy between asphaltene and solvent molecules in comparison with those between the pure components. From equation (4-4), we know that more compatible solute and solvent would lead to smaller  $\chi$  values as they tend to have comparable solubility parameters. To evaluate  $\chi$  for asphaltene-heptol system, there are three parameters to be determined:  $V_{heptol}$ ,  $\delta_{asp}$  and  $\delta_{heptol}$ . The solubility parameter of heptol,  $\delta_{heptol}$ , is computed on a volume average basis of toluene and n-heptane:<sup>254</sup>

$$\delta_{heptol} = \Phi_{heptane} \delta_{heptane} + \Phi_{toluene} \delta_{toluene} \quad (4-5)$$

The molar volume of heptol is calculated on a molar average basis:

$$V_{heptol} = y_{heptane} V_{heptane} + y_{toluene} V_{toluene} \quad (4-6)$$

where  $y_i$  is mole fraction of heptane or toluene.

The Hildebrand solubility parameter of asphaltenes is hard to determine since asphaltenes are a complex molecular mixture containing over tens of thousands of molecular species with varying solubility parameters. However, by definition, asphaltenes are a solubility class, which means that the solubility parameters of the asphaltene species fall within a relatively narrow range, despite their wide range of molecular structure and composition. Thus an average and representative solubility parameter can be used in equation (4-5) without sacrificing too much of scientific insights when interpreting the results. The Hildebrand solubility parameter,  $\delta_{asp}$ , of asphaltenes has been determined both experimentally and theoretically. The reported values in the open literature range from 19 to 22 MPa<sup>1/2</sup>.<sup>127, 135, 139</sup> Thus, for the petroleum asphaltenes precipitated by n-heptane, a value of 20 MPa<sup>1/2</sup> would be a satisfactory approximation and was used in this study. In the calculation of  $\chi$ , Hildebrand solubility parameters of solvents were used: 18.3 MPa<sup>1/2</sup> for toluene and 15.3 MPa<sup>1/2</sup> for heptane.<sup>255</sup>

The calculated  $\chi$  value as shown in Figure 4.10 decreases with increasing toluene volume fraction in heptol ( $\Phi_T$ ). As mentioned early, a smaller  $\chi$  value would represent a more miscible environment of the asphaltenes with the solvents. Thus the results of Figure 4.10 suggest that in heptol of higher toluene volume fraction ( $\Phi_T$ ) and hence a lower  $\chi$  value, the solvent phase is favorable for asphaltene molecules which are well solvated by the solvent molecules due to similar

interactions between aromatic rings in asphaltene molecules. In this case, asphaltene molecules are free to swell and consequently exhibit a steric repulsion among the swelled tails and loops. With decreasing  $\Phi_T$ , the solvent became more aliphatic and apolar, an environment unfavorable for highly poly-aromatic asphaltene molecules. As a result,  $\chi$  value increased due to the enlarged difference in the interaction energy of solvent with asphaltenes and with the solvent. Under such an unfavorable condition, the asphaltene molecules tend to stay together, leading to an attraction as detected by AFM force measurements. The transition of the interaction force between asphaltene surfaces in heptol from repulsion to attraction corresponds to a  $\chi$  value of about 1.0.

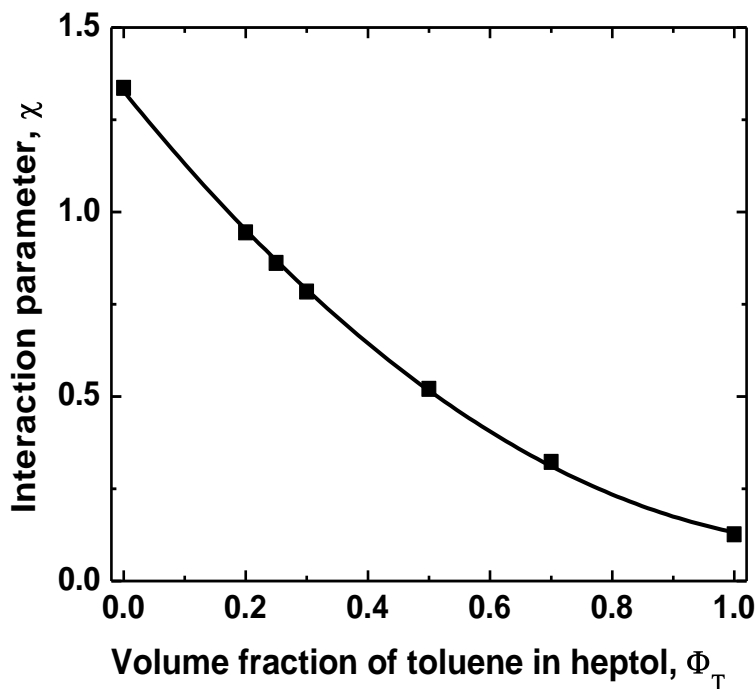


Figure 4.10. Interaction parameter of asphaltene/heptol as a function of  $\Phi_T$  of heptol

It is evident that the calculated interaction parameter  $\chi$  conforms well to the results of AFM force measurements with a clear correlation between adhesion

forces and  $\chi$  value: a system of larger  $\chi$  value leads to a larger adhesion as shown in Figure 4.11. The plot also indicates that the relatively constant adhesion force plateau (0.13 mN/m) occurs in a range of  $\chi = 0.3$  to 1.0. At lower  $\chi$  values, the adhesion force decreased sharply and became negligible ( $\chi$  is below 0.1 from Figure 4.11), indicating a system absent of asphaltene aggregation.

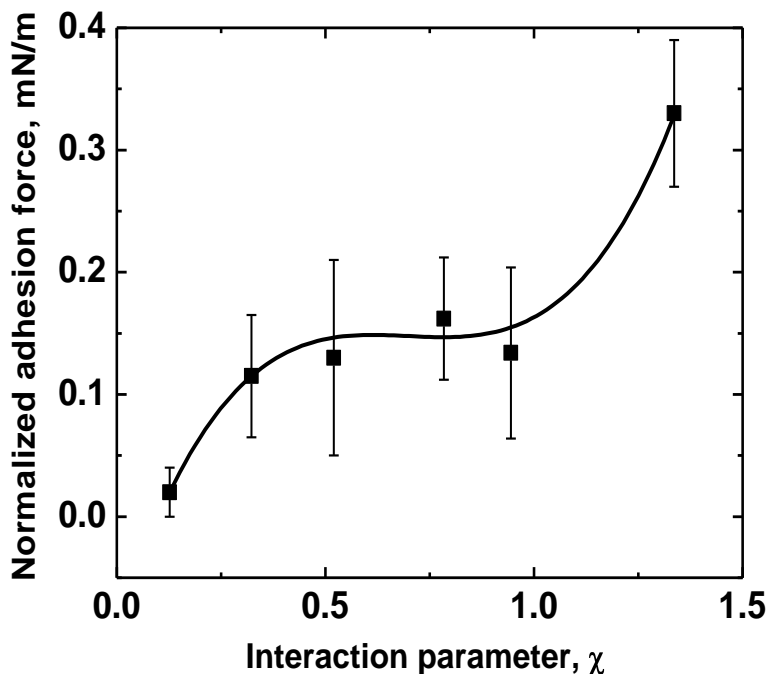


Figure 4.11. Relationship of adhesion force to interaction parameter of asphaltenes-heptol

#### 4.5 Conclusions

The colloidal forces between LB asphaltene films in heptol of varying volume fraction of toluene were measured using AFM colloidal probe technique. The AFM force measurements provide a direct evaluation on molecular interactions of asphaltenes in organic solvents, indicating directly the molecular aggregation/flocculation of asphaltenes in various solvent mixtures of toluene-heptane. The estimation of the interaction parameter of heptol with asphaltene

provides an alternative to evaluate the strength of interaction between asphaltene-asphaltene in heptol. By combining the results, the nature of asphaltene interaction in organic solvents was revealed. The following conclusions are drawn from this study.

The composition of the organic solvent has a significant impact on the nature of colloidal forces between asphaltene surfaces. By increasing toluene content in heptol,  $\Phi_T$ , the interaction forces change from attractive to repulsive. In the good solvents (heptols with  $\Phi_T$  greater than 0.2), the repulsion originates from the steric forces and the force profiles can be well described with the scaling theory of polymer brushes. In the poor solvents (heptol with  $\Phi_T$  less than 0.2), van der Waals attraction was determined to be the driving force for asphaltene aggregation and precipitation. The influence of van der Waals forces on molecular aggregation wanes with increasing  $\Phi_T$ .

The interaction parameter  $\chi$  between asphaltenes and heptol was calculated according to Flory-Huggins model. The  $\chi$  value was found to decrease with increasing  $\Phi_T$ , indicating relatively similar molecular interactions between poly-aromatic asphaltenes and major components of toluene in heptol as a good solvent (high  $\Phi_T$ ). Such interactions lead to swelling of asphaltene molecules giving rise to repulsive interaction between asphaltene films in a good solvent. The results conform well to the AFM force measurements. It was estimated that a  $\chi$  value of less than 0.1 is required to avoid asphaltene aggregation in organic solvents where adhesion force approaches zero.

# Chapter 5 Wettability Control Mechanism of Highly Contaminated Hydrophilic Silica/Alumina Surfaces by an Ethyl Cellulose\*

## 5.1 Introduction

Wettability of solids is known to play a critical role in many natural and industry processes, in particular in the area of life science and nanotechnology. For example, protein adsorption is largely controlled by hydrophobic interactions which greatly depend on the wettability of the surface on which protein adsorbs.<sup>256, 257</sup> The design of a super-hydrophobic surface similar to that of lotus leaf is of special interest in nanotechnology for the development of self-cleaning materials.<sup>258, 259</sup> During heavy oil processing, for example, two main challenges: demulsification of water-in-oil emulsions and removal of organic-contaminated solids, are both related to surface wettability. The organic-rich solids and emulsified water droplets, both oil wettable, are detrimental to downstream operation and need to be removed.<sup>7, 11</sup> Although chemical addition can be used to help break water-in-oil (w/o) emulsions,<sup>160</sup> solids removal usually depends on enhanced mechanical forces by, for example, centrifugation. The difficulty of both demulsification and solids removal is magnified by the presence of an extremely viscous, solids-stabilized rag layer in the form of mixed emulsions.<sup>3-5, 25</sup> In our previous study,<sup>155</sup> biodegradable ethyl cellulose (EC) was found to be an effective demulsifier for breaking water-in-diluted bitumen emulsions.<sup>155, 169</sup> The

---

\* Submitted paper: Wang, S.; Segin N.; Wang K.; Masliyah, J.; Xu, Z. *Journal of Physical Chemistry C*



addition of EC to the organic phase was found to cause a significant reduction in diluted bitumen-water interfacial tension. Water droplets were shown to flocculate and coalesce in diluted bitumen solutions containing EC, depending on EC concentration. In this study, we investigate the potential of EC as a wettability modifier of solids from oil-wet to water-wet in the context of heavy oil processing. The effect of EC addition on wettability of asphaltene- or bitumen-contaminated hydrophilic silica and alumina surfaces is determined by contact angle measurements. The mechanism of wettability alteration by EC addition was determined by atomic force microscope (AFM) imaging before and after soaking both hydrophilic silica and alumina surfaces with pre-adsorbed asphaltenes or bitumen in EC-containing toluene solutions for varying periods of time.

In heavy oil processing, the presence of oil-wet and bi-wettable solids usually causes the most challenging problems in water-in-oil (w/o) emulsions.<sup>7-9, 29, 166</sup>

These solids can accumulate at oil-water interface to cause Pickering-enhanced stabilization of w/o emulsions. As measured by Wu et al., solids occupy about 21% of the interfacial materials that stabilize w/o emulsions.<sup>6</sup> Highly water-wettable solids are known to contribute little to destabilization of w/o emulsions.

A combination of asphaltenes and solids leads to the most stable w/o emulsions.<sup>164, 260-262</sup> Fine water droplets stabilized by oil-wet solids and

asphaltenes tend to accumulate between the bulk water and heavy oil (diluted-bitumen) phases, forming a distinct intermediate layer of extremely high viscosity.

This layer is known as rag (sludge) layer which hinders effective water-oil phase separation.<sup>4-6, 164, 165, 260</sup> Oil-wet solids are naturally carried over to the oil phase,

which may cause equipment fouling and/or catalyst poisoning in downstream refining process.<sup>8</sup> The organic-rich solids mainly consist of ultra-fine aluminosilicate clay particles that are originally hydrophilic. Due to contact with heavy oil in reservoir or during oil processing, a layer of “asphaltene-like” organic materials is anchored/attached to the surface of the initially hydrophilic solids.<sup>8, 9</sup> Resins can also adsorb on hydrophilic surfaces, but their adsorption could be highly reversible. When switching to a good solvent, the adsorbed resins gradually desorb, making the solids less hydrophobic.<sup>168</sup> Removal of highly contaminated and hence hydrophobic solids can be extremely challenging even with centrifuges, since the particle size of clays can be as small as a few tenths of microns.<sup>7</sup> When the contaminated solids are washed with good solvents such as toluene or naphtha, not all the organic contaminants can be removed due to irreversible adsorption of heavy petroleum components such as asphaltenes on the clays surface.<sup>8, 9</sup> It is therefore of great importance to increase wettability of contaminated (oil-wet) solids in an oil phase so that they can migrate to the aqueous phase and become inactive in stabilizing w/o emulsions.

Adding a chemical modifier to make solid surfaces more water-wettable can enhance solids partitioning into the aqueous phase. For a chemical modifier to increase wettability of organic-rich solids in heavy oil processing, it has to be soluble in the heavy oil for delivery and either adsorb on top of the contaminating organics or displace the organic contaminants from the solid surface. To achieve the purpose of surface alteration, the chemical modifier has to be amphiphilic and of large molecular weight so that its hydrophobic segments may bind with the

hydrophobic contaminants on the solids surface. In this manner, the hydrophilic segments (groups) are exposed to the liquids, leading to the formation of hydrophilic particles, as schematically shown in Figure 5.1a. However, this conformation of chemical modifier is entropically unfavourable in a bulk oil phase in which most of the molecules are apolar. Preferably, the modifier has functional groups that can compete for the hydrophilic binding sites on the solid substrate with the contaminating organic species, thereby displacing the hydrophobic contaminants from the solid surface, as schematically shown in Figure 5.1b. In this case, it is extremely important to control the number of hydrophilic groups so that a sufficient number of active hydrophilic groups are available upon adsorption to make the solid surface hydrophilic.

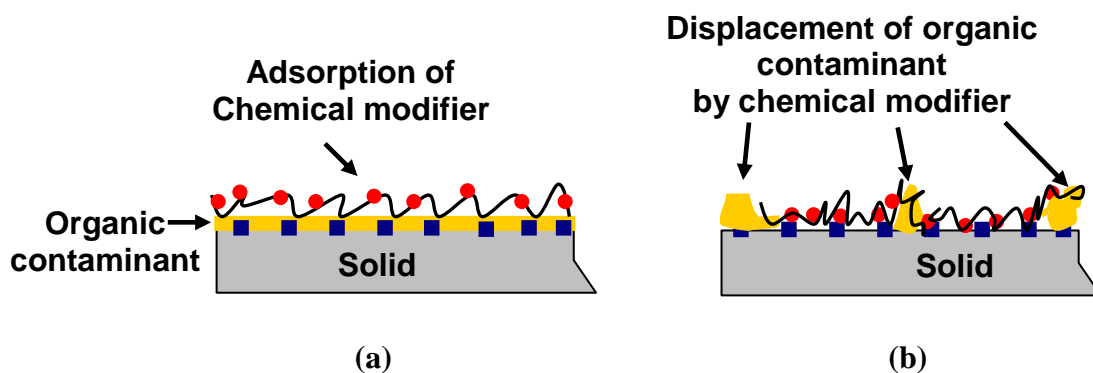


Figure 5.1. Effect of amphiphilic chemical modifier on organic contaminated solid surface (red circles and blue squares are polar groups on chemical modifier and solid surface, respectively). (a) Chemical modifiers adsorb on the top of organic contaminants through non-specific interaction and leave the polar segments exposed; (b) Chemical modifiers displace the organic contaminant and adsorb on the solid surface

In addition, with oil as the continuous phase, the chemical modifier has to be delivered through the oil phase. Thus an oil-soluble, amphiphilic modifier is needed. A demulsifier that adsorbs at w/o interfaces is a good candidate for this

purpose. Fundamentally, the demulsifier weakens the interfacial film by penetrating the original protective film and displacing the interfacial materials while its presence at the interface provides an opportunity for water droplet flocculation and/or coalescence.<sup>160</sup> A similar mechanism can be applied to a solid-oil interface for wettability modification. In this case, the demulsifier needs to access the binding sites such as -OH groups on hydrophilic silica and alumina surfaces; similar to those occurred at a water-oil interface. For breaking w/o emulsions and avoiding formation of rag layers, demulsifiers should modify both the surface properties of the solids in the bulk oil phase and the oil-water interfacial properties.

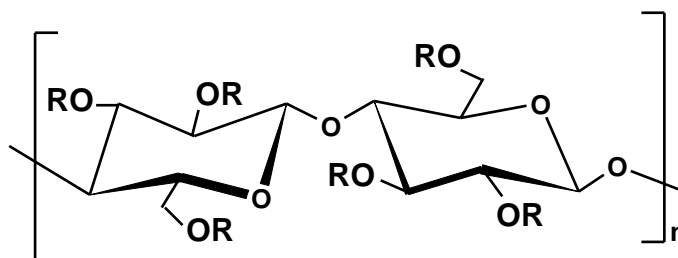


Figure 5.2. Molecular structure of ethyl cellulose (EC)<sup>169</sup>

As reported previously, EC is an effective demulsifier for water-in-diluted bitumen emulsions.<sup>155, 169</sup> It is a linear polymer with a backbone of cellulose structure (Figure 5.2). The side hydroxyl groups on the backbone are partly substituted by ethoxyl groups, making EC oil-soluble while maintaining its amphiphilic nature. The ethoxyl side groups are relatively short and separated by a linkage oxygen atom between glucose rings such that the intermolecular

association of EC molecules is minimized to avoid the formation of hydrophobic layers once adsorbed on solid surfaces through hydrogen bonds between hydroxyl groups and oxygen atoms in EC chains and on solid surfaces. These molecular characteristics of EC make it an ideal candidate for our purpose of exploring its ability to increase wettability of heavy oil-contaminated solids in heavy oil processing.

## **5.2 Experimental**

In the current study, silica and alumina were chosen as the solid surfaces to be investigated as they represent the basic components of clays. Asphaltenes represent the heaviest components of heavy oil and are known to be the major components contaminating solids in heavy oil. Asphaltenes as well as bitumen are therefore used, as the organic materials to contaminate solid surfaces. Quartz crystal microbalance with dissipation function (QCM-D) was used to determine the adsorption of EC in toluene solutions on asphaltenes pre-adsorbed on silica and alumina surfaces. During the soaking experiments, hydrophilic silica surfaces were dip-coated with a layer of asphaltenes or bitumen, and then immersed in EC-in-toluene solutions for a varying period of time. The contact angle of a water droplet on the treated surfaces was measured and the nano resolution morphology of the treated surfaces was determined by AFM. Langmuir isotherms were obtained for asphaltenes+EC films at toluene/water interface to compensate for the results acquired at solid/oil interface. All of the experiments were conducted to explore the potential and mechanisms of EC in increasing the water-wettability of the organic-contaminated solids in heavy oil.

### **5.2.1 Materials and chemicals**

Asphaltenes in vacuum distillation feed bitumen, provided by Syncrude Canada Ltd, were precipitated according to the procedure described in Chapter 2.1. Ethyl cellulose (EC), purchased from Sigma-Aldrich, was used as received. Properties of EC can be found in Chapter 2.1. HPLC grade toluene, purchased from Fisher Scientific, was used as the solvent. Three types of alkylchlorosilanes (dimethyldichlorosilane, butyltrichlorosilane and octyltrichlorosilane) from Fisher Scientific were used as silane coupling agent to modify the hydrophilic silica surface to become hydrophobic. Milli-Q water was used in the water contact angle measurements.

Silica wafers purchased from NanoFab (University of Alberta, Canada), and alumina wafers (University wafer, Massachusetts, USA) of finish C-plane were used as the model solids to represent building blocks of clays. Prior to their use, silica and alumina wafers were cut into 1 cm by 1 cm square pieces and cleaned according to the procedure described in Chapter 2.1.

### **5.2.2 Preparation of hydrophobic silica surfaces**

To evaluate the effect of EC on the wettability of the chemically-hydrophobized solid surfaces, the hydrophilic silica wafers were hydrophobized chemically by immersion in 5 mM alkylchlorosilane-in-toluene solution for 12 hours. The chlorosilanes chemically bond to hydroxyl (–OH) groups on hydrophilic silica surfaces, leaving the alkyl groups extending from the solid surface and thus making the surface hydrophobic. The silanized silica wafers were found to be highly hydrophobic with contact angles of water from 80° to 102°. The

hydrophobized surfaces are highly stable in toluene due to the covalent coupling between the chlorosilanes and the hydroxyl (-OH) groups on the solid surfaces.<sup>263</sup>

### 5.2.3 QCM-D adsorption experiment

QCM-D (Q-sense E4 system, Sweden) was used to measure the adsorption of asphaltenes and EC on quartz crystal sensors coated with silica and alumina. The operation procedures were described in Chapter 2.4. The Sauerbrey relation illustrated by equation (2-2) was used to calculate the mass uptake during asphaltene and EC adsorption:

$$\Delta m = -\frac{C \times \Delta f}{n} \quad (2-2)$$

### 5.2.4 Soaking experiment

In order to understand the wettability alteration mechanism of asphaltene- and bitumen-contaminated solids by EC adsorption, soaking experiments were carried out using procedures schematically described in Figure 5.3. In each test, silica or alumina wafers (1 cm by 1 cm) were immersed in 50 ppm asphaltenes- or 500 ppm bitumen-in-toluene solutions for 1 hour, after which they were removed from the toluene solution and rinsed with about 20 mL pure toluene to remove any residual asphaltene/bitumen solutions and loosely attached asphaltenes/bitumen. The asphaltene- or bitumen-coated wafers were then immediately soaked in 130 ppm EC-in-toluene solutions for a varying period of time from 1 to 12 hours. The samples were then taken out of the EC solution, rinsed with toluene and then blow-dried with nitrogen. Sampling in a time domain (i.e., as a function of time) in EC solution allows evaluation of dynamic structural changes of the asphaltene/bitumen layers pre-adsorbed on hydrophilic solid surfaces. For the

convenience of discussion, the samples were labelled as follows: AE-i for asphaltene-coated surface soaked in EC solution, with i representing the amount of time (in hours) that the sample was soaked in EC solution ( $i = 0, 1, 2, 3, 4, 5, 6, 7,$  and  $12$  hours); and BE-i for bitumen-coated surfaces soaked in EC solution for  $i = 0, 1, 2, 3, 4, 5, 6$  and  $7$  hours.

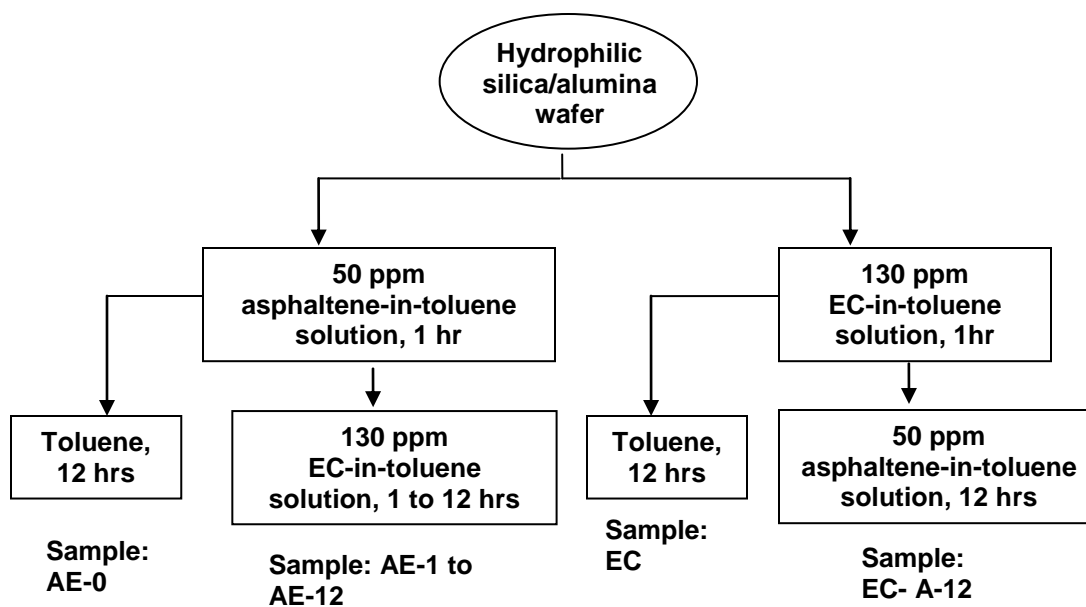


Figure 5.3. Soaking experiment procedures and corresponding sample codes. (Note: To prepare bitumen-coated surface, the 50 ppm asphaltene-in-toluene solution was replaced with 500 ppm bitumen-in-toluene solution and the same experimental procedures was followed with samples being labelled as BE in place of AE)

As a control to study the stability of immobilized asphaltenes and bitumen on hydrophilic wafer surfaces, an asphaltene- or bitumen-coated wafer was placed in pure toluene for 12 hours. Control tests were also conducted by immersing a bare wafer in 130 ppm EC-in-toluene solutions for 1 hour, followed by soaking in pure toluene for 12 hours. To study the binding of asphaltenes with EC in toluene, the



EC-coated wafer obtained here was placed in 50 ppm asphaltene- or 500 ppm bitumen-in-toluene solutions for 12 hours.

The prepared surfaces were characterized by contact angle measurements and AFM imaging. Water contact angle was measured to determine changes in the surface wettability as a consequence of compositional and conformational change of organic contaminants on hydrophilic solid surface. Topographical images of different samples, obtained by AFM, were used to observe changes in the structure of the surface layer.

### **5.2.5 Contact angle measurement**

Static contact angles of water on sample surfaces prepared in the soaking experiment were measured using a drop shape analyzer (DSA100, Krüss, Germany) equipped with an optical microscope and illumination system. Details of operation were described in Chapter 2.5.2.

### **5.2.6 AFM imaging**

AFM topographical images of the sample surfaces prepared in the soaking experiment were obtained using an Agilent 5500 Molecular Imaging Microscope (Agilent Technologies, Inc., Chandler, AZ) operated under AAC mode in air using silicon nitrate cantilevers (RTESP, Veeco, Santa Barbara, CA), with a nominal resonance frequency of 200-300 kHz. Details of operation were described in Chapter 2.2.5.

### **5.2.7 Langmuir compression isotherms of asphaltenes+EC films**

Langmuir isotherms of asphaltenes+EC films were obtained at toluene/water interface according to the procedure described in Chapter 2.3.2. Briefly, 20  $\mu$ L of

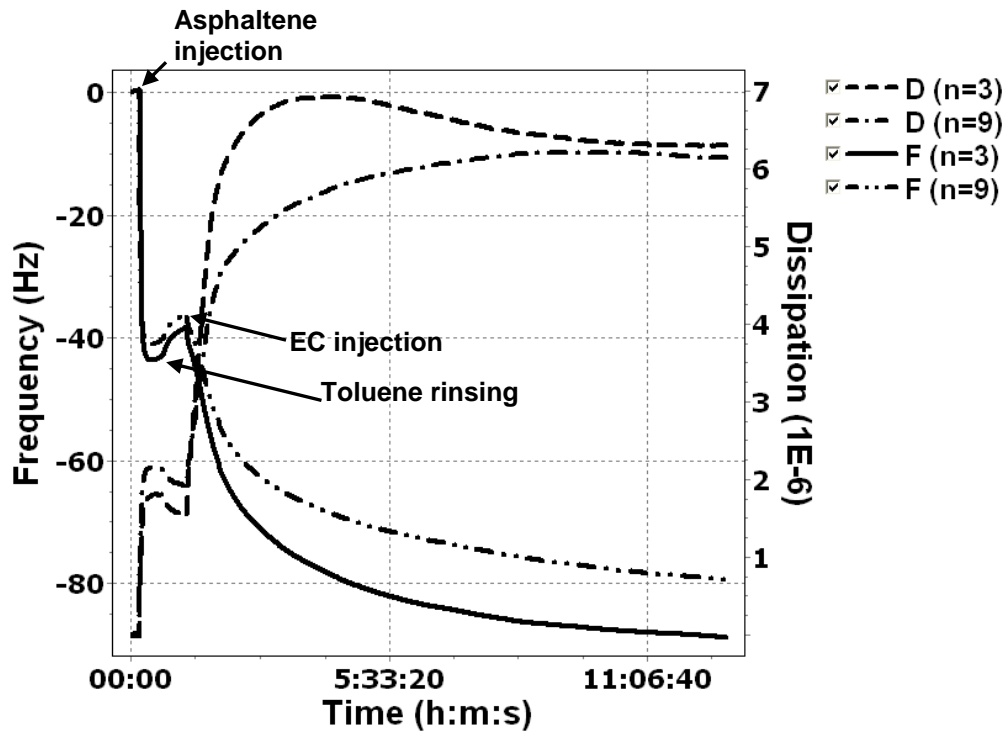
1 mg/mL asphaltene-in-toluene solution was spread on the water phase. After 20 minutes, about 100 mL toluene was added on top of the water phase. The asphaltene film was equilibrated for 30 minutes and then compressed with a barrier compression speed of 10 mm/min to obtain the interfacial pressure-area isotherm. To investigate the effect of EC on an asphaltene film at toluene/water interface, the asphaltene film was prepared in the same procedure as above. Then 20  $\mu$ L of 1 mg/mL EC-in-toluene was added to the toluene phase. EC was allowed to diffuse to the interface for 2 hours and then the interfacial film was compressed to obtain the pressure-area isotherm. Isotherms of EC alone and under effect of asphaltenes were obtained using the same procedure. The four interfacial films- 1) asphaltenes, 2) asphaltenes under effect of EC, 3) EC, and 4) EC under effect of asphaltenes- are termed as: asp, asp-EC, EC, and EC-asp, respectively.

## **5.3 Results and discussion**

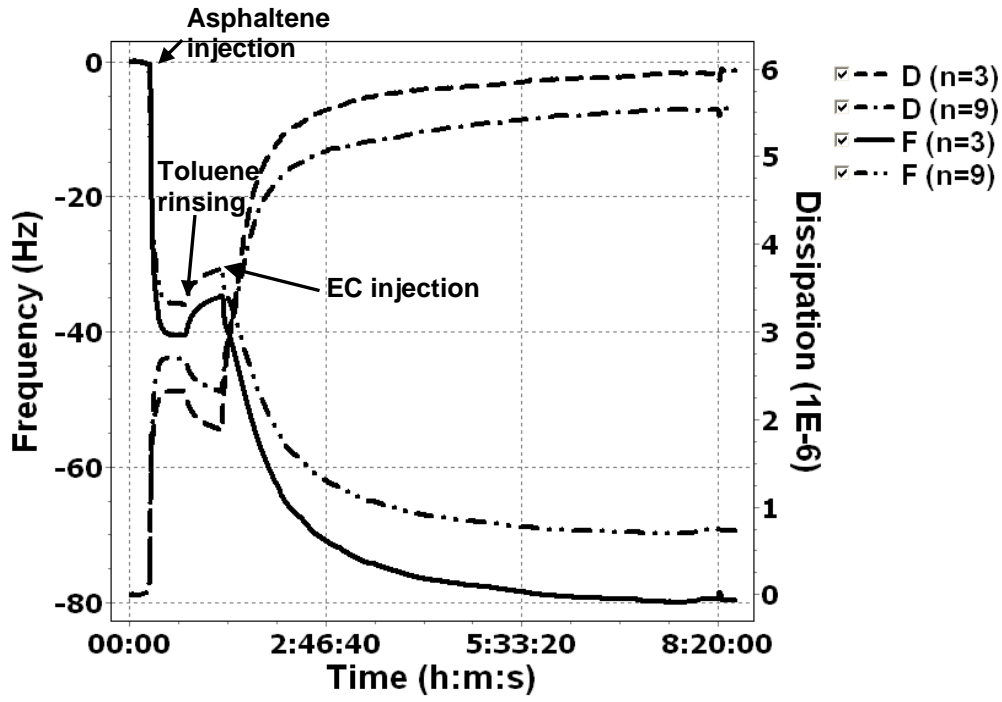
### **5.3.1 Adsorption of EC on asphaltene pre-adsorbed surface**

The QCM-D E4 system (Q-sense, Sweden) recorded the frequency and dissipation shift of all the seven harmonics. For the reason of simplicity, only two harmonics ( $n=3$  and  $n=9$ ) are shown in Figure 5.4a. In this study, we used the third overtone to determine the frequency and dissipation shifts, and calculate corresponding mass uptake. Adsorption of asphaltenes on silica surface led to a decrease of frequency by about -43 Hz and an increase in dissipation by  $\sim 2.0 \times 10^{-6}$ . Adsorption reached equilibrium after 1 hour, indicating a slow adsorption process characteristic of large asphaltene molecule systems. After rinsing with toluene for 30 minutes, a slight increase in the frequency and decrease in the dissipation were

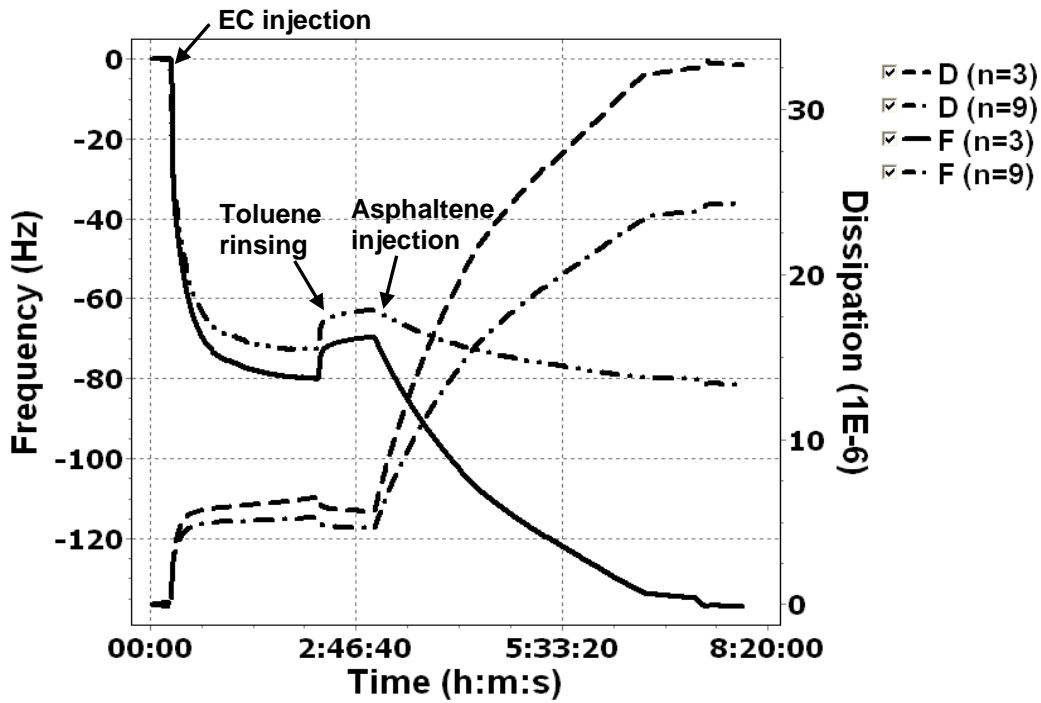
observed, indicating removal of loosely adsorbed asphaltenes from the surface. Since the changes in frequency and dissipation are not significant, most of asphaltenes on the solid surface are considered irreversibly adsorbed. The ratio of the frequency shift to the dissipation shift is quite low ( $< 0.2 \times 10^{-6}/\text{Hz}$ ), indicating that the adsorbed asphaltene layer is rigid and Sauerbrey relation of equation (2-2) is valid. Similar observations were reported by other researchers.<sup>15, 167, 168, 264</sup> Since the concentration of asphaltenes-in-toluene solution is very low (50 ppm), the viscosity and density of the solution can be approximated by the values of the pure solvent, i.e., toluene.<sup>167</sup> At equilibrium, the amount of asphaltenes adsorbed was calculated to be  $\sim 7 \text{ mg/m}^2$ , comparable to the values reported for similar systems.<sup>168, 264</sup>



(a)



(b)



(c)

Figure 5.4. Frequency and dissipation shift as a function of adsorption time in QCM-D experiments. (a) EC adsorption on asphaltene-coated silica surface; (b) EC adsorption on asphaltene-coated alumina surface; (c) Asphaltene adsorption on EC-coated silica surface

As also shown in Figure 5.4a, the contact with EC solutions of silica sensor surfaces pre-adsorbed with a layer of asphaltenes caused a further decrease in resonance frequency and increase in dissipation. The changes of  $f$  and  $D$  were fast in the first 4 hours after introducing EC solution, followed by a slow evolution. The shift in frequency and dissipation after introduction of EC is about -50 Hz and  $4.5 \times 10^{-6}$ , respectively. Using equation (2-2), the total mass uptake on the surface is calculated to be about  $15.5 \text{ mg/m}^2$ . An interesting observation is the distinct dissipation shift characteristics of the lower overtones ( $n=3$ ) after introduction of EC. The dissipation of the third overtone first increased to a larger degree and then decreased gradually to the level of the higher order overtones ( $n=5$  to 13). It is well documented that the lower order overtones are more sensitive to the outer region of the adsorbed layer (regions far away from the solid surface).<sup>15</sup> The characteristic changes in the dissipation of the third overtone indicate that, shortly after EC solution was introduced, the outer region of the film was softer than the inner region. The softness of the outer region of the film can be attributed to adsorption of EC, structural changes and/or trapping of the solvent with increased roughness of the film-liquid interface due to EC adsorption. With increasing contact time with EC solutions, the outer region of the film gradually became as rigid as the inner region, leading to a more homogeneous film across the thickness of the film. It should be noted that the results from the QCM-D tests could not distinguish whether EC simply adsorbed on pre-adsorbed asphaltenes or displaced them. Such information can be derived from the soaking experiments to be described later.

Similar results were obtained using an alumina-coated quartz crystal sensor as shown in Figure 5.4b. Considering similar surface characteristics of silica and alumina in toluene (e.g., both bear hydroxyl functional groups), this observation is not unexpected. The calculated mass of asphaltenes and asphaltenes+EC adsorbed is  $6.2 \text{ mg/m}^2$  and  $14.3 \text{ mg/m}^2$ , respectively. Over the duration of the experiment, the subtle change in dissipation profile of the third overtone as observed in Figure 5.4a for silica was absent, indicating that the build-up of EC films on asphaltenes pre-adsorbed on alumina is more uniform than that on the silica surface.

### **5.3.2 Adsorption of asphaltenes on EC pre-adsorbed surface**

Figure 5.4c shows that direct adsorption of EC on a hydrophilic silica surface caused a frequency shift of  $-70 \text{ Hz}$  and a dissipation shift of  $5.5 \times 10^{-6}$ , corresponding to a mass adsorption of  $12.5 \text{ mg/m}^2$  (density and viscosity of toluene were used in the calculation since 130 ppm EC-in-toluene solution is quite dilute). Rinsing with pure toluene caused only a small increase in  $f$ , and drop in  $D$ , indicating that most EC were irreversibly adsorbed on hydrophilic silica wafer. Subsequent adsorption of asphaltenes caused a large decrease of frequency for the lower order overtones ( $\Delta f_3 = -70 \text{ Hz}$ ). Apparently, a large amount of asphaltenes was adsorbed on the EC surface. Accompanied with asphaltene adsorption, a large increase in dissipation was also observed ( $\Delta D_{qm,3} = 26 \times 10^{-6}$ ), indicating a much softer and more rugged asphaltene film. Furthermore, the frequency shifts of the higher order overtones are quite small in comparison with  $\Delta f_3$ , for example,  $\Delta f_9 = -17 \text{ Hz}$ , indicating a more heterogeneous film from the inner to the outer region. As revealed by AFM imaging to be discussed later, asphaltenes only

randomly adsorbed on EC surface in the form of separate aggregates. Such layer is rough and would trap a large amount of toluene, which is likely the cause of both larger dissipation and frequency shifts.<sup>195, 196</sup>

The mass uptake in each adsorption event calculated by the Sauerbrey equation was shown in Figure 5.5. For EC adsorption after asphaltenes on silica, the total mass uptake (asphaltenes+EC) is about 15 mg/m<sup>2</sup>. However, for EC adsorption directly on silica surface, the mass uptake is about 13 mg/m<sup>2</sup>. The total mass uptake on silica in the two adsorption events is comparable. The mass uptake on alumina surface of asphaltenes+EC is similar to that on silica surface.

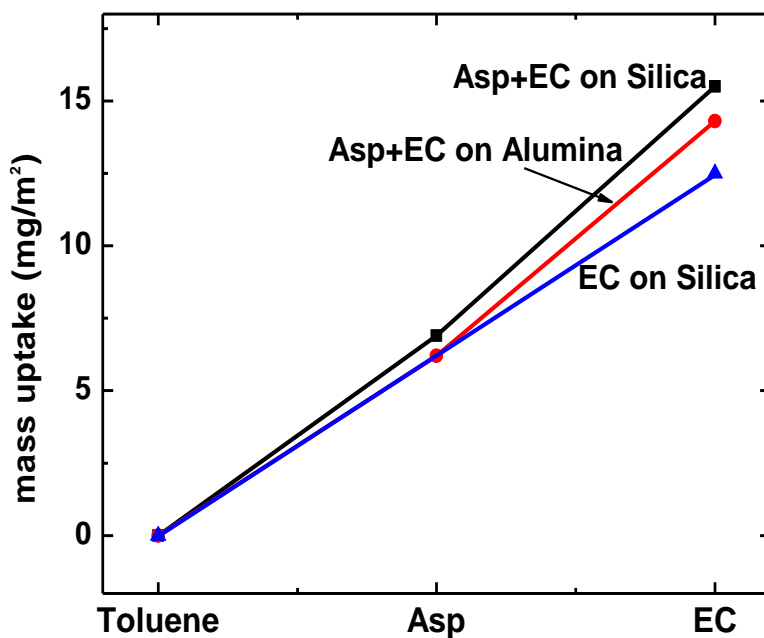


Figure 5.5. Mass uptake on QCM-D sensor surface in each adsorption event in Figure 5.4

To extract more structural information of the film during adsorption process, we plotted the  $\Delta D_{qcm}$  versus  $\Delta f$  in Figure 5.6, in which only the values of the third overtone are shown. For asphaltene adsorption on hydrophilic silica and alumina

surface, the slopes of  $\Delta D_{qcm}/\Delta f$  were very small, indicating the formation of a dense adsorbed layer on these two hydrophilic solid surfaces. Subsequent adsorption of EC caused only a slight increase in the slope values, ensuring applicability of Sauerbrey relationship. With continuous adsorption of EC, the slope of  $\Delta D_{qcm}/\Delta f$  decreased gradually, indicating an increasingly more rigid film due to increased packing of adsorbed molecules. For EC adsorption on a bare silica surface,  $\Delta D_{qcm}$  and  $\Delta f$  reached values comparable to those of EC adsorption on asphaltene surfaces. This finding suggests that whether EC adsorbed on asphaltene pre-adsorbed silica surface or directly on the bare hydrophilic silica surface, the adsorbed film would eventually become dominated by EC. Adsorption of asphaltenes on the EC surface, on the other hand, led to a larger slope value for  $\Delta D_{qcm}/\Delta f$ , indicating a much more loosely adsorbed asphaltene layer than that adsorbed directly on silica or alumina surfaces. The distinct linear relationship between  $\Delta D_{qcm}$  and  $\Delta f$  suggests that there is no conformational change during adsorption of asphaltenes on EC.<sup>265</sup>

The difference between asphaltene layers adsorbed on EC and on solid surfaces indicates that the structural and viscoelastic properties of the adsorbed layers depend on the interactions of the asphaltene molecules with the surface. For asphaltene adsorption onto the hydrophilic silica or alumina surfaces, there can be multiple bonding between the polar groups of asphaltene molecules and that (mainly hydroxyl groups) of the hydrophilic solid surfaces. However, for asphaltene adsorption on EC surface, there are fewer such polar-polar bonds because most of the polar groups in EC have already been bonded with the



hydrophilic solid surface and hence unavailable for binding with polar groups of asphaltenes. The lack of hydrogen bonding between asphaltene molecules and the adsorbed EC molecules led to a probable physical adsorption of asphaltenes on EC surface, with a loosely packed conformation of the asphaltene molecules or aggregates. However, washing with toluene cannot easily remove these physically adsorbed asphaltenes due to the relatively large size of adsorbed asphaltene aggregates that enables greater van der Waals attractions between asphaltenes and the EC-coated surface. For EC adsorption on asphaltene pre-adsorbed silica surface, the  $\Delta D_{qcm}/\Delta f$  simulates the case of EC adsorption on bare silica surface, which implies similar bonding characteristics and adsorbed film properties in these two adsorption events of EC.

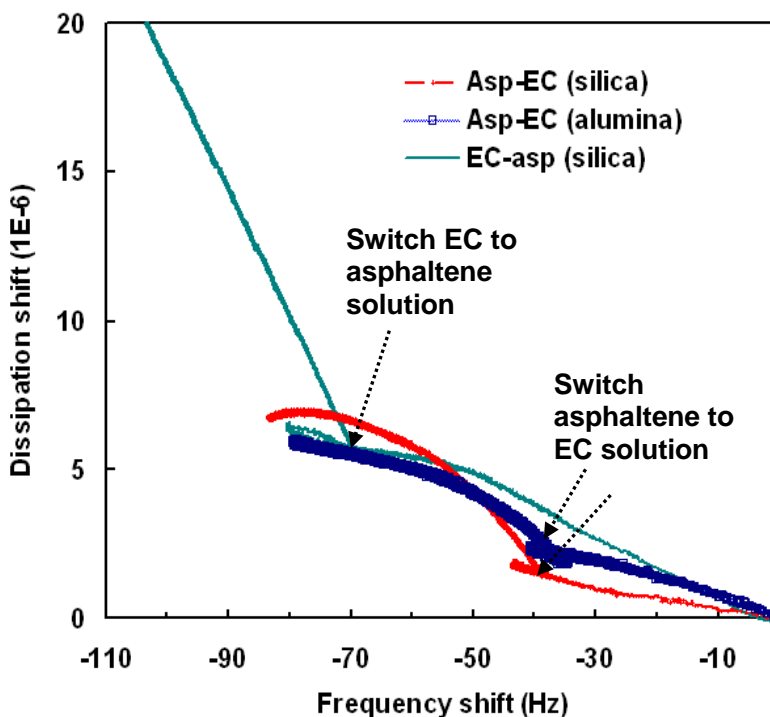
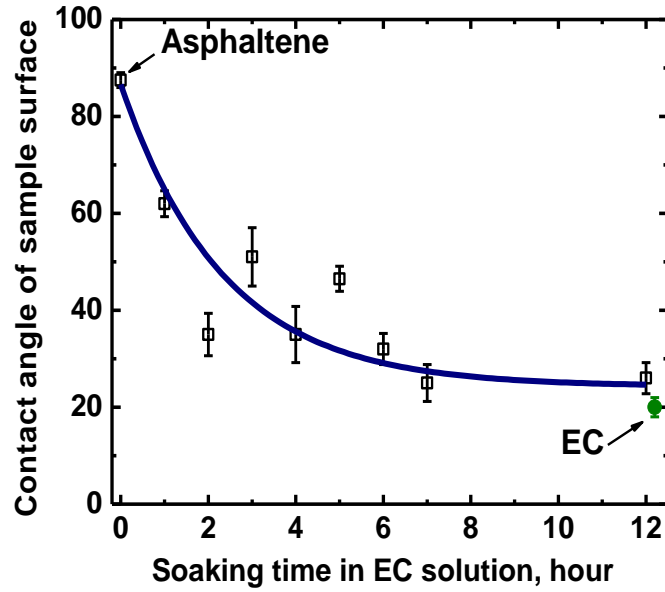


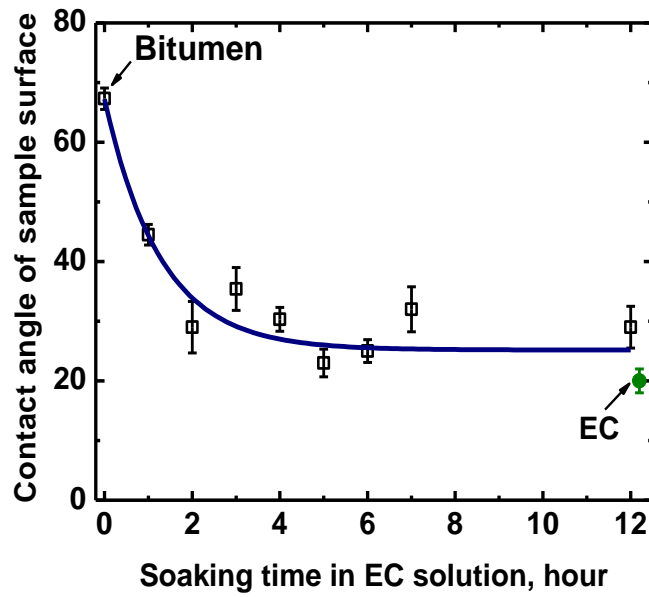
Figure 5.6.  $D_{qcm}$ - $f$  plot of the QCM-D adsorption results in Figure 5.4

### 5.3.3 Water wettability of sample surface

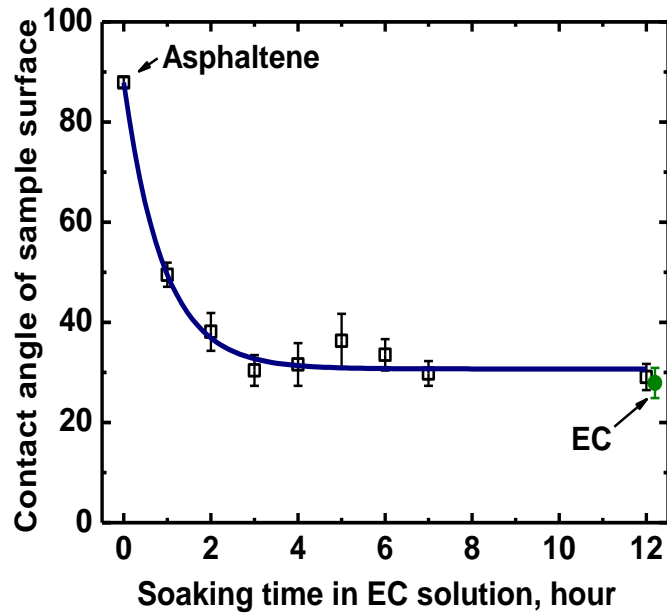
Contact angles of water on the surfaces prepared by soaking experiments are shown in Figure 5.7.



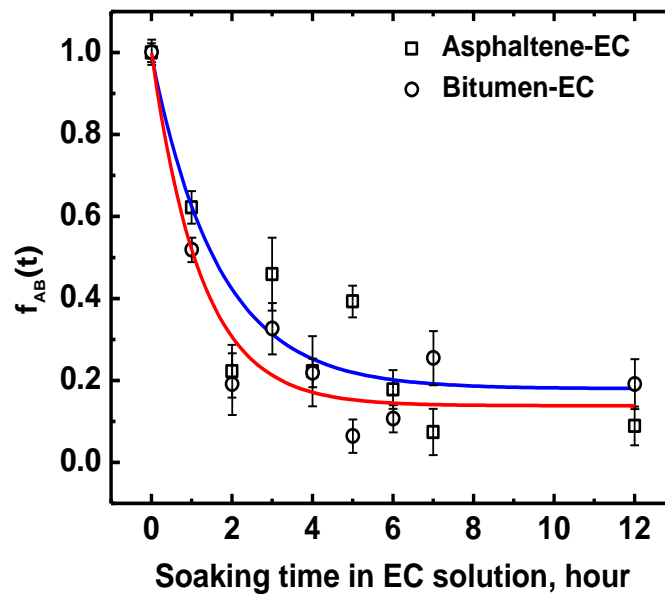
(a)



(b)



(c)



(d)

Figure 5.7. Water contact angles of the sample surfaces after soaking in EC-in-toluene solutions (Scatters: experiment data; Lines: fitted lines by exponential decay model). (a) Asphaltene-coated silica surfaces; (b) Bitumen-coated silica surfaces; (c) Asphaltene-coated alumina surfaces; (d)  $f_{AB}(t)$  profiles of plot (a) and (b) with the exponentially fitted curves by equation (5-1)

A bare silica surface had a water contact angle of less than 10°. Upon adsorption of asphaltenes or bitumen the water contact angle increased to 88±2° for asphaltenes and 67±2° for bitumen. This asphaltene or bitumen layer is considered to be irreversibly adsorbed on silica as it did not dissociate from the silica surface after soaking in toluene for 12 hours. After soaking in EC-in-toluene solution, however, the water contact angle on the asphaltene- and bitumen-coated surfaces decreased significantly, indicating a change to a more water-wettable surface. The water contact angle reduced rapidly in the first 4 hours, followed by a gradual reduction and finally levelled off after 7 hours at a value of 25°-30°. Such a contact angle value is comparable to that of water on an EC-adsorbed silica surface (~20°). The afore-mentioned observation suggests an “EC-like” surface be obtained after exposure of the asphaltene pre-adsorbed surfaces to EC solutions. This finding is consistent with the conclusions derived from the adsorption measurement using QCM-D (Figures 5.4 to 5.6). Similar change of contact angles was obtained for the alumina surface with pre-adsorbed asphaltenes (Figure 5.7c). The decrease in the water contact angles was more rapid for bitumen-coated surfaces than for asphaltene-coated surfaces. Quantitatively, one can use Cassie equation given below to estimate the coverage of asphaltene or bitumen films as a function of exposure time to EC solutions.

$$f_{AB}(t) = -\frac{\theta(t) - \theta_{EC}}{\theta_{AB} - \theta_{EC}} \quad (5-1)$$

where  $f_{AB}(t)$  is the fraction coverage of asphaltene or bitumen at exposure time  $t$ ,  $\theta(t)$  is the contact angle measured at exposure time  $t$ ,  $\theta_{EC}$  (=20°) and  $\theta_{AB}$  (=88° or

67°) are the contact angles of water on EC and asphaltene- or bitumen-covered surfaces, respectively. The calculated  $f_{AB}(t)$  profiles as a function of exposure time to EC solutions shown in Figure 5.7d can be well described by an exponential function of equation (5-2) below, represented by the fitted curve.

$$Y = A_0 \exp(-\alpha x) + Y_0 \quad (5-2)$$

The decay parameter  $\alpha$  for bitumen film ( $\alpha=0.82$ ) is higher than that for asphaltenes film ( $\alpha =0.60$ ) (Table 5.1), suggesting that bitumen films are easier to be displaced by EC than asphaltene films or that EC adsorbs more readily on bitumen film than on asphaltene films. Both follow a first order rate process. To distinguish whether displacement of adsorbed film by EC or EC adsorption on the adsorbed asphaltenes or bitumen films is responsible for the observed increase in water wettability, AFM imaging is performed.

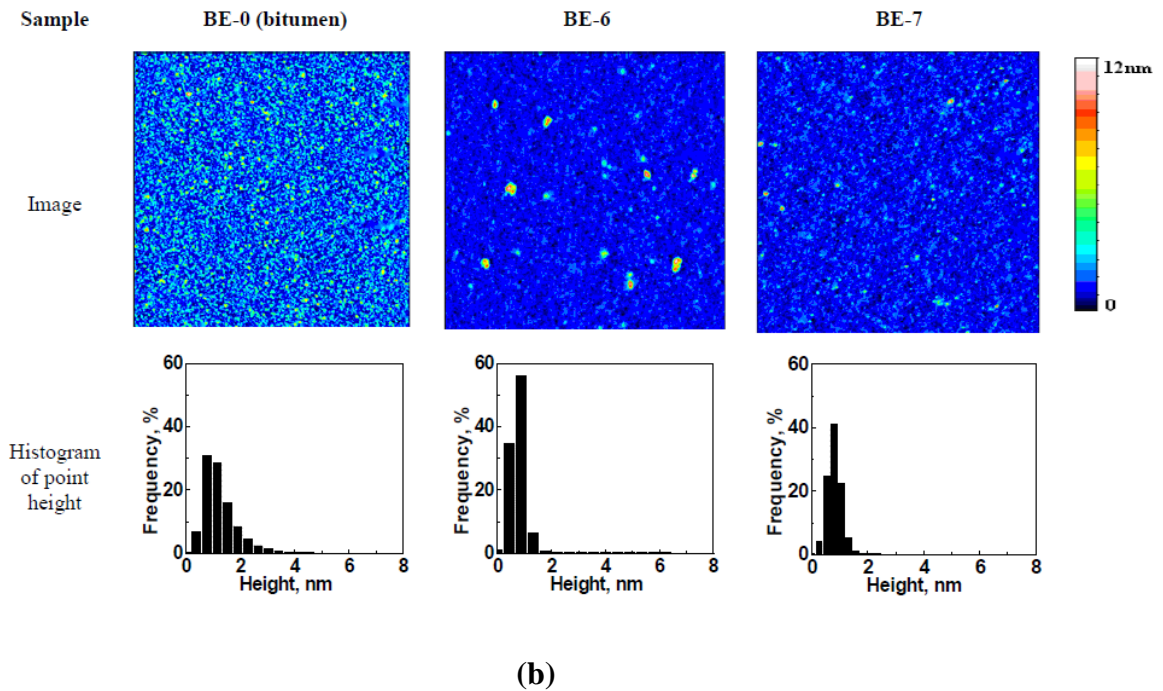
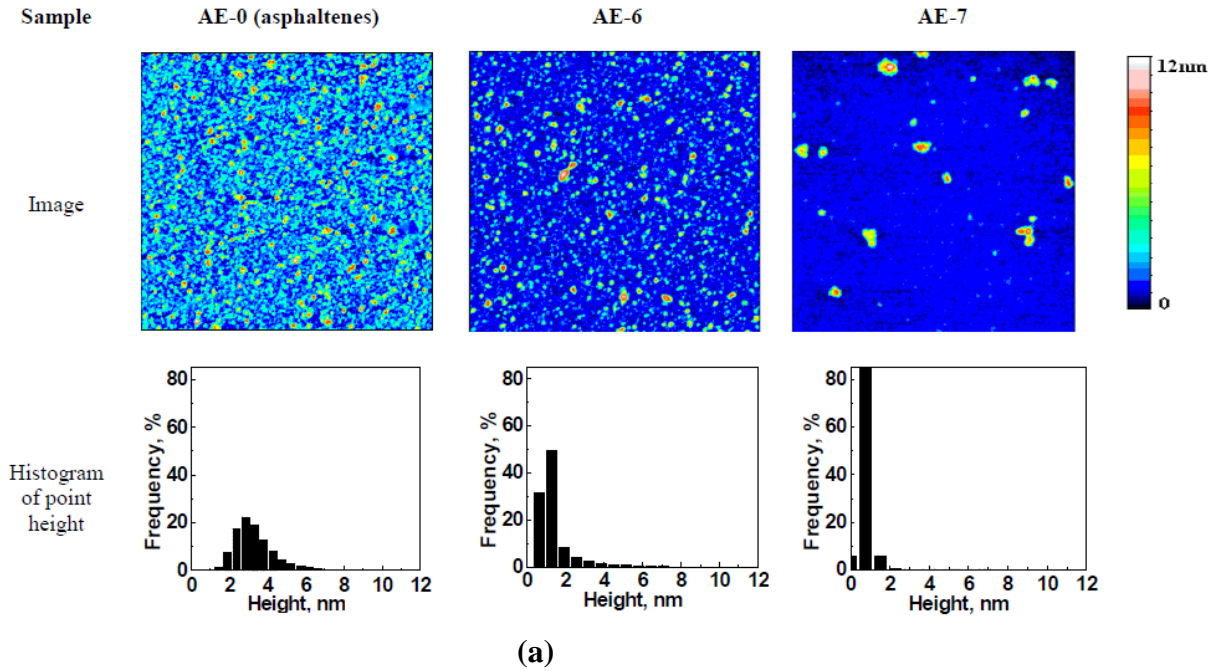
Table 5.1. Fitting parameters of Figure 5.7d by exponential equation (5-2)

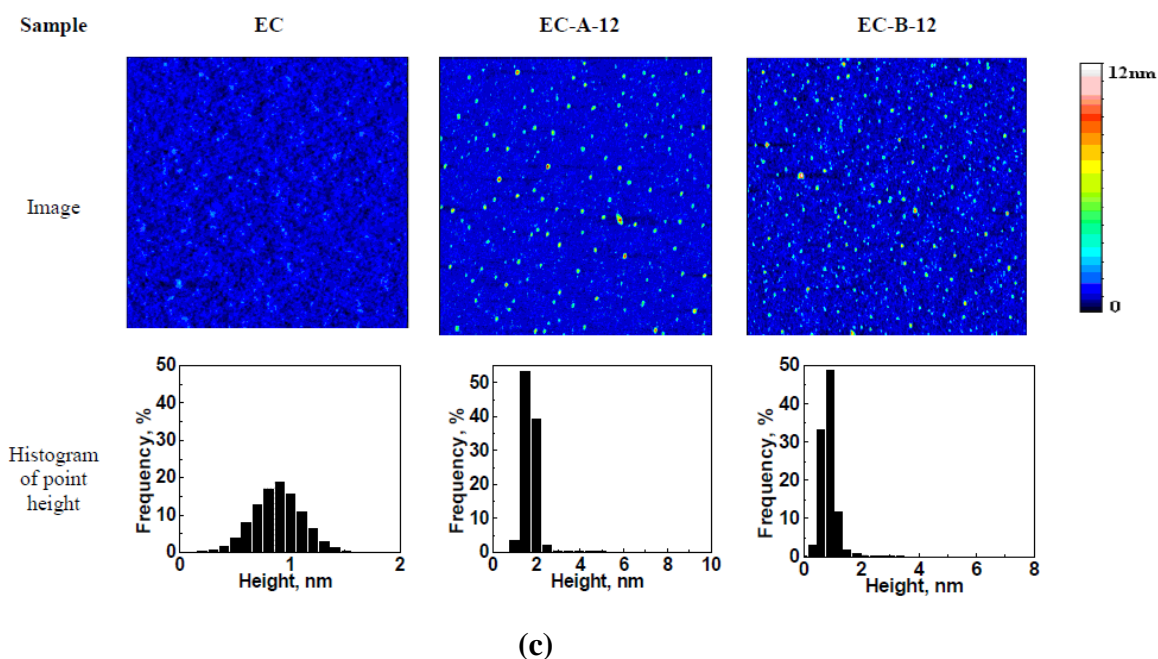
Parameters	Asphaltenes-EC	Bitumen-EC
$A_0$	0.82	0.86
$\alpha$	0.60	0.82
$Y_0$	1.65	1.22

### 5.3.4 Topography of sample surface

Topographical images of the sample surfaces with hydrophilic silica as substrate in the soaking experiments are shown in Figure 5.8. Images of AE0 (asphaltene-coated surface, Figure 5.8a) and BE0 (bitumen-coated surface, Figure 5.8b) show typical topographical features of asphaltenes and bitumen adsorbed on a hydrophilic silica surface, both randomly distributed in the form of closely packed

colloid-like nano-aggregates, with an average root-mean-square roughness of  $\sim 1$  nm.<sup>155, 251</sup> In contrast, the image of EC (Figure 5.8c) shows a more uniform and much flatter surface morphology with an average surface roughness less than 0.5 nm, comparable to the roughness of the silica wafer itself.



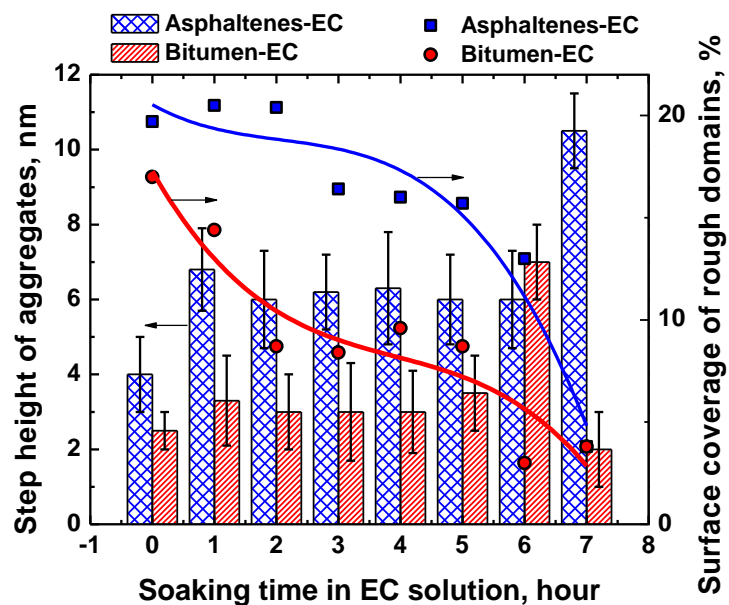


(c) Figure 5.8. AFM topographical images of the samples in soaking experiment. (a) Asphaltenes and AE-*i* (asphaltene-coated sample surface soaked in EC-in-toluene solution for *i* hours, *i* = 0, 6, and 7); (b) Bitumen and BE-*i* (bitumen-coated sample surface soaked in EC-in-toluene solution for *i* hours, *i* = 0, 6, and 7); (c) EC (EC-coated sample surface), EC-A-12 (EC-coated sample surface soaked in asphaltene-in-toluene solution for 12 hours) and EC-B-12 (EC-coated sample surface soaked in bitumen-in-toluene solution for 12 hours). The dimension of images is  $2 \mu\text{m} \times 2 \mu\text{m}$

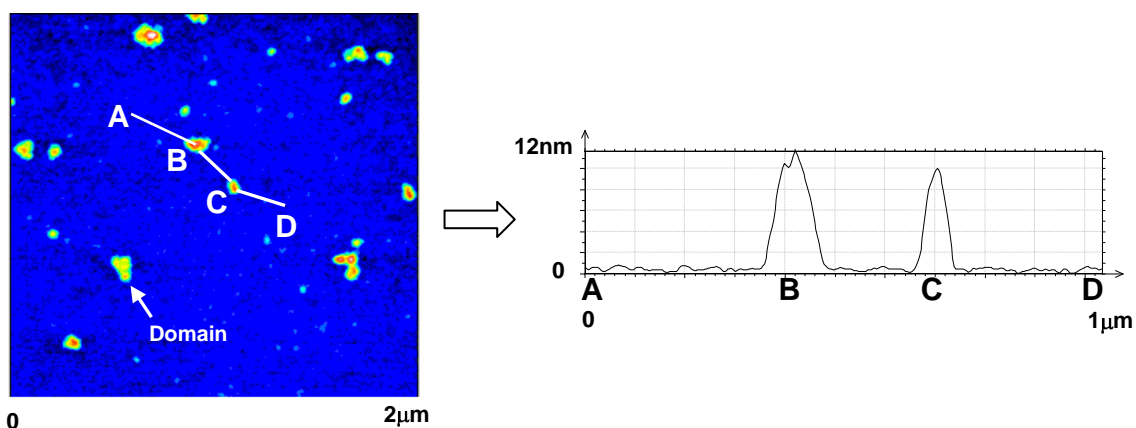
Surface topography of asphaltene-coated surfaces as a function of soaking time in EC solutions is shown in Figure 5.8a. When the soaking time is less than 7 hours, surface topography of asphaltene films on silica (AE-1 to AE-6) shows two distinct changes: some aggregates grew in size while the discrete flat areas expanded on the surface. These two changes are much clearer in Image AE-7 (7 hours of soaking time), showing higher rough domains (the larger aggregates) and much larger flat open areas. The AFM images suggest that EC displaced asphaltenes by pushing them to form larger aggregates.

In order to analyze the displacement process in more detail, a statistical analysis of the surface features of the images was performed. Histograms of the data point height on each sample surface were obtained using the image analysis software of AFM instrument and they are shown under each image. For the asphaltene surface (image AE-0 in Figure 5.8a), the aggregate height distribution has a broad peak at  $2.9 \pm 1.6$  nm. With increasing soaking time, the distribution of the histogram began to develop in two manners: firstly, the distribution peak became narrower and higher (in surface coverage) and shifted to the left (flat area), indicating that the flat area began to dominate on the surface; secondly, the height of rough domains shifted further to the right (the higher data point), a sign that the aggregates grew in height. The flat area on the surface is considered to be locations where EC dominates. Figure 5.9a shows the calculated surface coverage and step height distribution of the rough domains (asphaltene or bitumen aggregates). The step height distribution of the aggregates was estimated by drawing a line across the large domains as shown in Figure 5.9b and statistically analysing the step heights using an image analysis software. It is observed that increasing soaking time decreased the surface coverage of the rough domains from  $\sim 20\%$  (AE-0, BE-0) to  $\sim 4\%$  (AE-7, BE-7), accompanied by a slow increase up to 6 hours and a sharp increase between 6 and 7 hours of soaking time for the rough domain heights. This sudden increase in the domain height of the aggregates coincides with a drastic breakdown of asphaltene layers, as indicated by a clear separation between the flat areas and domains.





(a)



(b)

Figure 5.9. Statistical analysis of the AFM images in Figure 5.8. (a) Step height of the aggregates (columns) and surface coverage of the domains with height  $> 0.5$  nm (Dots: calculated data from images; Lines: polynomial fitting curve) as a function of soaking time in EC-in-toluene solution; (b) Step height profile across asphaltene (bitumen) domains (A, B, C and D correspond to four locations on the image along the line A $\rightarrow$ B $\rightarrow$ C $\rightarrow$ D)

Combined with  $f_{AB}(t)$  profile, results of the AFM imaging would suggest initial adsorption of EC on asphaltene films to cover an increasing area with soaking time. This observation accounts for a quick uptake of EC by asphaltene-adsorbed

silica sensors in QCM-D and the corresponding rapid decrease in contact angle of water on asphaltene films with soaking time. The adsorbed EC then compete for the polar bonding sites on the hydrophilic solid surface with asphaltenes by penetrating and displacing the asphaltene films. Due to the cross-link nature of the asphaltene layer as that formed at w/o interfaces,<sup>145-147, 160</sup> the adsorbed asphaltenes are unlikely to lose quickly all their bonds with the silica surfaces, leading to a slow shrinkage in contact area of asphaltenes with silica surfaces, until EC finally breaks all the connections to push them away from the surface. At the same time, the water contact angle of the sample surface continued to decrease gradually until levelled off at a value similar to that of EC-covered silica surface. Since the QCM-D tests showed no sign of asphaltenes detaching from the solid surface, instead there was a continuous increase in the uptake of material on asphaltene-adsorbed sensor surfaces, the adsorbed asphaltenes are likely pushed into larger size aggregates in the form of “islands” sporadically distributed on the silica surface. It is of course quite possible that stronger adsorption of EC may partially compensate for the loss of asphaltenes from sensor surfaces, exhibiting an overall increase in the mass adsorbed on the sensor surface albeit, at a decreased extent. Based on the results from this study, a process of EC displacing asphaltenes from the silica surface, illustrated in Figure 5.10, is suggested. Two processes are highlighted. First, the EC molecules, being more surface active than asphaltenes, adsorb on the surface and/or at the defects of the asphaltene layers, followed by a displacement process, in which EC penetrates the asphaltene films

and weakens the binding between asphaltenes and substrates, and gradually squeezes the asphaltene aggregates into small areas to form higher domains.

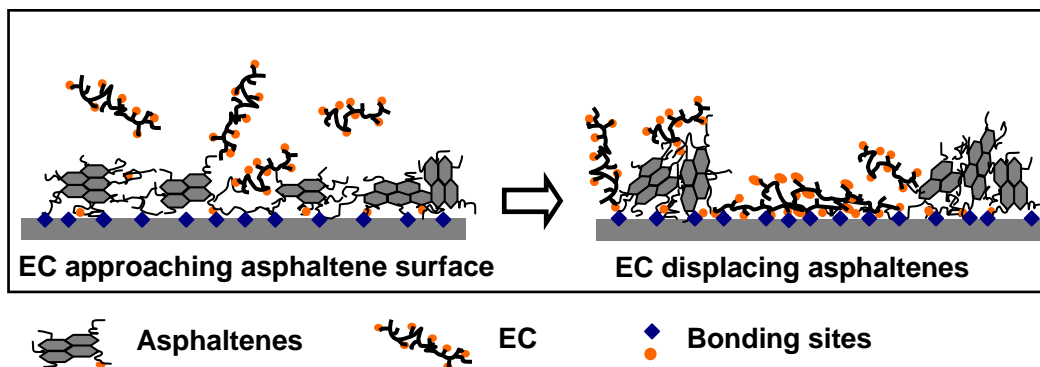


Figure 5.10. Schematics of asphaltenes displacement by EC on a hydrophilic solid surface

Figure 5.10 also shows the structural basis of asphaltenes being displaced by EC. Asphaltene molecules are composed of fused aromatic sheets connected by aliphatic chains, with polar functional groups and hetero-atoms dotted in the side chains.<sup>16, 50, 52, 266</sup> However, the distribution of polar groups on asphaltenes is not dense and uniform. When adsorbing on the hydrophilic silica and alumina surfaces, the asphaltene layer cannot occupy all the binding sites on the solid surface, providing opportunities for sequential adsorption of EC. For EC molecules, the polar (e.g., hydroxyl) binding groups are uniformly distributed along the polymeric chains and of higher density compared with asphaltenes, so that each EC molecule can form multiple bindings with the hydrophilic solid surfaces. With these structural characteristics, the EC molecules are expected to lie on the solid surface once adsorbed although tails and loops of EC chains can also be present (higher dissipation in Figure 5.4 and 5.6). The structural differences between asphaltenes and EC can be seen in AFM images (Figure 5.8),

where asphaltenes are in the form of randomly distributed nano-aggregates while EC on silica surface is much more smooth and flatter. Once EC molecules penetrate the asphaltene layer and bind to the solid surface, they “grab” the solid surface more tightly than asphaltenes due to their higher number of binding sites per molecule. In this manner, the adsorbed EC gradually expands to compete for more binding sites on the solid surface and pushes away the neighbouring asphaltenes. Therefore the driving force for EC to displace adsorbed asphaltenes is its higher number of stronger hydrogen binding sites towards hydroxyl groups on hydrophilic solid surface as illustrated in Figure 5.10.

The same phenomena are expected to occur on alumina surfaces due to similarity of the surface chemistry of alumina surface with that of silica. At neutral state, the hydrophilic alumina surface also has a layer of hydroxyl group (Al-OH),<sup>267</sup> which makes possible for hydrogen bonding during adsorption of asphaltenes or EC and displacement of asphaltenes by EC.

The effect of EC on bitumen-coated surfaces is very similar to that of asphaltene-coated surfaces, but the displacement process of bitumen by EC is faster. As seen in Figure 5.8b, after soaking for 6 hours, large bitumen aggregates were formed on the surface (BE-6). After 7 hours of soaking, only a few bitumen aggregates were observed, implying that bitumen nearly detached completely from the solid surface (BE-7). This observation was not unexpected since bitumen contains many of the smaller polar molecules such as resins. Resins are able to adsorb on hydrophilic silica surfaces but this adsorption is mostly reversible,<sup>168</sup> indicating that bitumen would be more easily displaced by EC.

Another control experiment was carried out to show the irreversibility of the displacement of asphaltenes and bitumen by EC. Here, a silica wafer was first coated by a layer of EC and then soaked in asphaltene- or bitumen-in-toluene solution for 12 hours. The AFM images of the two samples in Figure 5.8c (EA-12 and EB-12) show only sparsely scattered aggregates of asphaltenes or bitumen on EC surfaces. The lateral size of these aggregates is in tens of nanometers with a height of a few nanometers. These observations are in agreement with the QCM-D adsorption experiments which suggested a rough and loosely adsorbed asphaltene layer (Figure 5.4c and 5.6) Despite of asphaltene adsorption, the contact angle of the surface remains quite low,  $16.2 \pm 2.7^\circ$ . As we can note here, although the EC-coated surface had a low water contact angle (Figure 5.7), there was little asphaltene adsorption since EC had blocked the polar bonding sites on the solid surface. These observations would imply that interactions between asphaltenes and EC play an insignificant role in determining the final occupation of the silica surface. From AFM colloidal force measurements performed in our laboratory, this observation was confirmed by the observed repulsive forces between asphaltene-coated and EC-coated surfaces in toluene solutions. It is the competition for the hydrophilic binding sites on the silica surface that induced the displacement of asphaltenes by EC. Higher surface affinity of EC ensured its occupation of hydrophilic silica and alumina surfaces.

### **5.3.5 Langmuir isotherms of asphaltenes+EC films at toluene/water interface**

The Langmuir isotherms of asphaltenes+EC films at toluene/water interface further confirmed the displacement of asphaltenes by EC.

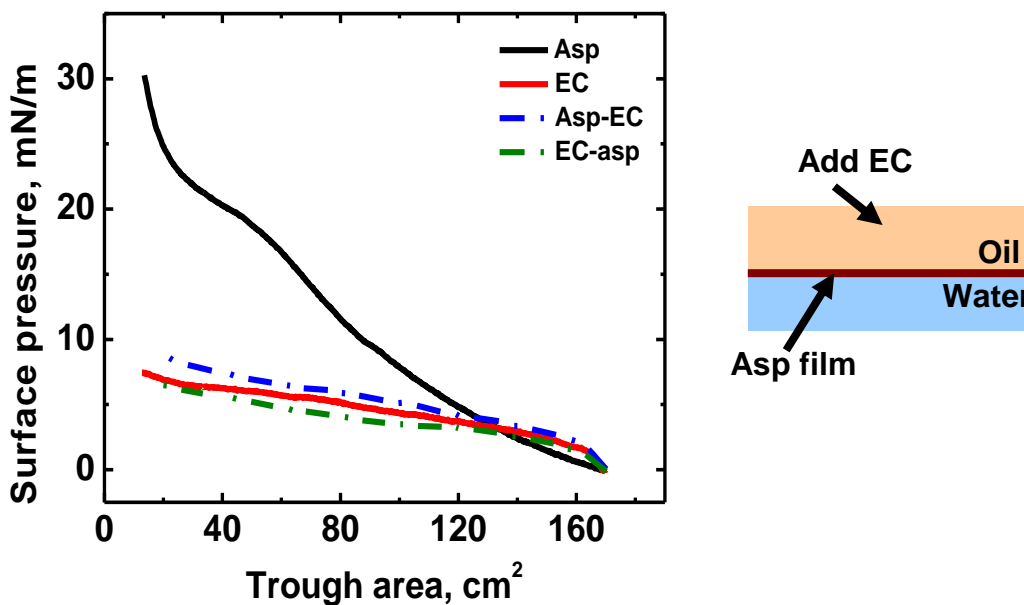


Figure 5.11. Langmuir isotherms of asphaltenes+EC films at toluene/water interface

As shown in Figure 5.11, the Langmuir isotherm of asphaltene film distinguished from those of EC, asp-EC (asphaltenes under effect of EC), and EC-asp (EC under effect of asphaltenes), with the latter three interfacial films showing similar characteristics during compression. The similarity of asp-EC to EC film indicated that the original asphaltene film has been gradually displaced by EC and the interfacial film was dominated by EC. The similarity of EC-asp to EC film showed that asphaltenes had little effect on EC film already formed at toluene/water interface. All the four Langmuir isotherms confirmed that EC is more interfacially active than asphaltenes and EC can irreversibly displace asphaltenes from the toluene/water interface. The thickness of EC, asp-EC and EC-asp films measured by spectroscopic ellipsometry (SOPRA GES 5) is in the range of 0.6 to 0.7 nm, much thinner than that of an asphaltene film (3-4 nm). As demonstrated earlier in Figure 1.3 and in the introduction part of this chapter,

similar phenomena are expected to occur at the oil/solid and oil/water interfaces. These Langmuir isotherms obtained at toluene/water interface confirmed the irreversible displacement of asphaltenes by EC on a solid surface in toluene.

### 5.3.6 Effect of EC on water wettability of silane-treated hydrophobic silica surfaces

The contact angle of water on the silanized hydrophobic silica surfaces before and after immersing in EC-in-toluene solution for 12 hours is given in Table 5.2.

Table 5.2. Water contact angle of silanized silica surface treated with EC

Silane type	Water contact angle		
	Clean hydrophilic silica surface	Silanized (S-) silica	S-silica treated with EC/toluene solution
dimethyldichlorosilane	<10°	80.9±0.8°	67.7±1.5°
butyltrichlorosilane		96.6±0.3°	62.8±3.3°
octyltrichlorosilane		102.1±0.7°	67.5±1.3°

As can be seen, the contact angle of water on freshly silanized silica surfaces increased with the number of carbons in alkylchlorosilanes. Upon exposure to 130 ppm EC-in-toluene solution for 12 hours, the contact angles of water on all the hydrophobized surfaces decreased to 60°~70°. This substantial decrease indicates some adsorption of EC on hydrophobized silica surfaces, although much lower than on asphaltene- or bitumen-adsorbed hydrophilic silica or alumina surfaces. Furthermore, if the EC-adsorbed surface was sonicated in the 130 ppm EC-in-toluene solution for 1 minute, the contact angle of water on the resultant surface returned almost to the value for the original silanized-silica surfaces. This observation would indicate weak adsorption of EC on silanized silica surfaces, a

characteristic of physisorption. Lack of specific binding, such as hydrogen bond between EC and silanized silica surfaces of methyl-terminal chemistry is responsible for the weak physical adsorption.

Figure 5.12 shows topographical images of the butyltrichlorosilane-treated silica surface and of EC on the silanized silica surface. The freshly silanized silica surface shows a relatively flat and featureless image. In comparison, EC on silanized silica wafer surfaces has a network structure with an almost constant height of the chains of EC network. This feature is absent for EC on a hydrophilic surface (Figure 5.8c) where a flat surface was observed. On the hydrophobic silica surface, however, due to lack of polar groups on the silanized silica surface, intra- and inter-molecular interaction between hydroxyl polar groups on EC may play a major role in the adsorption of EC and contribute to the formation of the network structure (e.g., the network structure is probably a way to fold the polar groups in EC), leading to relatively weak van der Waals forces that are responsible for adsorption of EC on chemically hydrophobized surfaces. In general, through physical adsorption, EC can increase the water wettability, i.e., smaller contact angle, of the silanized silica surface to an intermediate degree. Clearly stronger, multi-point specific binding (anchoring) of EC with solid surfaces is the key in controlling wettability of contaminated solid surfaces and their behaviour in colloidal systems, such as solids-stabilized emulsions.



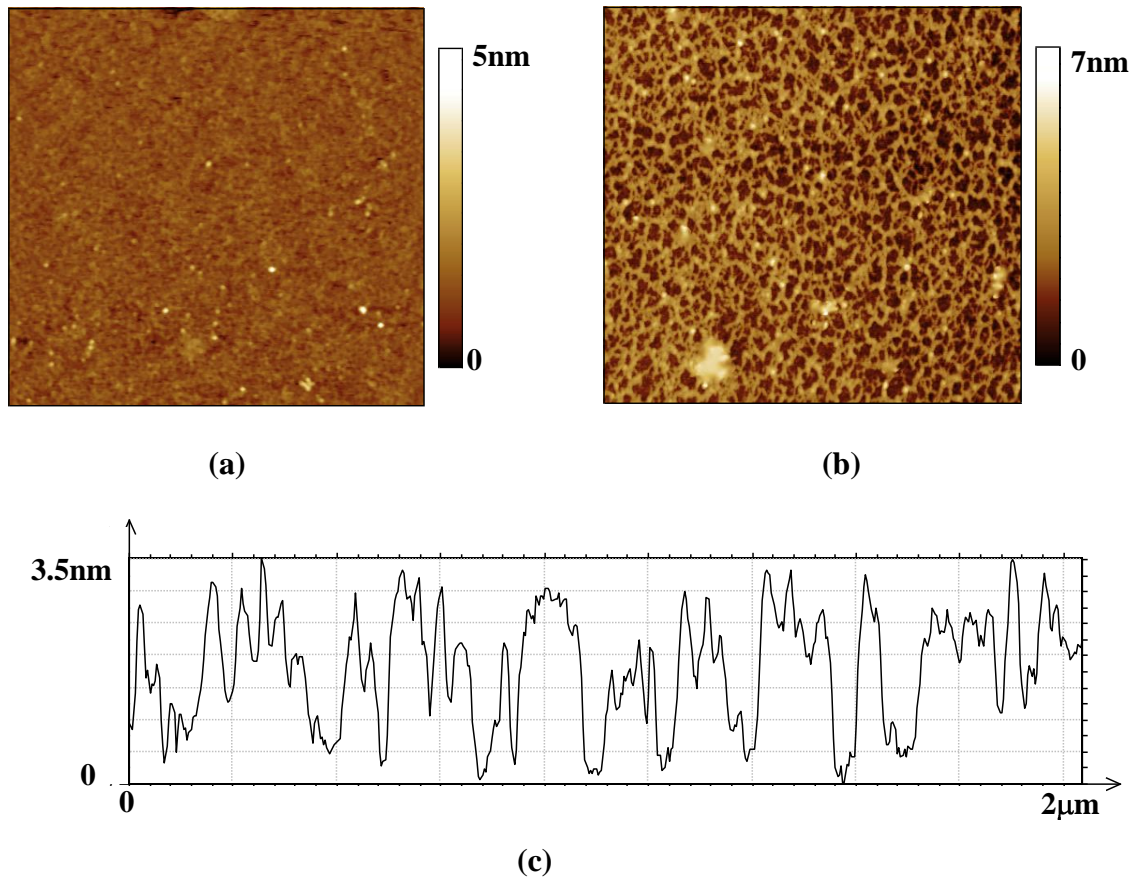


Figure 5.12. AFM image of: (a) Butyltrichlorosilane-treated silica surface and (b) EC on butyltrichlorosilane-treated silica surface; and (c) Height profile of EC image in (b). The dimension of the images is  $2 \mu\text{m} \times 2 \mu\text{m}$

### 5.3.7 Solids removal with EC addition in froth treatment in oil sands processing

Due to increased water wettability under the influence of EC adsorption, asphaltene- or bitumen-coated fines solids become more hydrophilic thereby have lower potential in stabilizing water-in-oil emulsions. It was shown by Feng et al.,<sup>169</sup> that EC was an effective emulsifier for bitumen froth (essentially a 5 wt% water-in-naphtha diluted bitumen emulsion stabilized by asphaltenes and fine solids) that contains 10 wt% fine solids. They noted that significant amounts of the fine solids settled with the coalesced water to the bottom of the emulsions in a

graduated cylinder. Some of these fine solids were associated with the emulsified water droplets (e.g., solids at the water/oil interface). For weathered ores containing large percentage of hydrophobic solids, EC was shown to be less effective in water removal. It is assumed that solids consumed considerable amount of EC since higher dosage of EC was required for effective water removal.<sup>155</sup> This observation implies that EC acts at both water/oil and solid/oil interfaces, which is desirable for preventing rag layer formation, since rag layer is a complex inter-connected mixture of flocculated fine solids, water droplets and multiple emulsions.<sup>3,5</sup>

#### **5.4 Conclusions**

In this study, ethyl cellulose (EC), an effective demulsifier for water-in-diluted bitumen emulsions, was shown to decrease the surface hydrophobicity of organic-contaminated solids. Both the QCM-D and the soaking experiments showed that the pre-adsorbed asphaltenes/bitumen on hydrophilic silica/alumina was displaced by EC in toluene solution. During the displacement by EC, asphaltenes and bitumen were compressed by EC to form a heterogeneous layer of larger aggregate sizes. These aggregates were sparsely scattered on the surface while EC covered most of the silica surface. The displacement occurred because of its higher number of hydroxyl groups per EC molecule thus a stronger affinity to the hydrophilic silica surface than asphaltenes. The interaction between EC and asphaltenes/bitumen played minimal role in asphaltene/bitumen displacement by EC from hydrophilic silica and alumina surfaces. The EC-dominated surface became more hydrophilic and thus facilitated the solid partitioning into the

aqueous phase during the froth treatment process in oil sands engineering. EC adsorption on the silanized hydrophobic silica surface resulted in an intermediate water contact angle ( $60^{\circ}$ - $70^{\circ}$ ). The major findings from this study shed the light on controlling wettability of organic-contaminated solids using chemicals, especially appropriate demulsifiers of w/o emulsions, to improve processability of heavy oils.

## Chapter 6 Summaries and Conclusions

The performance of bitumen froth cleaning operation is critical to the quality of bitumen product and the subsequent bitumen upgrading operation. A competitive froth treatment process aims at maximizing bitumen recovery while maintaining high quality of the bitumen product. Currently, there are mainly two commercial bitumen froth cleaning processes: a naphtha-based and a paraffin-based process. Removal of residual emulsified water droplets and fine solids from diluted bitumen remains a challenge for the naphtha-based process. A quantitative evaluation of asphaltene-asphaltene interactions in an organic system is necessary for improving naphtha-based process. For the purpose of technology improvement, this work is initiated to obtain a fundamental understanding of the bitumen froth treatment process. Specifically, interactions of asphaltene-asphaltene in organic solvents and wettability control of solids using chemical modifiers are investigated.

Experimentally, the aggregation/interaction of asphaltene in organic solvents was determined by surface force measurements using atomic force microscopy (AFM) in the form of colloidal probe technique. The effects of aromaticity of the solvents, temperature and water content of the solvents on asphaltene-asphaltene interactions were determined. For solid wettability control, the potential of ethyl cellulose (EC), an effective demulsifier for water-in-diluted bitumen emulsion, as a surface wettability modifier of the organic-contaminated solids was explored. The effect of EC addition on the wettability of asphaltene- or bitumen-contaminated hydrophilic silica and alumina surfaces was determined by contact

angle measurements. The mechanism of wettability alteration by EC addition was determined by QCM-D and AFM topographical imaging.

The major findings and contributions of this work are listed below.

## **6.1 Major conclusions**

1) The interaction forces between asphaltenes in solvents are determined to be highly sensitive to the aromaticity of the organic solvents. In good solvents (high aromaticity), there exists a steric repulsive force between asphaltenes. The force profile can be well described by the scaling theory developed for polymer brushes. In poor solvents (low aromaticity), van der Waals attraction is determined to be the driving force for asphaltene precipitation. When tuning the aromaticity of the solvents from good solvents to poor solvents, there is a gradual transition from repulsive to attractive forces, indicating a possibility of controlling asphaltene interaction/aggregation through tuning the aromaticity of the organic solvents.

For asphaltene-asphaltene interactions in toluene, the presence of a trace amount of water slightly reduces the repulsive force while temperature in the range of 25 °C to 40 °C has negligible effect on the interactive forces, indicating that the aromaticity of solvents is dominant in controlling asphaltene stability, at least in the range of parameters investigated in this study.

2) Ethyl cellulose (EC) is able to decrease the surface hydrophobicity of the asphaltene- and bitumen-contaminated solids. In toluene solution, EC gradually displaces the organic contaminants (asphaltenes/bitumen) on the hydrophilic silica/alumina surfaces. The displacement occurs because of the higher number of hydroxyl groups per EC molecule thus a stronger affinity to the hydrophilic

silica/alumina surface of EC than asphaltenes and bitumen. The EC-dominated surface becomes more hydrophilic, with a water contact angle of about 30°. Treating the organic-contaminated solids with EC is anticipated to enhance solids removal during bitumen froth cleaning.

## **6.2 Major contributions**

1) The colloidal probe technique of atomic force microscopy (AFM), in combination with the Langmuir-trough upstroke technique, was successfully applied to the study of asphaltenes-asphaltene interactions in organic medium using the surface force measurement. The author addressed the contamination problems that might be encountered in organic solvents and pointed that great care in selecting appropriate auxiliaries of the AFM fluid cell should be taken for force measurement in organic solvents.

2) For the first time, the interaction forces between asphaltene surfaces in organic solvents were systematically and quantitatively determined. It was found that aromaticity of solvents, rather than temperature and water content in solvents, is the dominant factor determining asphaltene aggregation in organic solvents. The transition point from good solvents to poor solvents in terms of solvent aromaticity was determined. The results could help predict the onset of asphaltene precipitation during bitumen dilution.

3) The nature of the forces between asphaltene surfaces in poor and good solvents was clearly identified by quantitative fitting of the force profiles with theoretical models, which provided insight into precipitation mechanisms of asphaltenes in crude oil. The successful application of the scaling theory for polymer brushes to

the repulsive forces between asphaltene surfaces addresses the polymeric properties of asphaltene molecules adsorbed on a hydrophilic silica surface.

4) This work demonstrated the possibility of using chemical modifiers, especially appropriate demulsifiers for water-in-oil emulsions, to reduce the surface hydrophobicity of the organic-contaminated solids and thus enhance their removal from bitumen froth. The successful application of EC to solid wettability control established the criteria for selecting such chemical modifiers and demonstrated a potential direction for the development of such type of chemicals.

### **6.3 Suggestions for future work**

For evaluation and prediction of asphaltene association/aggregation, more work needs to be conducted as listed below:

1) Study the surface forces in “real oil” system, e.g., naphtha. In this study, the interactions between asphaltene surfaces were measured in the model oil – heptol (mixture of toluene and heptane). Heptol is a very simple model solvent. Heptol can be used to evaluate the relative aromaticity of the solvents but cannot represent the complex structure of real oils, e.g., cyclic saturates and fused aromatic sheets in naphtha. Force measurements need to be extended to real oil system in order to more accurately evaluate asphaltene aggregation in industrial processes.

2) Study the effect of non-asphaltenic components of bitumen on asphaltene-asphaltene interactions, e.g., resins. It is reported that resins are capable of reducing asphaltene aggregation and precipitation. Presence of resins might affect the interactions between asphaltenes-asphaltenes in a given solvent. Bitumen also

contains some natural surfactants, such as naphthenic acids. With asphaltenes being the most polar fraction of bitumen, interactions between asphaltenes might also be mediated by these surfactants. It would be beneficial to study the synergistic effect of various components in bitumen on asphaltene aggregation by direct force measurements.

For solid wettability control, ethyl cellulose (EC) was shown to be able to make the organic-contaminated solid surface more water-wet, which provides an opportunity for the treatment of the hydrophobic solids by chemical modifiers. More work needs to be conducted in this respect:

- 1) Use high concentrations of asphaltenes/bitumen-in-toluene solutions to contaminate solid surfaces. As a mechanistic study, this work used a concentration of asphaltene-in-toluene solution lower than the concentration of an industry system. To simulate an industry system, concentrations of asphaltene and bitumen solutions close to industrial operations need to be employed. In addition, the dosage of EC can be varied according to the organic content of the hydrophobic solids.
- 2) Establish a systematic procedure for screening and developing chemical modifiers that can control the surface wettability of the hydrophobic solids. Since this study clarified the mechanism for solids wettability control by EC, a series of chemical modifiers of similar type as EC can be tested.
- 3) Apply EC and other selected chemical modifiers in upstream operations, e.g., during Denver cell flotation and evaluate their effect on solids removal from froth.



Specifically, the effect of these chemical additives on rag layer formation is worthy of investigation.

## References

1. Masliyah, J. H., *Fundamentals of Oilsands Extraction (ChE534 text book)*. 2006.
2. Long, Y. C.; Dabros, T.; Hamza, H., *Fuel* **2002**, 81, 1945-1952.
3. Romanova, U. G.; Yarranton, H. W.; Schramm, L. L.; Shelfantook, W. E., *Canadian Journal of Chemical Engineering* **2004**, 82, 710-721.
4. Saadatmand, M.; Yarranton, H. W.; Moran, K., *Industrial & Engineering Chemistry Research* **2008**, 47, 8828-8839.
5. Czarnecki, J.; Moran, K.; Yang, X. L., *Canadian Journal of Chemical Engineering* **2007**, 85, 748-755.
6. Wu, X. A., *Energy & Fuels* **2008**, 22, 2346-2352.
7. Sparks, B. D.; Kotlyar, L. S.; O'Carroll, J. B.; Chung, K. H., *Journal of Petroleum Science and Engineering* **2003**, 39, 417-430.
8. Kotlyar, L. S.; Sparks, B. D.; Woods, J. R.; Chung, K. H., *Energy & Fuels* **1999**, 13, 346-350.
9. Kotlyar, L. S.; Sparks, B. D.; Woods, J. R.; Raymond, S.; Le Page, Y.; Shelfantook, W., *Petroleum Science and Technology* **1998**, 16, 1-19.
10. Kilpatrick, P. K.; Spiecker, P. M., *Encyclopedic handbook of emulsion technology*. Johan Sjöblom Ed. ed.; Marcel Dekker, Inc.: New York, 2001.
11. Sjöblom, J.; Aske, N.; Auflem, I. H.; Brandal, O.; Havre, T. E.; Saether, O.; Westvik, A.; Johnsen, E. E.; Kallevik, H., *Advances in Colloid and Interface Science* **2003**, 100, 399-473.
12. Sztukowski, D. M.; Jafari, M.; Alboudwarej, H.; Yarranton, H. W., *Journal of Colloid and Interface Science* **2003**, 265, 179-186.
13. Robert N. Tipman, Y.-C. L., *US Patent, No5876592* **1999**.
14. Czarnecki, J.; Moran, K., *Energy & Fuels* **2005**, 19, 2074-2079.
15. Hannisdal, A.; Ese, M. H.; Hemmingsen, P. V.; Sjöblom, J., *Colloids and Surfaces a-Physicochemical and Engineering Aspects* **2006**, 276, 45-58.
16. O. C. Mullins, E. Y. S., A. Hammami and A. G. Marshall, *Asphaltenes, heavy oils, and petroleomics*. Springer: New York 2007.

17. McLean, J. D.; Kilpatrick, P. K., *Journal of Colloid and Interface Science* **1997**, 196, 23-34.
18. Kumar, K.; Nikolov, A. D.; Wasan, D. T., *Industrial & Engineering Chemistry Research* **2001**, 40, 3009-3014.
19. Wu, X.; van de Ven, T. G. M.; Czarnecki, J., *Colloids and Surfaces a-Physicochemical and Engineering Aspects* **1999**, 149, 577-583.
20. Oliver C. Mullins, E. Y. S., *Structures and Dynamics of Asphaltenes*. Plenum Press, New York: 1998.
21. Hong, E.; Watkinson, P., *Fuel* **2004**, 83, 1881-1887.
22. Yang, X. L.; Hamza, H.; Czarnecki, J., *Energy & Fuels* **2004**, 18, 770-777.
23. Andersen, S. I.; del Rio, J. M.; Khvostitchenko, D.; Shakir, S.; Lira-Galeana, C., *Langmuir* **2001**, 17, 307-313.
24. Murgich, J.; Merino-Garcia, D.; Andersen, S. I.; del Rio, J. M.; Galeana, C. L., *Langmuir* **2002**, 18, 9080-9086.
25. Gu, G.; Zhang, L.; Xu, Z.; Mashyah, J., *Energy & Fuels* **2007**, 21, 3462-3468.
26. Jiang, T. M.; Hirasaki, G.; Miller, C.; Moran, K.; Fleury, M., *Energy & Fuels* **2007**, 21, 1325-1336.
27. Chen, F.; Finch, J. A.; Xu, Z.; Czarnecki, J., *Journal of Adhesion Science and Technology* **1999**, 13, 1209-1224.
28. Dang-Vu, T.; Jha, R.; Wu, S. Y.; Tannant, D. D.; Masliyah, J.; Xu, Z. H., *Energy & Fuels* **2009**, 23, 2628-2636.
29. Kotlyar, L. S.; Sparks, B. D.; Woods, J.; Capes, C. E.; Schutte, R., *Fuel* **1995**, 74, 1146-1149.
30. Tharanivasan, A. K.; Svrcek, W. Y.; Yarranton, H. W.; Taylor, S. D.; Merino-Garcia, D.; Rahimi, P. M., *Energy & Fuels* **2009**, 23, 3971-3980.
31. Joshi, N. B.; Mullins, O. C.; Jamaluddin, A.; Creek, J.; McFadden, J., *Energy & Fuels* **2001**, 15, 979-986.
32. Yarranton, H. W., *Journal of Dispersion Science and Technology* **2005**, 26, 5-8.
33. Merino-Garcia, D.; Murgich, J.; Andersen, S. I., *Petroleum Science and Technology* **2004**, 22, 735-758.

34. Mohamed, R. S.; Ramos, A. C. S.; Loh, W., *Energy & Fuels* **1999**, 13, 323-327.
35. Ortega-Rodriguez, A.; Cruz, S. A.; Gil-Villegas, A.; Guevara-Rodriguez, F.; Lira-Galeana, C., *Energy & Fuels* **2003**, 17, 1100-1108.
36. Pacheco-Sanchez, J. H.; Alvarez-Ramirez, F.; Martinez-Magadan, J. M., *Energy & Fuels* **2004**, 18, 1676-1686.
37. Kuznicki, T.; Masliyah, J. H.; Bhattacharjee, S., *Energy & Fuels* **2009**, 23, 5027-5035.
38. Kuznicki, T.; Masliyah, J. H.; Bhattacharjee, S., *Energy & Fuels* **2008**, 22, 2379-2389.
39. Holmberg, K., *Handbook of Applied Surface and Colloid Chemistry*. John Wiley & Sons, Ltd: New York, 2001.
40. Israelachvili, J. N., *Faraday Discussions of the Chemical Society* **1978**, 65, 20-24.
41. Ducker, W. A.; Senden, T. J.; Pashley, R. M., *Nature* **1991**, 353, 239-241.
42. Butt, H. J.; Cappella, B.; Kappl, M., *Surface Science Reports* **2005**, 59, 1-152.
43. Long, J.; Zhang, L. Y.; Xu, Z. H.; Masliyah, J. H., *Langmuir* **2006**, 22, 8831-8839.
44. Long, J.; Li, H.; Xu, Z.; Masliyah, J. H., *Aiche Journal* **2006**, 52, 371-383.
45. Long, J.; Xu, Z. H.; Masliyah, J. H., *Colloids and Surfaces a-Physicochemical and Engineering Aspects* **2006**, 281, 202-214.
46. Liu, J. J.; Xu, Z. H.; Masliyah, J., *Canadian Journal of Chemical Engineering* **2004**, 82, 655-666.
47. Liu, J. J.; Xu, Z. H.; Masliyah, J., *Colloids and Surfaces a-Physicochemical and Engineering Aspects* **2005**, 260, 217-228.
48. Liu, J. J.; Zhang, L. Y.; Xu, Z. H.; Masliyah, J., *Langmuir* **2006**, 22, 1485-1492.
49. Wang, J. X.; Buckley, J., *Journal of Dispersion Science and Technology* **2007**, 28, 425-430.
50. Dickie, J. P.; Yen, T. F., *Analytical Chemistry* **1967**, 39, 1847-1852.
51. Strausz, O. P.; Mojelsky, T. W.; Faraji, F.; Lown, E. M.; Peng, P., *Energy & Fuels* **1999**, 13, 207-227.

52. Strausz, O. P.; Mojelsky, T. W.; Lown, E. M., *Fuel* **1992**, 71, 1355-1363.
53. Payzant, J. D.; Lown, E. M.; Strausz, O. P., *Energy & Fuels* **1991**, 5, 445-453.
54. Sheu, E. Y., *Journal of Physics-Condensed Matter* **2006**, 18, S2485-S2498.
55. Sirota, E. B., *Energy & Fuels* **2005**, 19, 1290-1296.
56. Coelho, R. R.; Hovell, I., *Petroleum Science and Technology* **2007**, 25, 41-54.
57. Zhang, L. Y.; Lawrence, S.; Xu, Z. H.; Masliyah, J. H., *Journal of Colloid and Interface Science* **2003**, 264, 128-140.
58. Yen, T. F.; Boucher, L. J.; Dickie, J. P.; Tynan, E. C.; Vaughan, G. B., *Journal of the Institute of Petroleum* **1969**, 55, 87-99.
59. Speight, J. G., *The chemistry and technology of petroleum*. 2nd ed.; Marcel Dekker: New York, 1991.
60. Fossen, M.; Kallevik, H.; Knudsen, K. D.; Sjoblom, J., *Energy & Fuels* **2007**, 21, 1030-1037.
61. Fossen, M.; Sjoblom, J.; Kallevik, H.; Jakobsson, J., *Journal of Dispersion Science and Technology* **2007**, 28, 193-197.
62. Spiecker, P. M.; Gawrys, K. L.; Kilpatrick, P. K., *Journal of Colloid and Interface Science* **2003**, 267, 178-193.
63. Wattana, P.; Fogler, H. S.; Yen, A.; Garcia, M. D.; Carbognani, L., *Energy & Fuels* **2005**, 19, 101-110.
64. Ostlund, J. A.; Wattana, P.; Nyden, M.; Fogler, H. S., *Journal of Colloid and Interface Science* **2004**, 271, 372-380.
65. Kaminski, T. J.; Fogler, H. S.; Wolf, N.; Wattana, P.; Mairal, A., *Energy & Fuels* **2000**, 14, 25-30.
66. Groenzin, H.; Mullins, O. C.; Eser, S.; Mathews, J.; Yang, M. G.; Jones, D., *Energy & Fuels* **2003**, 17, 498-503.
67. Espinat, D.; Fenistein, D.; Barre, L.; Frot, D.; Briolant, Y., *Energy & Fuels* **2004**, 18, 1243-1249.
68. Yen, T. F.; Erdman, J. G.; Pollack, S. S., *Analytical Chemistry* **1961**, 33, 1587-1594.
69. Zhang, Y.; Takanohashi, T.; Sato, S.; Saito, I.; Tanaka, R., *Journal of the Japan Petroleum Institute* **2004**, 47, 32-36.

70. Yen, T. F.; Wu, W. H.; Chilingar, G. V., *Energy Sources* **1984**, 7, 203-235.
71. Durand, E.; Clemancey, M.; Lancelin, J. M.; Verstraete, J.; Espinat, D.; Quoineaud, A. A., *Energy & Fuels* **2010**, 24, 1051-1062.
72. Merdrignac, I.; Espinat, D., *Oil & Gas Science and Technology-Revue De L Institut Francais Du Petrole* **2007**, 62, 7-32.
73. Gawrys, K. L.; Blankenship, G. A.; Kilpatrick, P. K., *Langmuir* **2006**, 22, 4487-4497.
74. Gray, M. R., *Energy & Fuels* **2003**, 17, 1566-1569.
75. Aguilera-Mercado, B.; Herdes, C.; Murgich, J.; Muller, E. A., *Energy & Fuels* **2006**, 20, 327-338.
76. Strausz, O. P.; Lown, E. M.; Alberta Energy Research Institute., *The chemistry of Alberta oil sands, bitumens and heavy oils*. Alberta Energy Research Institute: Calgary, Alta., 2003.
77. Groenzin, H.; Mullins, O. C., *Energy & Fuels* **2000**, 14, 677-684.
78. Long, J.; Xu, Z. H.; Masliyah, J. H., *Langmuir* **2007**, 23, 6182-6190.
79. Murgich, J., *Molecular Simulation* **2003**, 29, 451-461.
80. Mullins, O. C., *Spe Journal* **2008**, 13, 48-57.
81. Strausz, O. P.; Peng, P.; Murgich, J., *Energy & Fuels* **2002**, 16, 809-822.
82. Monte, M. B. M.; Coelho, R. R.; Middea, A., *Petroleum Science and Technology* **2004**, 22, 991-1001.
83. Badre, S.; Goncalves, C. C.; Norinaga, K.; Gustavson, G.; Mullins, O. C., *Fuel* **2006**, 85, 1-11.
84. Mullins, O. C.; Martinez-Haya, B.; Marshall, A. G., *Energy & Fuels* **2008**, 22, 1765-1773.
85. Becker, C.; Qian, K. N.; Russell, D. H., *Analytical Chemistry* **2008**, 80, 8592-8597.
86. Rogel, E.; Leon, O.; Torres, G.; Espidel, J., *Fuel* **2000**, 79, 1389-1394.
87. Merino-Garcia, D.; Andersen, S. I., *Petroleum Science and Technology* **2003**, 21, 507-525.
88. Gawrys, K. L.; Kilpatrick, P. K., *Instrumentation Science & Technology* **2004**, 32, 247-253.

89. Takanohashi, T.; Sato, S.; Saito, I.; Tanaka, R., *Energy & Fuels* **2003**, 17, 135-139.
90. Headen, T. F.; Boek, E. S.; Stellbrink, J.; Scheven, U. M., *Langmuir* **2009**, 25, 422-428.
91. Roux, J. N.; Broseta, D.; Deme, B., *Langmuir* **2001**, 17, 5085-5092.
92. Ravey, J. C.; Espinat, D., *Trends in Colloid and Interface Science Iv*, Zulauf, M.; Lindner, P.; Terech, P., Eds. 1990; Vol. 81, pp 127-130.
93. Durand, E.; Clemancey, M.; Lancelin, J. M.; Verstraete, J.; Espinat, D.; Quoineaud, A. A., *Journal of Physical Chemistry C* **2009**, 113, 16266-16276.
94. Acevedo, S.; Castillo, J.; Fernandez, A.; Goncalves, S.; Ranaudo, M. A., *Energy & Fuels* **1998**, 12, 386-390.
95. Andreatta, G.; Bostrom, N.; Mullins, O. C., *Langmuir* **2005**, 21, 2728-2736.
96. Groenzin, H.; Mullins, O. C., *Journal of Physical Chemistry A* **1999**, 103, 11237-11245.
97. Andreatta, G.; Goncalves, C. C.; Buffin, G.; Bostrom, N.; Quintella, C. M.; Arteaga-Larios, F.; Perez, E.; Mullins, O. C., *Energy & Fuels* **2005**, 19, 1282-1289.
98. Pineda, L. A.; Trejo, F.; Ancheyta, J., *Petroleum Science and Technology* **2007**, 25, 105-119.
99. Gawrys, K. L.; Spiecker, P. M.; Kilpatrick, P. K., *Petroleum Science and Technology* **2003**, 21, 461-489.
100. Wang, J. X.; Buckley, J. S., *Energy & Fuels* **2003**, 17, 1445-1451.
101. Castillo, J.; Fernandez, A.; Ranaudo, M. A.; Acevedo, S., *Petroleum Science and Technology* **2001**, 19, 75-106.
102. da Silva, S. M. C.; Rajagopal, K., *Petroleum Science and Technology* **2004**, 22, 1073-1085.
103. Carbonezi, C. A.; de Almeida, L. C.; Araujo, B. C.; Lucas, E. F.; Gonzalez, G., *Energy & Fuels* **2009**, 23, 1249-1252.
104. Pillon, L. Z., *Petroleum Science and Technology* **2001**, 19, 863-873.
105. Tan, X. L.; Fenniri, H.; Gray, M. R., *Energy & Fuels* **2009**, 23, 3687-3693.
106. Khvostichenko, D. S.; Andersen, S. I., *Energy & Fuels* **2008**, 22, 3096-3103.

107. Andersen, S. I.; Birdi, K. S., *J. Colloid Interface Sci.* **1991**, 142, 497-502.
108. Oh, K.; Ring, T. A.; Deo, M. D., *Journal of Colloid and Interface Science* **2004**, 271, 212-219.
109. Rogel, E., *Langmuir* **2004**, 20, 1003-1012.
110. Rogel, E., *Langmuir* **2002**, 18, 1928-1937.
111. Sheu, E. Y.; Detar, M. M.; Storm, D. A.; Decanio, S. J., *Fuel* **1992**, 71, 299-302.
112. Merino-Garcia, D.; Andersen, S. I., *Journal of Dispersion Science and Technology* **2005**, 26, 217-225.
113. Agrawala, M.; Yarranton, H. W., *Industrial & Engineering Chemistry Research* **2001**, 40, 4664-4672.
114. Duda, Y.; Lira-Galeana, C., *Fluid Phase Equilibria* **2006**, 241, 257-267.
115. Liu, Y. C.; Sheu, E. Y.; Chen, S. H.; Storm, D. A., *Fuel* **1995**, 74, 1352-1356.
116. Barre, L.; Simon, S.; Palermo, T., *Langmuir* **2008**, 24, 3709-3717.
117. Toulhoat, H.; Prayer, C.; Rouquet, G., *Colloids and Surfaces a-Physicochemical and Engineering Aspects* **1994**, 91, 267-283.
118. Marques, J.; Merdrignac, I.; Baudot, A.; Barre, L.; Guillaume, D.; Espinat, D.; Brunet, S., *Oil & Gas Science and Technology-Revue De L Institut Francais Du Petrole* **2008**, 63, 139-149.
119. Buckley, J. S.; Hirasaki, G. J.; Liu, Y.; Von Drasek, S.; Wang, J. X.; Gil, B. S., *Petroleum Science and Technology* **1998**, 16, 251-285.
120. Stachowiak, C.; Viguie, J. R.; Grolier, J. P. E.; Rogalski, M., *Langmuir* **2005**, 21, 4824-4829.
121. Porte, G.; Zhou, H. G.; Lazzeri, V., *Langmuir* **2003**, 19, 40-47.
122. Sheu, E. Y.; Detar, M. M.; Storm, D. A., International Symposium on Asphaltene Particles in Fossil Fuel Exploration, Recovery, Refining and Production Processes, JUL 13-17, 1992, 155-165.
123. Lin, J. R.; Yen, T. F., International Symposium on Asphaltene Particles in Fossil Fuel Exploration, Recovery, Refining and Production Processes, JUL 13-17, 1992, 171-184.



124. Rogel, E.; Leon, O.; Contreras, E.; Carbognani, L.; Torres, G.; Espidel, J.; Zambrano, A., *Energy & Fuels* **2003**, 17, 1583-1590.
125. Prunelet, A.; Fleury, M.; Cohen-Addad, J. P., *Comptes Rendus Chimie* **2004**, 7, 283-289.
126. Buenrostro-Gonzalez, E.; Lira-Galeana, C.; Gil-Villegas, A.; Wu, J. Z., *Aiche Journal* **2004**, 50, 2552-2570.
127. Ting, P. D.; Hirasaki, G. J.; Chapman, W. G., *Petroleum Science and Technology* **2003**, 21, 647-661.
128. Sabbagh, O.; Akbarzadeh, K.; Badamchi-Zadeh, A.; Svrcek, W. Y.; Yarranton, H. W., *Energy & Fuels* **2006**, 20, 625-634.
129. Lopez-Chavez, E.; Pacheco-Sanchez, J. H.; Martinez-Magadan, J. M.; Castillo-Alvarado, F. D.; Soto-Figueroa, C.; Garcia-Cruz, I., *Petroleum Science and Technology* **2007**, 25, 19-39.
130. Vargas, F. M.; Gonzalez, D. L.; Creek, J. L.; Wang, J. X.; Buckley, J.; Hirasaki, G. J.; Chapman, W. G., *Energy & Fuels* **2009**, 23, 1147-1154.
131. Taylor, S. D.; Czarnecki, J.; Masliyah, J., *Fuel* **2001**, 80, 2013-2018.
132. Buckley, J. S., *Energy & Fuels* **1999**, 13, 328-332.
133. Correra, S., *Petroleum Science and Technology* **2004**, 22, 943-959.
134. Pazuki, G. R.; Nikookar, M., *Fuel* **2006**, 85, 1083-1086.
135. Mousavi-Dehghani, S. A.; Mirzayi, B.; Vafaic-Sefti, M., *Brazilian Journal of Chemical Engineering* **2008**, 25, 523-534.
136. Johansson, B.; Friman, R.; Hakanpaa-Laitinen, H.; Rosenholm, J. B., *Advances in Colloid and Interface Science* **2009**, 147-48, 132-143.
137. Mitchell, D. L.; Speight, J. G., *Fuel* **1973**, 52, 149-152.
138. Wiehe, I. A., *Fuel Science & Technology International* **1996**, 14, 289-312.
139. Wang, J. X.; Buckley, J. S., *Energy & Fuels* **2001**, 15, 1004-1012.
140. Redelius, P., *Energy & Fuels* **2004**, 18, 1087-1092.
141. de Sousa, M. D.; de Oliveira, G. E.; Lucas, E. F.; Gonzalez, G., *Surface and Colloid Science*, Galembeck, F., Ed. 2004; Vol. 128, pp 283-287.
142. Akbarzadeh, K.; Alboudwarej, H.; Svrcek, W. Y.; Yarranton, H. W., *Fluid Phase Equilibria* **2005**, 232, 159-170.

143. Mannistu, K. D.; Yarranton, H. W.; Masliyah, J. H., *Energy & Fuels* **1997**, 11, 615-622.
144. Tu, Y.; O'Carroll, J. B.; Kotlyar, L. S.; Sparks, B. D.; Ng, B. D.; Chung, K. H.; Cuddy, G., *Fuel* **2005**, 84, 653-660.
145. Freer, E. M.; Radke, C. J., *Journal of Adhesion* **2004**, 80, 481-496.
146. Sztukowski, D. M.; Yarranton, H. W., *Langmuir* **2005**, 21, 11651-11658.
147. Bouriati, P.; El Kerri, N.; Graciaa, A.; Lachaise, J., *Langmuir* **2004**, 20, 7459-7464.
148. Spiecker, P. M.; Gawrys, K. L.; Trail, C. B.; Kilpatrick, P. K., *Colloids and Surfaces a-Physicochemical and Engineering Aspects* **2003**, 220, 9-27.
149. Jeribi, M.; Almir-Assad, B.; Langevin, D.; Henaut, I.; Argillier, J. F., *Journal of Colloid and Interface Science* **2002**, 256, 268-272.
150. Zhang, L. Y.; Lopetinsky, R.; Xu, Z. H.; Masliyah, J. H., *Energy & Fuels* **2005**, 19, 1330-1336.
151. Yeung, A.; Dabros, T.; Masliyah, J.; Czarnecki, J., *Colloids and Surfaces a-Physicochemical and Engineering Aspects* **2000**, 174, 169-181.
152. Moran, K.; Yeung, A.; Masliyah, J., *Langmuir* **1999**, 15, 8497-8504.
153. Tambe, D. E.; Sharma, M. M., *Advances in Colloid and Interface Science* **1994**, 52, 1-63.
154. Eley, D. D.; Hey, M. J.; Lee, M. A., *Colloids and Surfaces* **1987**, 24, 173-182.
155. Feng X, M. P., Gao S, Wang S, Wu SY, Masliyah JH, Xu Z., *Langmuir* **2010**, 26.
156. Xu, Y. M.; Wu, J. Y.; Dabros, T.; Hamza, H.; Venter, J., *Energy & Fuels* **2005**, 19, 916-921.
157. Djuve, J.; Yang, X.; Fjellanger, I. J.; Sjoblom, J.; Pelizzetti, E., *Colloid and Polymer Science* **2001**, 279, 232-239.
158. Sjoblom, J.; Soderlund, H.; Lindblad, S.; Johansen, E. J.; Skjarvo, I. M., *Colloid and Polymer Science* **1990**, 268, 389-398.
159. Daniel-David, D.; Le Follotec, A.; Pezron, I.; Dalmazzone, C.; Noik, C.; Barre, L.; Komunjer, L., *Oil & Gas Science and Technology-Revue De L Institut Francais Du Petrole* **2008**, 63, 165-173.

160. Angle, C. W., *Encyclopedic handbook of emulsion technology*. Johan Sjöblom Ed. ed.; Marcel Dekker, Inc.: New York, 2001.
161. Zhang, L. Y.; Xu, Z. H.; Mashyah, J. H., *Langmuir* **2003**, 19, 9730-9741.
162. Ese, M. H.; Sjöblom, J.; Djuve, J.; Pugh, R., *Colloid and Polymer Science* **2000**, 278, 532-538.
163. Kim, Y. H.; Wasan, D. T., *Industrial & Engineering Chemistry Research* **1996**, 35, 1141-1149.
164. Sullivan, A. P.; Kilpatrick, P. K., *Industrial & Engineering Chemistry Research* **2002**, 41, 3389-3404.
165. Poindexter, M. K.; Marsh, S. C., *Energy & Fuels* **2009**, 23, 1258-1268.
166. Bensebaa, F.; Kotlyar, L. S.; Sparks, B. D.; Chung, K. H., *Canadian Journal of Chemical Engineering* **2000**, 78, 610-616.
167. Abudu, A.; Goual, L., *Energy & Fuels* **2009**, 23, 1237-1248.
168. Ekholm, P.; Blomberg, E.; Claesson, P.; Auflem, I. H.; Sjöblom, J.; Kornfeldt, A., *Journal of Colloid and Interface Science* **2002**, 247, 342-350.
169. Feng, X. H.; Xu, Z. H.; Masliyah, J., *Energy & Fuels* **2009**, 23, 451-456.
170. Strausser, Y. E.; Heaton, M. G., *American Laboratory* **1994**, 26, 20-&.
171. Binnig, G.; Rohrer, H., *Helvetica Physica Acta* **1982**, 55, 726-735.
172. Binnig, G.; Quate, C. F.; Gerber, C., *Physical Review Letters* **1986**, 56, 930-933.
173. Passeri, D.; Bettucci, A.; Rossi, M., *Analytical and Bioanalytical Chemistry* **2010**, 396, 2769-2783.
174. Alexander, J.; Magonov, S.; Moeller, M., *Journal of Vacuum Science & Technology B* **2009**, 27, 903-911.
175. S. Magonov; Alexander, J., , *Application Note, Agilent Technologies, Inc.* **2008**.
176. Oliver, R. A., *Reports on Progress in Physics* **2008**, 71.
177. Giessibl, F. J., *Reviews of Modern Physics* **2003**, 75, 949-983.
178. Aske, N.; Kallevik, H.; Sjöblom, J., *Energy & Fuels* **2001**, 15, 1304-1312.

179. Kluge, D.; Abraham, F.; Schmidt, S.; Schmidt, H. W.; Fery, A., *Langmuir* **2010**, 26, 3020-3023.
180. Verbelen, C.; Christiaens, N.; Alsteens, D.; Dupres, V.; Baulard, A. R.; Dufrene, Y. F., *Langmuir* **2009**, 25, 4324-4327.
181. Nussio, M. R.; Voelcker, N. H.; Sykes, M. J.; Flavel, B. S.; Miners, J. O.; Shapter, J. G., *International Conference on Nanoscience and Nanotechnology*, 2008; pp 121-124.
182. Zlatanova, J.; Lindsay, S. M.; Leuba, S. H., *Progress in Biophysics & Molecular Biology* **2000**, 74, 37-61.
183. Rief, M.; Pascual, J.; Saraste, M.; Gaub, H. E., *Journal of Molecular Biology* **1999**, 286, 553-561.
184. Rief, M.; Oesterhelt, F.; Heymann, B.; Gaub, H. E., *Science* **1997**, 275, 1295-1297.
185. Drew, M. E.; Chworos, A.; Oroudjev, E.; Hansma, H.; Yamakoshi, Y., *Langmuir* **2010**, 26, 7117-7125.
186. Ebner, A.; Wildling, L.; Zhu, R.; Rankl, C.; Haselgrubler, T.; Hinterdorfer, P.; Gruber, H. J., *Stm and Afm Studies On*, 2008; Vol. 285, pp 29-76.
187. Auletta, T.; de Jong, M. R.; Mulder, A.; van Veggel, F.; Huskens, J.; Reinhoudt, D. N.; Zou, S.; Zapotoczny, S.; Schonherr, H.; Vancso, G. J.; Kuipers, L., *Journal of the American Chemical Society* **2004**, 126, 1577-1584.
188. Jacob H. Masliyah; Bhattacharjee, S., *Electrokinetic and Colloid Transport Phenomena* Wiley-Interscience: Hoboken, N.J., **2006**.
189. Luckham, P. F., *Advances in Colloid and Interface Science* **1991**, 34, 191-215.
190. Taunton, H. J.; Toprakcioglu, C.; Fetters, L. J.; Klein, J., *Macromolecules* **1990**, 23, 571-580.
191. Taunton, H. J.; Toprakcioglu, C.; Fetters, L. J.; Klein, J., *Nature* **1988**, 332, 712-714.
192. Solovyev, A.; Zhang, L. Y.; Xu, Z. H.; Masliyah, J. H., *Energy & Fuels* **2006**, 20, 1572-1578.
193. Petkov, J. T.; Gurkov, T. D.; Campbell, B. E.; Borwankar, R. P., *Langmuir* **2000**, 16, 3703-3711.

194. Alvarez, L.; Diaz, M. E.; Montes, F. J.; Galan, M. A., *Fuel* **2010**, 89, 691-702.
195. Hook, F.; Rodahl, M.; Brzezinski, P.; Kasemo, B., *Langmuir* **1998**, 14, 729-734.
196. Rodahl, M.; Hook, F.; Fredriksson, C.; Keller, C. A.; Krozer, A.; Brzezinski, P.; Voinova, M.; Kasemo, B., *Faraday Discussions* **1997**, 107, 229-246.
197. Richter, R. P. The Formation of Solid-Supported Lipid Membranes and Two-Dimensional Assembly of Proteins. Université Bordeaux I – Institut Européen de Chimie et Biologie, 2004.
198. Grace, R., S., L. L., Ed, *American Chemical Society: Washington, DC* **1992**.
199. Yarranton, H. W.; Alboudwarej, H.; Jakher, R., *Industrial & Engineering Chemistry Research* **2000**, 39, 2916-2924.
200. Gafonova, O. V.; Yarranton, H. W., *Journal of Colloid and Interface Science* **2001**, 241, 469-478.
201. Aston, D. E.; Berg, J. C., *Journal of Pulp and Paper Science* **1998**, 24, 121-125.
202. Hartley, P. G.; Grieser, F.; Mulvaney, P.; Stevens, G. W., *Langmuir* **1999**, 15, 7282-7289.
203. Mulvaney, P.; Perera, J. M.; Biggs, S.; Grieser, F.; Stevens, G. W., *Journal of Colloid and Interface Science* **1996**, 183, 614-616.
204. Snyder, B. A.; Aston, D. E.; Berg, J. C., *Langmuir* **1997**, 13, 590-593.
205. Basu, S.; Sharma, M. M., *Journal of Colloid and Interface Science* **1996**, 181, 443-455.
206. Yoon, R. H. G., D.; Aksoy, B. S.; Czarnecki, J.; Leung, A., *CIM* **1995**.
207. Wu, X.; Czarnecki, J.; Hamza, N.; Masliyah, J., *Langmuir* **1999**, 15, 5244-5250.
208. Wu, X.; Dabros, T.; Czarnecki, J., *Langmuir* **1999**, 15, 8706-8713.
209. Wu, X.; Laroche, I.; Masliyah, J.; Czarnecki, J.; Dabros, T., *Colloids and Surfaces a-Physicochemical and Engineering Aspects* **2000**, 174, 133-146.
210. Liu, J. J.; Xu, Z. H.; Masliyah, J., *Langmuir* **2003**, 19, 3911-3920.
211. Liu, J. J.; Xu, Z. H.; Masliyah, J., *Aiche Journal* **2004**, 50, 1917-1927.

212. Li, H.; Long, J.; Xu, Z.; Masliyah, J. H., *Energy & Fuels* **2005**, 19, 936-943.
213. Li, M. Y.; Xu, M. J.; Ma, Y.; Wu, Z. L.; Christy, A. A., *Colloids and Surfaces a-Physicochemical and Engineering Aspects* **2002**, 197, 193-201.
214. Marra, J.; Hair, M. L., *Macromolecules* **1988**, 21, 2349-2355.
215. Marra, J.; Hair, M. L., *Macromolecules* **1988**, 21, 2356-2362.
216. Salehi, M.; Johnson, S. J.; Liang, J. T., *Langmuir* **2008**, 24, 14099-14107.
217. Costello, B. A. D.; Luckham, P. F.; Tadros, T. F., *Langmuir* **1992**, 8, 464-468.
218. Plunkett, M. A.; Rutland, M. W., *Journal of Adhesion Science and Technology* **2002**, 16, 983-996.
219. Plunkett, M. A.; Rodner, S.; Bergstrom, L.; Rutland, M. W., *Journal of Adhesion Science and Technology* **2002**, 16, 965-981.
220. Gennes, P.-G. d., *Scaling Concepts in Polymer Physics*. Cornell University Press: Ithaca, N. Y., 1979.
221. Flory, P. J., *Principles of polymer chemistry*. Cornell University Press: Ithaca, 1953
222. Alexander, S., *Journal De Physique* **1977**, 38, 983-987.
223. Degennes, P. G., *Advances in Colloid and Interface Science* **1987**, 27, 189-209.
224. Degennes, P. G., *Macromolecules* **1982**, 15, 492-500.
225. Degennes, P. G., *Macromolecules* **1981**, 14, 1637-1644.
226. Degennes, P. G., *Macromolecules* **1980**, 13, 1069-1075.
227. Milner, S. T., *Science* **1991**, 251, 905-914.
228. Milner, S. T.; Witten, T. A.; Cates, M. E., *Europhysics Letters* **1988**, 5, 413-418.
229. Milner, S. T.; Witten, T. A.; Cates, M. E., *Macromolecules* **1988**, 21, 2610-2619.
230. Efremova, N. V.; Bondurant, B.; O'Brien, D. F.; Leckband, D. E., *Biochemistry* **2000**, 39, 3441-3451.

231. Kenworthy, A. K.; Hristova, K.; Needham, D.; McIntosh, T. J., *Biophysical Journal* **1995**, 68, 1921-1936.
232. Mendez, S.; Andrzejewski, B. P.; Canavan, H. E.; Keller, D. J.; McCoy, J. D.; Lopez, G. P.; Curro, J. G., *Langmuir* **2009**, 25, 10624-10632.
233. Cuenot, S.; Gabriel, S.; Jerome, R.; Jerome, C.; Fustin, C. A.; Jonas, A. M.; Duwez, A. S., *Macromolecules* **2006**, 39, 8428-8433.
234. Hansen, P. L.; Cohen, J. A.; Podgornik, R.; Parsegian, V. A., *Biophysical Journal* **2003**, 84, 350-355.
235. Yamamoto, S.; Ejaz, M.; Tsujii, Y.; Matsumoto, M.; Fukuda, T., *Macromolecules* **2000**, 33, 5602-5607.
236. Butt, H. J.; Kappl, M.; Mueller, H.; Raiteri, R.; Meyer, W.; Ruhe, J., *Langmuir* **1999**, 15, 2559-2565.
237. Marsh, D., *Biophysical Journal* **2004**, 86, 2630-2633.
238. Schwartz, D. K., *Surface Science Reports* **1997**, 27, 245-334.
239. Acevedo, S.; Ranaudo, M. A.; Garcia, C.; Castillo, J.; Fernandez, A., *Energy & Fuels* **2003**, 17, 257-261.
240. Israelachvili, J. N., *Intermolecular and Surface Forces*. Academic Press, 3<sup>rd</sup> edition: 2003.
241. Cosultchi, A.; Bosch, P.; Lara, V. H., *Colloid and Polymer Science* **2003**, 281, 325-330.
242. Wiehe, I. A., *Process Chemistry of Petroleum Macromolecules*. CRC Press: 2008.
243. Evdokimov, I. N.; Eliseev, N. Y.; Akhmetov, B. R., *Fuel* **2003**, 82, 817-823.
244. Pina, A.; Mougin, P.; Behar, E., *Oil & Gas Science and Technology-Revue De L Institut Francais Du Petrole* **2006**, 61, 319-343.
245. Schabron, J. F.; Speight, J. G., *Petroleum Science and Technology* **1998**, 16, 361-375.
246. Andersen, S. I.; Speight, J. G., *Journal of Petroleum Science and Engineering* **1999**, 22, 53-66.
247. Andersen, S. I.; Christensen, S. D., *Energy Fuels* **2000**, 14, 38-42.
248. Rogel, E., *Energy & Fuels* **1997**, 11, 920-925.

249. Mutelet, F.; Ekulu, G.; Solimando, R.; Rogalski, M., *Energy & Fuels* **2004**, 18, 667-673.
250. Desando, M. A.; Ripmeester, J. A., *Fuel* **2002**, 81, 1305-1319.
251. Wang, S. Q.; Liu, J. J.; Zhang, L. Y.; Xu, Z. H.; Masliyah, J., *Energy & Fuels* **2009**, 23, 862-869.
252. Lewis, J. A., *Journal of the American Ceramic Society* **2000**, 83, 2341-2359.
253. Fotland, P.; Askvik, K. M., *Colloids and Surfaces a-Physicochemical and Engineering Aspects* **2008**, 324, 22-27.
254. Burke, J., *AIC Book and Paper Group Annual* **Aug. 1984**, 3, 13-58.
255. Barton, A. F. M., *CRC handbook of solubility parameters and other cohesion parameters* CRC Press: 1983.
256. Sigal, G. B.; Mrksich, M.; Whitesides, G. M., *Journal of the American Chemical Society* **1998**, 120, 3464-3473.
257. Elwing, H.; Welin, S.; Askendal, A.; Nilsson, U.; Lundstrom, I., *Journal of Colloid and Interface Science* **1987**, 119, 203-210.
258. Li, X. Y.; Du, X.; He, J. H., *Langmuir* **2010**, 26, 13528-13534.
259. Cheng, Y. T.; Rodak, D. E.; Wong, C. A.; Hayden, C. A., *Nanotechnology* **2006**, 17, 1359-1362.
260. Sztukowski, D. M.; Yarranton, H. W., *J Colloid Interface Sci* **2005**, 285, 821-33.
261. Sztukowski, D. M.; Yarranton, H. W., *Journal of Dispersion Science and Technology* **2004**, 25, 299-310.
262. Vander Kloet, J.; Schramm, L. L.; Shelfantook, B., *Colloids and Surfaces a-Physicochemical and Engineering Aspects* **2001**, 192, 15-24.
263. Slavov, S. V.; Chuang, K. T.; Sanger, A. R., *Journal of Physical Chemistry* **1996**, 100, 16285-16292.
264. Dudasova, D.; Silset, A.; Sjoblom, J., *Journal of Dispersion Science and Technology* **2008**, 29, 139-146.
265. Volden, S.; Zhu, K. Z.; Nystrom, B.; Glomm, W. R., *Colloids and Surfaces B-Biointerfaces* **2009**, 72, 266-271.
266. Sheremata, J. M.; Gray, M. R.; Dettman, H. D.; McCaffrey, W. C., *Energy & Fuels* **2004**, 18, 1377-1384.



267. Franks, G. V.; Meagher, L., *Colloids and Surfaces a-Physicochemical and Engineering Aspects* **2003**, 214, 99-110.